# Vienna Rectifier with Gallium Nitride (GaN) Devices

By

Yutong Zhu

A thesis submitted in partial fulfillment of
requirements for the degree of

Master of Science
(Electrical and Computer Engineering)

at the

**University of Wisconsin – Madison**

2016

# Vienna Rectifier with Gallium Nitride (GaN) Devices

By

Yutong Zhu

Under the supervision of Professor Yehui Han

at University of Wisconsin - Madison

Approved by _____

Yehui Han

Date _____

# *Abstract*

As the technology on wide bandgap materials such as gallium-nitride (GaN) has advanced rapidly, commercial GaN power devices with satisfying performance are available now. It is widely-known that GaN-based switching devices have several advantages over traditional Si-based switching devices, such as lower ON-resistance, faster switching speed, better thermal conductivity, and smaller size. However, researchers have not yet fully explored and applied GaN devices in many important power conversion applications such as power rectifiers.

The three-phase three-level three-switch Vienna rectifier has advantages of low input current harmonics, low blocking voltage stress on the power semiconductor devices, high power density, high efficiency, and high reliability, and is widely used in many power applications. It is a good candidate topology to demonstrate GaN applications.

In this thesis, a three-phase three-level three-switch Vienna rectifier is designed utilizing GaN FETs. The advantages and challenges of utilizing GaN FETs in Vienna rectifiers are discussed. The topology and operation principles of the Vienna rectifier are carried out. The control of the Vienna rectifier is introduced based on two types of the current control strategies, the instantaneous current control and the direct power control. A simulation model is established and run in MATLAB/Simulink to verify theoretical analysis. To provide a comparative analysis of GaN FET and Si MOSFET based Vienna rectifiers, two prototypes are built with each type of the power devices on a similar scale. Experiment results and design experience of GaN FET based and Si MOSFET based Vienna rectifier systems are presented.

Advantages and benefits of applying GaN FET devices in the Vienna rectifier are concluded based on simulation and experimental results. It proves the promising potentials of GaN power devices in Vienna rectifier applications.

# *Acknowledgement*

I would like to thank my advisor Professor Yehui Han, for his guidance and support to my graduate study and research at Wisconsin Electric Machines and Power Electronics Consortium (WEMPEC) in University of Wisconsin-Madison. His enthusiasm in power electronics and patience with his students always inspire me to pursue the best and face the challenges with courage.

It is great pleasure for me to spend my graduate life with the WEMPEC family. The WEMPEC faculties are giving the most comprehensive and the best arranged lectures in power electronics, controls, electric machines and power grids, and I have learnt a lot from them. The WEMPEC students establish harmonic research atmosphere and I have enjoyed the great collaboration with them.

I would love to thank my parents, Jinling Zhu and Xiaoyun Feng, and my husband, Haichuan Tang, for their understanding and support during my graduate life. I would like to extend my sincere love and best wishes to them. Great thanks to all my friends in USA and China, for the pleasant and sad time we spent together.

# *Table of Contents*

***Abstract*** ..... I

***Acknowledgement*** ..... II

***Table of Contents*** ..... III

***List of Figures*** ..... VII

***List of Tables*** ..... XII

***Nomenclature*** ..... XIII

***Introduction*** ..... XV

Research Overview ..... XV

Summary of Chapters ..... XV

***Chapter 1*** ..... 1

***State-of-the-Art Review*** ..... 1

1.1 Unidirectional Rectifier Topologies ..... 1

1.1.1 Passive Systems ..... 4

1.1.2 Hybrid Systems ..... 6

1.1.3 Active Systems ..... 8

1.2 Wide Bandgap Semiconductor Power Devices ..... 14

1.2.1 Material Properties ..... 15

1.2.2 Existing Wide Bandgap Devices ..... 19

1.3 Research Opportunities and Challenges ..... 25

***Chapter 2*** ..... 28

***Vienna Rectifier Topology & Operation*** ..... 28

2.1 General Topology of Three-Level Rectifiers ..... 28

2.1.1 Single-phase Three-level Rectifying Circuit Topology ..... 28

2.1.2 Three-phase Three-level Rectifying Circuit Topology ..... 30

2.2 Vienna Rectifier Topology and Operation ..... 32

2.2.1 Bipolar Bidirectional Switch ..... 32

2.2.2 Topology of Vienna Rectifier ..... 34

2.2.3 Operation of Vienna Rectifier ..... 35

2.2.3.1 Basic Operation of Vienna Rectifier ..... 35

2.2.3.2 Voltage Space Vector of Vienna Rectifier ..... 37
2.3 Modulation of Vienna Rectifier ..... 42
2.3.1 Space Vector PWM (SVPWM) Based Modulation ..... 43
2.3.2 PWM Carrier Based Modulation ..... 44
***Chapter 3*** ..... 48
***Control of the Vienna Rectifier*** ..... 48
3.1 Mathematical Model of Vienna Rectifier System ..... 48
3.1.1 Model in Three-Phase Stationary (ABC) Reference Frame ..... 48
3.1.2 Model in Two-Phase Stationary (αβ) Reference Frame ..... 49
3.1.3 Model in Two-Phase Rotating (dq) Reference Frame ..... 50
3.2 Controller Structure ..... 52
3.3 Current Controller ..... 53
3.4 DC Output Voltage Controller ..... 56
3.5 Voltage Balance Controller ..... 61
3.6 Direct Power Controller (DPC) ..... 66
***Chapter 4*** ..... 72
***Simulation of the Vienna Rectifier*** ..... 72
4.1 Simulation Model of the Vienna Rectifier ..... 72
4.1.1 Power Circuit Simulation Model ..... 73
4.1.1.1 Build Power Circuit Model in MATLAB / Simulink ..... 73
4.1.1.2 Parameter Design of the Power Circuit ..... 75
4.1.2 Control Circuit Simulation Model ..... 76
4.1.2.1 Instantaneous Current Controller ..... 77
4.1.2.2 DPC Based Current Controller ..... 78
4.1.2.3 DC Voltage Controller ..... 80
4.1.2.4 Voltage Balancing Controller ..... 81
4.1.3 Modulator Simulation Model ..... 82
4.1.4 Summary of the Vienna Rectifier Simulation Model ..... 83
4.2 Simulation Results of the Vienna Rectifier ..... 84
4.2.1 Simulation Results of the Vienna Rectifier Based on Instantaneous Current Control (ICC) ..... 84

4.2.2 Simulation Results of the Vienna Rectifier Based on Direct Power Control (DPC) 89
4.2.3 Simulation Results of the Vienna Rectifier with Load Change ..... 90
4.2.4 Summary of Simulation Results of Vienna Rectifier ..... 92
***Chapter 5*** ..... 93
***Experiments of the Vienna Rectifier*** ..... 93
5.1 The Hardware Design of the Vienna Rectifier ..... 94
5.1.1 The Power Circuit Hardware Design ..... 95
5.1.2 The Driver circuit Hardware Design ..... 95
5.1.2.1 The Driver Circuit Hardware Design of the Si MOSFET ..... 95
5.1.2.2 The Driver circuit Hardware Design of the GaN FET ..... 96
5.1.3 The Sensing Circuit Hardware Design ..... 98
5.1.3.1 The AC Voltage Sensing Circuit Hardware Design ..... 99
5.1.3.2 The DC Voltage Sensing Circuit Hardware Design ..... 100
5.1.3.3 The AC Current Sensing Circuit Hardware Design ..... 101
5.1.4 The DSP Control Circuit Hardware Design ..... 102
5.1.5 The Power Supplier Hardware Design ..... 102
5.1.6 The Prototypes of the Vienna Rectifier Systems ..... 103
5.2 The Software Design of the Vienna Rectifier ..... 106
5.3 Experiment Results of the Vienna Rectifier ..... 109
5.3.1 Si MOSFET Based Vienna Rectifier Prototype with ICC control ..... 109
5.3.2 Si MOSFET Based Vienna Rectifier Prototype with DPC control ..... 111
5.3.3 GaN FET Based Vienna Rectifier Prototype with ICC Control ..... 112
5.3.4 GaN FET Based Vienna Rectifier Prototype with DPC Control ..... 114
5.3.5 Summary of Experimental Results ..... 116
5.4 Comparison between the GaN FET Based and Si MOSFET Based Vienna Rectifiers ..... 116
5.4.1 Comparison on Power Densities and Sizes of the GaN FET and Si MOSFET Devices and Drivers ..... 116
5.4.2 Comparison on Power Losses on the GaN FET and Si MOSFET Devices 117

5.4.3 Comparison on Current Qualities of the GaN FET and Si MOSFET Based Vienna Rectifier Systems ..... 118
***Chapter 6*** ..... 119
***Conclusions, Contributions and Future Work*** ..... 119
6.1 Conclusions ..... 119
6.2 Contributions ..... 121
6.3 Future Work ..... 122
***Appendix*** ..... 123
***Bibliography*** ..... 124

# *List of Figures*

**Fig. 1.1 Rectifiers classification based on power flow direction and converter types** ..... 2
**Fig. 1.2 Classification of unidirectional three-phase rectifier topologies into passive, hybrid, and active systems [9]** ..... 3
**Fig. 1.3 (a) Topology of diode rectifier; (b) Topology of thyristor rectifier** ..... 5
**Fig. 1.4 Minnesota rectifier using third harmonic injection into all three phases** ..... 7
**Fig. 1.5 Korea rectifier using third harmonic injection always into one phase** .. 7
**Fig. 1.6 (a) Y-connection phase-modular rectifier; (b) Δ-connection phase-modular rectifier** ..... 9
**Fig. 1.7 Single-switch three-phase rectifier operating in DCM** ..... 10
**Fig. 1.8 Three-switch Vienna rectifier** ..... 11
**Fig. 1.9 Six-switch Vienna rectifier** ..... 12
**Fig. 1.10 Two bipolar bidirectional switch structures** ..... 13
**Fig. 1.11 NPC-converter-based unidirectional rectifier** ..... 14
**Fig. 1.12 Concentration of intrinsic carriers in semiconductor vs. temperature** ..... 16
**Fig. 1.13 The specific on-resistance vs. breakdown voltage** ..... 17
**Fig. 1.14 The structure of EPC GaN FET** ..... 23
**Fig. 1.15 Illustration of cascode solution** ..... 24
**Fig. 2.1 (a) Symbolic topology of single-phase three-level rectifying circuit; (b) Equivalent ideal switch topology of single-phase three-level rectifying circuit** ..... 29
**Fig. 2.2 Symbolic topology of three-phase three-level rectifying circuit** ..... 30
**Fig. 2.3 Equivalent ideal switch topology of three-phase three-level rectifying circuit** ..... 31
**Fig. 2.4 Switch implementation with one power electronics device and four diodes and its operation modes** ..... 33

**Fig. 2.5 Topology of Vienna rectifier** ..... 34
**Fig. 2 6 Voltage space vector of Vienna rectifier** ..... 42
**Fig. 2.7 Control flowchart of the Vienna Rectifier SVPWM** ..... 43
**Fig. 2.8 (a)Architecture of the modulator of the Vienna rectifier system; (b) Pulse-width modulation using two 180°-phase-shifted triangular carrier signals at $\phi_N = 10°$ in ( $i_a > 0, i_b < 0$ , $i_c < 0$ ) section** ..... 47
**Fig. 3.1 Basic controller structure of the Vienna Rectifier system. (Signal paths being equal to all three phases are shown in double lines)** ..... 53
**Fig. 3.2 State block diagram of the current controller** ..... 55
**Fig. 3.3 Model of the DC side of the Vienne Rectifier with a resistive load** ..... 56
**Fig. 3.4 State block diagram of the DC output voltage controller** ..... 60
**Fig. 3.5 Pulse-width modulation and switching sequence illustrating the self stability of an unbalanced output voltage** ..... 62
**Fig. 3.6 (a) Vienna rectifier connection and neutral point current direction for the switching state $(S_a, S_b, S_c) = (0, -1, -1)$ for $\phi_N = 10°$; (b) Vienna rectifier connection and neutral point current direction for the switching state $(S_a, S_b, S_c) = (1, 0, 0)$ for $\phi_N = 10°$** ..... 64
**Fig. 3.7 Influence of a DC component $\Delta m$ added to all three modulation indexes on the switching sequence of the rectifier system for $\phi_N = 10°$** .... 65
**Fig. 3.8 DPC controller structure of the Vienna rectifier system. (Signal paths being equal to all three phases are shown in double lines)** ..... 69
**Fig. 3.9 State block diagram of decoupled power control loops in the DPC system** ..... 71
**Fig. 3.10 State block diagram of simplified active power control loop in the DPC system** ..... 71
**Fig. 4.1 Structure of the simulation model of the Vienna rectifier system** ..... 73
**Fig. 4.2 (a) Simulation model of the power circuit of the Vienna rectifier system; (b) Detailed simulation model of the rectifying subsystem in the power circuit** ..... 75
**Fig. 4.3 Structure of the simulation model of the control circuit** ..... 77

**Fig. 4.4 (a) State block diagram of the instantaneous current controller; (b) Function of the instantaneous current controller** ..... 78
**Fig. 4.5 State block diagram of the DPC based current controller** ..... 79
**Fig. 4.6 Function of the modulation index generating section in the DPC based current controller** ..... 80
**Fig. 4.7 State block diagram of the DC voltage controller** ..... 81
**Fig. 4.8 State block diagram of the voltage balancing controller** ..... 81
**Fig. 4.9 (a) State block diagram of the modulator based on the carrier based PWM modulation; (b) State block diagram of the PWM generator in the modulator** ..... 82
**Fig. 4.10 (a) State block diagram of the Vienna rectifier system simulation model with the instantaneous current control strategy; (b) State block diagram of the Vienna rectifier system simulation model with the direct power control strategy** ..... 84
**Fig. 4.11 Simulation results of the ICC based Vienna rectifier system in the rated operating condition with $f_s = 100$ kHz, and $R_L = 110$ Ω** ..... 85
**Fig. 4.12 FFT analysis results of the ICC based Vienna rectifier in the rated operating condition with $f_s = 100$ kHz, and $R_L = 110$ Ω** ..... 86
**Fig. 4.13 Simulation results of the ICC based Vienna rectifier system in the low frequency operating condition with $f_{s\_low} = 10$ kHz** ..... 87
**Fig. 4.14 Simulation results of the ICC based Vienna rectifier system in the high frequency operating condition with $f_{s\_high} = 500$ kHz** ..... 88
**Fig. 4.15 Simulation results of the DPC based Vienna rectifier system in the rated operating condition with $f_s = 100$ kHz, and $R_L = 110$ Ω** ..... 89
**Fig. 4.16 FFT analysis results of the DPC based Vienna rectifier in the rated operating condition with $f_s = 100$ kHz, and $R_L = 110$ Ω** ..... 90
**Fig. 4.17 Simulation results of the ICC based Vienna rectifier system when the resistive load $R_L$ changes from 110 Ω to 80 Ω at 0.1 s** ..... 91

**Fig. 4.18 Simulation results of the DPC based Vienna rectifier system when the resistive load $R_L$ changes from 110 Ω to 80 Ω at 0.1 s** ..... 91
**Fig. 5.1 Structure of the hardware design of the Vienna rectifier system** ..... 94
**Fig. 5.2 Schematic of the driver circuit in the Si MOSFET based Vienna rectifier system** ..... 96
**Fig. 5.3 Schematic of the driver circuit with GaN FET in the GaN FET based Vienna rectifier system** ..... 97
**Fig. 5.4 Photo of a real driver circuit for the GaN FET** ..... 98
**Fig. 5.5 Schematic of the AC voltage sensing circuit in the Vienna rectifier system** ..... 100
**Fig. 5.6 Schematic of the DC voltage sensing circuit in the Vienna rectifier system** ..... 101
**Fig. 5.7 Schematic of the AC current sensing circuit in the Vienna rectifier system** ..... 101
**Fig. 5.8 Photo of the DSP development board** ..... 102
**Fig. 5.9 Photo of the prototype of the Si MOSFET based Vienna rectifier system** ..... 104
**Fig. 5.10 Photo of the prototype of the GaN FET based Vienna rectifier system** ..... 105
**Fig. 5.11 DSP Control Program Flow Chart** ..... 107
**Fig. 5.12 Experiment results of the Si MOSFET based Vienna rectifier system with ICC control** ..... 110
**Fig. 5.13 FFT analysis on AC mains current in the Si MOSFET based Vienna rectifier system with ICC control** ..... 110
**Fig. 5.14 Experiment results of the Si MOSFET based Vienna rectifier system with DPC control** ..... 111
**Fig. 5.15 FFT analysis on AC mains current in the Si MOSFET based Vienna rectifier system with DPC control** ..... 112
**Fig. 5.16 Experiment results of the GaN FET based Vienna rectifier system with ICC control** ..... 113

**Fig. 5.17 FFT analysis on AC mains current in the GaN FET based Vienna rectifier system with ICC control** ..... 114
**Fig. 5.18 Experiment results of the GaN FET based Vienna rectifier system with DPC control**..... 115
**Fig. 5.19 FFT analysis on AC mains current in the GaN FET based Vienna rectifier system with DPC control** ..... 115

# *List of Tables*

**Table 1.1 Material properties I** ..... 15
**Table 1.2 Material properties II** ..... 18
**Table 1.3 Comparison between 1200 V Si and SiC devices** ..... 21
**Table 1.4 Comparison between 200 V Si and GaN devices** ..... 25
**Table 2.1 Section division based on phase voltage polarity** ..... 35
**Table 2.2 Switching states in Section 2** ($u_a > 0$ , $u_b < 0$ , $u_c < 0$) ..... 36
**Table 2.3 Voltage space vectors of Vienna rectifier** ..... 38
**Table 4.1 Parameters of the power circuit of the Vienna rectifier system** ..... 75
**Table 5.1 Parameters of the selected Si MOSFET and GaN FET devices** ..... 93
**Table 5.2 Power supplying chips and their characteristics** ..... 103

# *Nomenclature*

**Symbol**

| | |
|---|---|
| $C_1$ , $C_2$ | DC side capacitors |
| $\delta_i$ | duty cycle |
| $f_N$ | grid frequency |
| $f_s$ | switching frequency |
| $i_a$ , $i_b$ , $i_c$ | AC phase currents in the ABC reference frame |
| $i_\alpha$ , $i_\beta$ | AC phase currents in the αβ reference frame |
| $i_d$ , $i_q$ | AC phase currents in the dq reference frame |
| $i_o$ | neutral point current |
| $L$ | AC side boost inductors |
| $m_i^*$ | modulation index |
| $R_L$ | resistive load |
| $p$ | active power |
| $q$ | reactive power |
| $S_i$ | switching state (function) |
| $S_{ij}$ , $SW_i$ | switch ON/OFF status |
| $T_{ABC-\alpha\beta}$ | Clark transforming matrix |
| $T_{\alpha\beta-dq}$ | Park transforming matrix |
| $u_{DC1}$ , $u_{DC2}$ | DC side voltages on output capacitors |
| $u_{DC}$ | DC side output voltage |
| $u_{ao}$ , $u_{bo}$ , $u_{co}$ | rectifier input voltages referring to neutral point |
| $u_{aN}$ , $u_{bN}$ , $u_{cN}$ | rectifier input voltages referring to mains ground in ABC reference frame |

| | |
|---|---|
| $\vec{u}_r$ | voltage space vector |
| $u_\alpha$ , $u_\beta$ | rectifier input voltages in αβ reference frame |
| $u_d$ , $u_q$ | rectifier input voltages in dq reference frame |
| ω | the speed of dq reference frame |
| θ | the angle of dq reference frame |

**Abbreviations**

| | |
|---|---|
| 2DEG | 2 dimensional electron gas |
| BFoM | Baliga's figure of merit |
| DPC | direct power control |
| FET | field effect transistor |
| GaN | gallium nitride |
| MOSFET | metal oxide semiconductor field effect transistor |
| PCB | printed circuit board |
| PWM | pulse width modulation |
| SiC | silicon carbide |
| SVPWM | space vector pulse width modulation |
| THD | total harmonic distortion |
| WBG | wide bandgap |

# *Introduction*

## Research Overview

The objective of this research is to design a Vienna rectifier using Gallium Nitride (GaN) FET devices to maximize advantages of the Vienna rectifier topology and GaN power devices. The promising potential of applying the GaN power devices in power electronics applications is concluded.

In this research, theoretical analysis, simulation study and experiments based on prototypes are carried out on the Vienna rectifier system with GaN FET devices. All the concepts and techniques to realize such a system is covered in this research.

## Summary of Chapters

**Chapter 1** presents the state-of-the-art review of rectifier topologies and wide bandgap semiconductor power devices. Based on the reviews, research opportunities are identified.
**Chapter 2** introduces the Vienna rectifier topology. Technical details, such as operation and modulation, of the Vienna rectifier are presented.
**Chapter 3** presents control of the Vienna rectifier system. Since control strategy largely determines the performance of the Vienna rectifier, two control strategies based on instantaneous current control and direct power control are introduced and compared.
**Chapter 4** develops the simulation model of the Vienna rectifier in MATLAB/Simulink and provides simulation results. Simulation results are presented to validate the theoretical analysis results.
**Chapter 5** presents the hardware design of the Vienna rectifier prototypes based on similar scaling GaN FET devices and Si MOSFET devices respectively. Experiences of hardware design are shared in this chapter. Experimental results are provided to compare the GaN FET and the Si MOSFET devices.
**Chapter 6** concludes the thesis and summarizes the contributions of this research. Future work is also proposed in this chapter.

# *Chapter 1*

# *State-of-the-Art Review*

This chapter presents the state-of-the-art review of existing unidirectional rectifier topologies. These topologies are classified into three categories including passive rectifier systems, hybrid rectifier systems, and active rectifier systems. The advantages and challenges of the Vienna rectifier system are also discussed. Wide bandgap (WBG) semiconductors are briefly reviewed in the second part of this chapter. Several existing WBG products are introduced. At the end of this chapter, based on the review of rectifier topologies, and WBG semiconductor, research opportunities are identified.

## 1.1 Unidirectional Rectifier Topologies

AC-DC converters, also known as rectifiers, are the most commonly used power electronics circuits in wide applications including adjustable-speeds drive (ASDs), uninterruptible power supplies (UPSs), HVDC systems, and utility interfaces with renewable energy sources such as solar photovoltaic systems (PVs), wind power, etc [1]-[7]. In general, rectifiers play the role of a front end in power chains by switching accessible three-phase AC power into specific DC power, which supplies following power systems. Since rectifiers directly connect the input AC mains to the DC bus, they may have problems of poor power quality in terms of injected current harmonics, resultant voltage distortion and poor power factor at input AC mains and slowly varying rippled DC output at load end, low efficiency, and large size of AC and DC filters [8]. In order to avoid these problems, researches focusing on improved power quality and advanced performance rectifiers have been carried out for a long time, and important achievements have been made.

The classification of rectifiers can be done in various ways in terms of different aspects. Based on the power flow direction, rectifiers can be divided into unidirectional ones and bidirectional ones. Based on converter types, the rectifiers can be classified as boost, buck, buck-boost, multilevel and multipulse AC-DC converters [8]. Fig. 1.1 shows the classification according to power flow direction and sub-classification based on converter

types. Other than converter types, rectifiers can also be classified by the switching components applied in the systems. Traditionally, rectifiers are developed using diodes and thyristors. Nowadays, MOSFETs, GTOs, and IGBTs are widely used in rectifier systems as well.

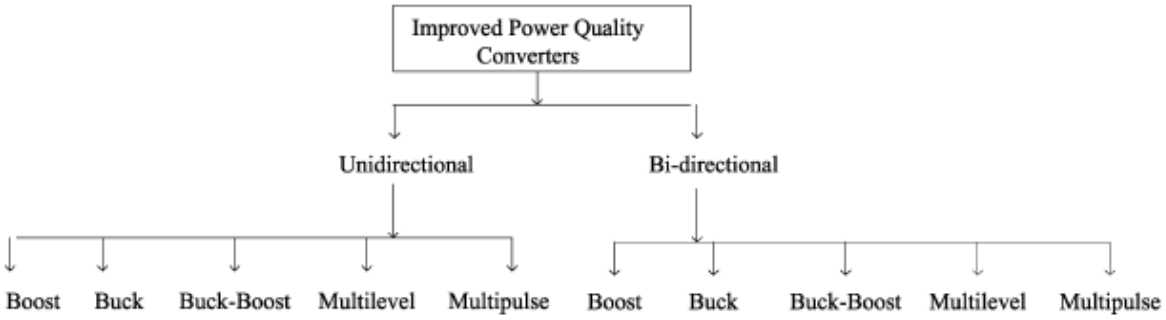


**Fig. 1.1 Rectifiers classification based on power flow direction and converter types [8]**

In addition to above classification methods, the unidirectional rectifiers can be divided into passive systems, hybrid systems and active systems as well [9]. Passive systems usually use diode or thyristor bridge without any active current control. This results in low-frequency harmonics in the mains currents and an uncontrolled output voltage. Hybrid systems partially integrate a passive rectifier and an active circuit part implemented with power semiconductors that can be actively switched OFF. As a result, hybrid systems exhibit either partly controlled mains currents or output voltage. Active systems employ fully controlled power semiconductors and achieve desired characteristics such as controlled output voltage and controlled sinusoidal mains currents. A more comprehensive comparison is presented in Fig. 1.2 [9].

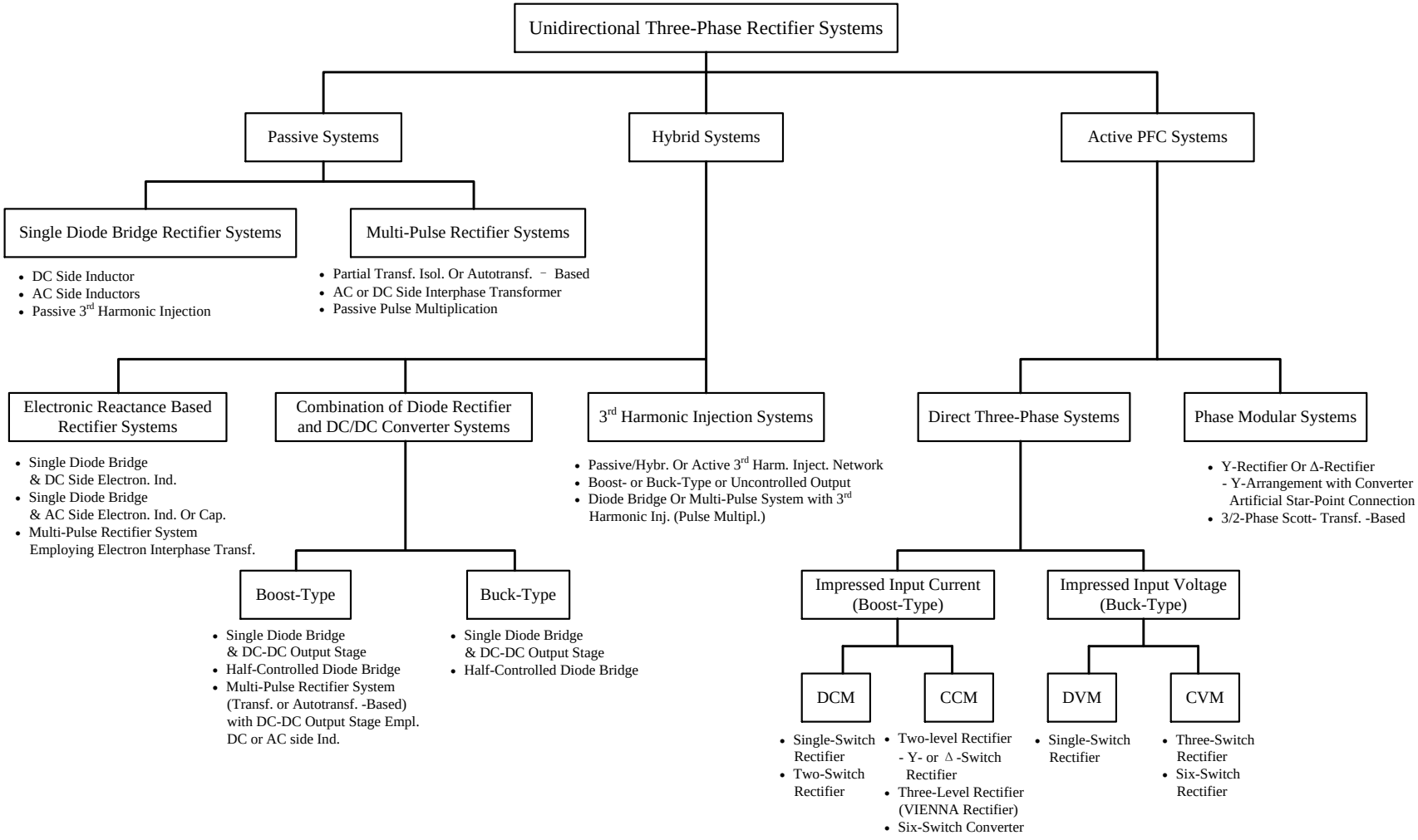


**Fig. 1.2 Classification of unidirectional three-phase rectifier topologies into passive, hybrid, and active systems [9]**

In the following discussion, unidirectional rectifier topologies with passive systems, hybrid systems and active systems will be introduced and discussed respectively.

### 1.1.1 Passive Systems

For purely passive systems, usually using three-phase diode/thyristor bridge shown in Fig. 1.3, the rectifier characteristics include:

1) Containing no turn-off semiconductors;

2) Working purely in mains-commutated mode;

3) Employing low frequency passive components (inductors and capacitors) for output voltage smoothing and mains current shaping;

4) Large low-frequency harmonics in mains currents, poor power factor, high THD;

5) Poor or even no output voltage regulation capability.

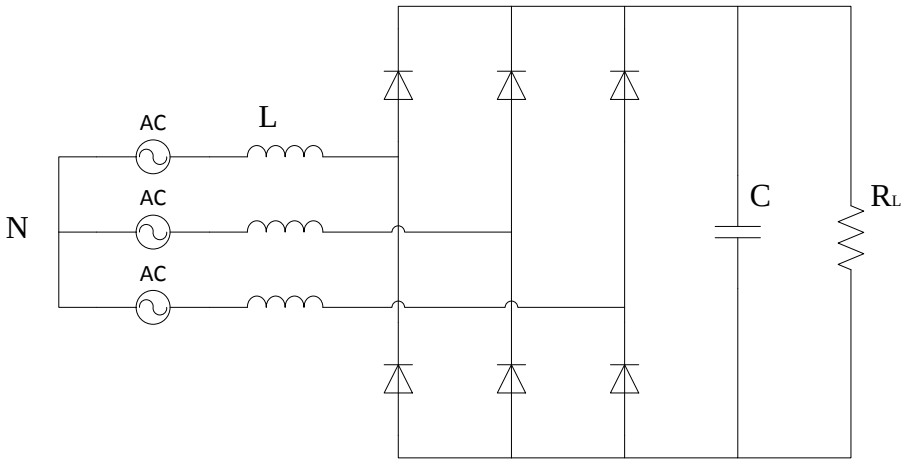


(a)

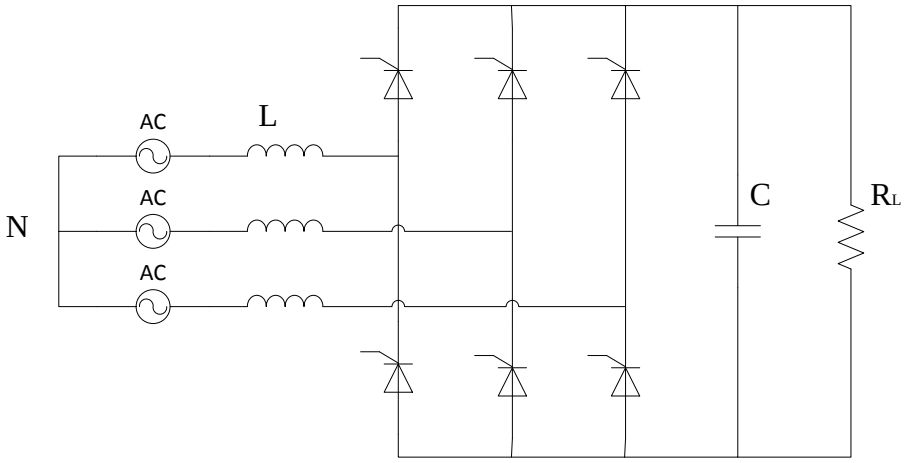


(b)

**Fig. 1.3 (a) Topology of diode rectifier; (b) Topology of thyristor rectifier**

In general, passive rectifier systems exhibit high mains current peaks, which lead to poor input current quality and power factor. However, this problem can be reduced if filter inductors are inserted in AC or DC side of the rectifier bridge. Adding filter inductors considerably improves system performance, but system THD is still above 30% and a power factor below 0.952 exists. In addition, the concept of passive third harmonic injection can be used to improve the input current quality according to [10] and a THD of 5% at full load can be achieved using this method. Moreover, the input current quality can also be enhanced with multi-pulse rectifier structure, which consists of two or more phase-shifted rectifier bridges connecting in parallel. Transformers are used for phase-shifting or isolation in multi-pulse rectifiers. Even though performance of passive systems can be improved with additional components or circuit design, the system size is big and its efficiency is low.

Considering the strong limitations of uncontrolled switches, i.e. diodes, or half-controlled switches, i.e. thyristors, passive systems are not suitable for applications where high input current quality and high power factor is required.

### 1.1.2 Hybrid Systems

Hybrid systems are developed based on passive systems by partially integrating full-controlled semiconductor devices, which can be turned off, into the systems. The hybrid systems fundamentally allow a regulation of the output voltage and a sinusoidal control of the mains current. However, there are limitations to output voltage regulation and mains current shaping. Furthermore, low frequency filter components of passive rectifier systems may be replaced/emulated by high-frequency PWM converters of relatively low rated power (electronic inductor [11], [12]), e.g., in the sense of an increase of the power density [9].

Third harmonic injection concepts form a major group of hybrid rectifier circuits. Here, current is injected by a passive or active injection network into either one phase or all three phases resulting in avoiding the zero mains current period in each phase. Therefore, nearly sinusoidal current flows in all phases. The most famous topology of third harmonic injection was proposed by Prof. N. Mohan in 1995 and is known as Minnesota rectifier [13], [14], as shown in Fig. 1.4. It uses a third harmonic current injection transformer to inject third harmonic currents into all three phases to achieve sinusoidal mains currents. The rectifier system shows a controlled output voltage and purely sinusoidal mains currents. The main drawback of the topology is the bulky, low-frequency current injection transformer, which has a high weight.

The bulky and heavy third harmonic injection transformer can be omitted if the current is always injected into only one phase. An interesting approach was proposed in [15], [16] and the basic structure of the rectifier system is given in Fig. 1.5. The system uses only a single inductor and three bidirectional, bipolar switches for injection of the third harmonic current into one phase. The current in the inductor L is modulated by the transistors S+ and S−. The three bidirectional switches always connect the phase with smallest (absolute) voltage value to the inductor.

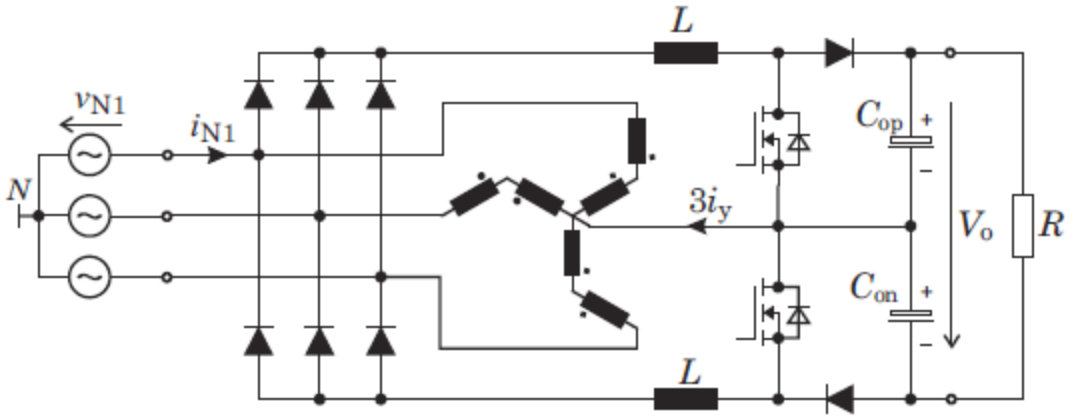


**Fig. 1.4 Minnesota rectifier using third harmonic injection into all three phases**

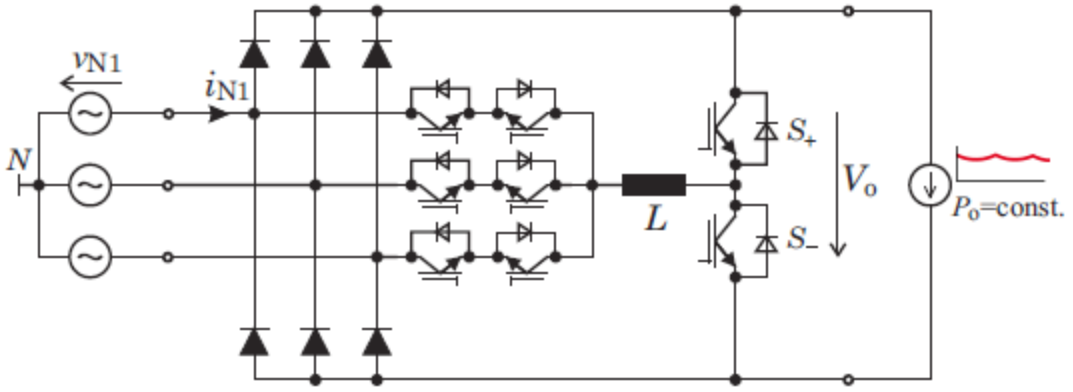


**Fig. 1.5 Korea rectifier using third harmonic injection always into one phase**

In conclusion, the rectifier function of the hybrid systems with third harmonic injection is implemented by a diode bridge on the input side. The active network for current shaping, injection, and voltage regulation, is arranged on the dc side, thus it may be considered essentially as a dc–dc converter working on a time-varying (six-pulse) dc input voltage [9]. Hence, the circuits are relatively simple and exhibit relatively low complexity control comparing with active three-phase converter systems. The characteristics of hybrid rectifiers are summarized as follows:

1) The diode rectifier circuit is commutated by mains while the active network is under forced commutation since it is implemented with power semiconductors that can be actively switched OFF;

2) Utilize low frequency and/or switching frequency passive components;

3) Limited output voltage regulation and/or sinusoidal mains current shaping can be achieved by turn-off power semiconductors.

### 1.1.3 Active Systems

Rectifier systems with active power factor correction (PFC) systems have outstanding advantages including high input current quality, low input current harmonics, high power factor, controllable output voltage regulation, high power density, etc. As a result, plenty of researches have been done in developing various active rectifier topologies. According to Fig. 1.2, the active rectifier topologies have two main branches, phase-modular systems and direct three-phase rectifier systems.

First, phase-modular systems use a single-phase rectifier stage for each phase to carry out active rectifier characteristics. The individual rectifier systems can be connected in star (Y-Rectifier [17], [18], as shown in Fig. 1.6(a)) or between phases (Δ-Rectifier [19], as shown in Fig. 1.6(b)). As the individual phase units provide independent output voltages ($V_{o1}$ $V_{o2}$ $V_{o3}$), in order to have common DC voltage ($V_o$) on the DC bus, isolated DC/DC converters are essential in each phase. Large capacitors are required in the DC bus of phase-modular rectifier as power flow pulsating, which is typical in single phase rectifier systems. Besides, balancing issues of three independent rectifier units need to be addressed. Overall, the phase-modular systems exhibit good active rectifier performance, but a DC/DC converter is typically required for each phase in the systems. Therefore, the phase-modular systems are not the top choice of active rectifiers in applications with specification of high power density.

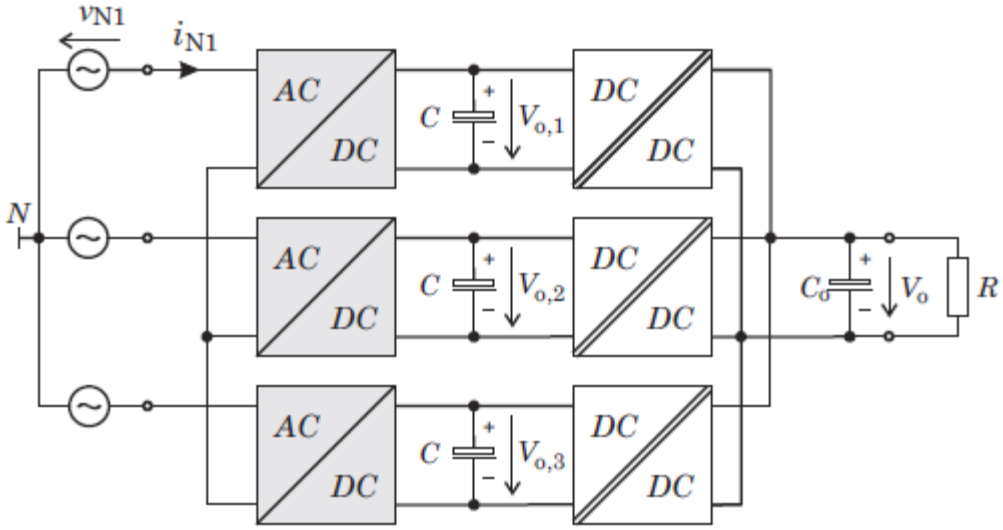


(a)

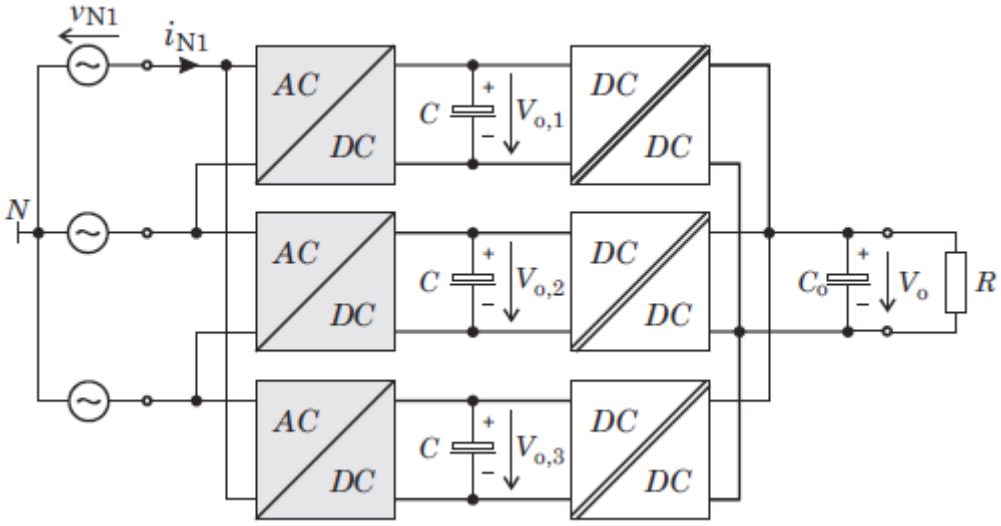


(b)

**Fig. 1.6 (a) Y-connection phase-modular rectifier; (b) Δ-connection phase-modular rectifier**

Second, direct three-phase rectifiers perform a direct energy conversion from the three-phase AC mains to the specific DC bus. Direct three-phase rectifier systems can be generally classified into boost-type and buck-type rectifier systems based on the voltage ratio. Typical buck-type rectifier systems, such as Three-Switch Buck Rectifier System [20] or Six-Switch Buck Rectifier System [21], operate in discontinuous conduction mode (DCM), thus extra input filtering capacitors are required due to discontinuous input currents and high current peak values. The high demand for filters limits the applications of buck-type rectifiers in high power density applications.

In general, boost-type rectifier systems are more popular and have more topologies. A very simple boost-type direct three-phase rectifier topology is shown in Fig. 1.7, named as single-switch three-phase boost rectifier [22], [23]. This system operates in discontinuous conduction mode (DCM) and the switch is modulated with a constant duty ratio. No PWM nor current measurement is required for this rectifier. However, since the system has discontinuous input current with high current peak values, there is a large demand in EMI filter as well.

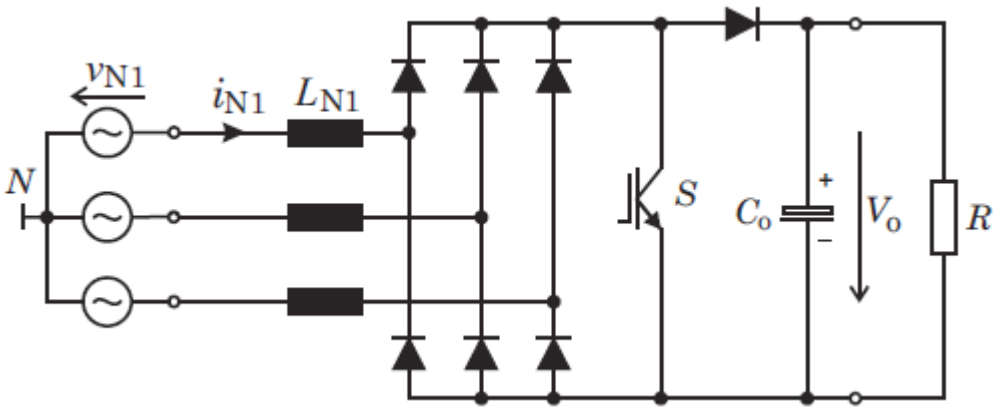


**Fig. 1.7 Single-switch three-phase rectifier operating in DCM**

Furthermore, direct three-phase rectifier systems can be divided into two-level and three-level topologies utilizing two and three voltage levels for PWM voltage formation. Compared with two-level rectifiers, three-level rectifiers outstand by smaller current ripples

and lower voltage stress on semiconductor switches. Since the current ripples are small, the size of boost inductors on the AC side is small. Moreover, due to low voltage stress on semiconductor switches, the switching loss is decreased, the filtering effort is reduced, and high frequency operation is enabled. As a result, capabilities of operating with high switching frequency and high power density make three-level rectifier suitable in corresponding applications. On the other hand, three-level rectifiers have some drawbacks. Usually, the complexity of three-level rectifier is high and an additional controller needs to be employed to balance the two output voltages. The advantages, however, overrule the drawbacks for applications where high power density is required.

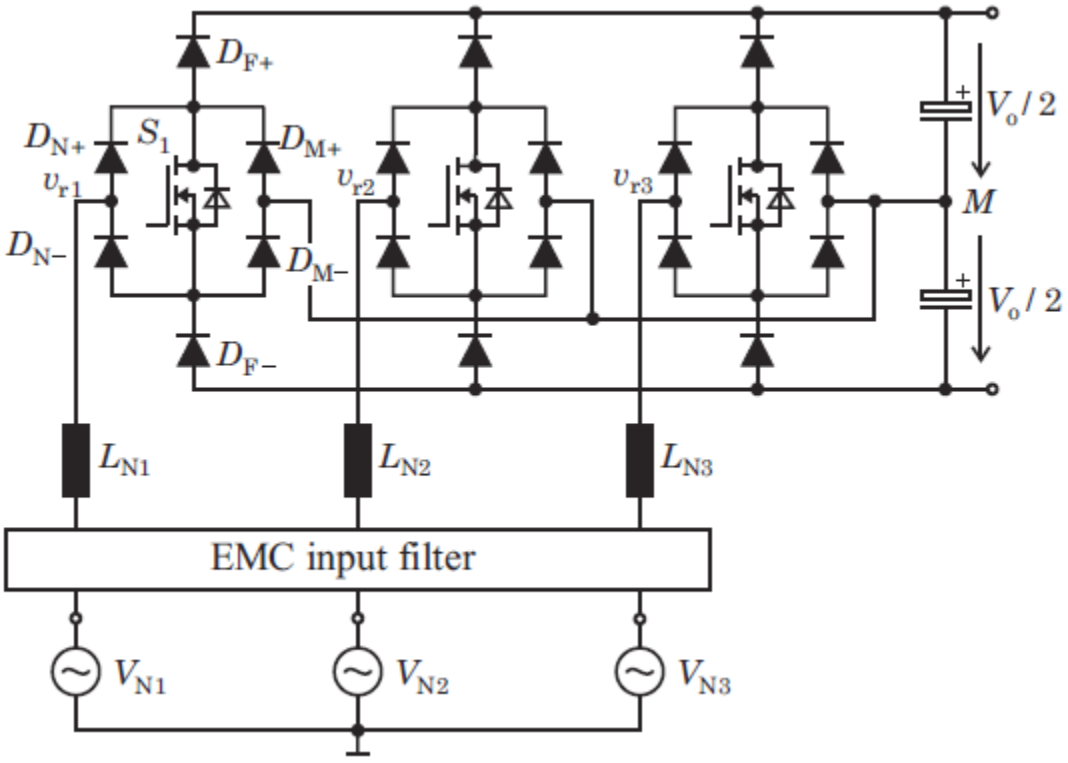


**Fig. 1.8 Three-switch Vienna rectifier**

The most famous representative of a unidirectional three-phase three-level rectifier topology is the Vienna rectifier, which is shown in Fig. 1.8 [24], [25]. This is the "original" Vienna rectifier implemented with only three switches, and all semiconductors (diodes and

active switches) are only stressed with half of the output DC voltage. The reliability of Vienna rectifier is pretty high because the DC output voltage can never be shorten. In each phase, two diodes are always conducting the current, which causes high conduction losses. The conduction loss problem of the original Three-Switch Vienna rectifier can be declined by slightly changing the topology in to Six-Switch Vienna rectifier [26], as shown in Fig. 1.9, to reduce number of conducting diodes.

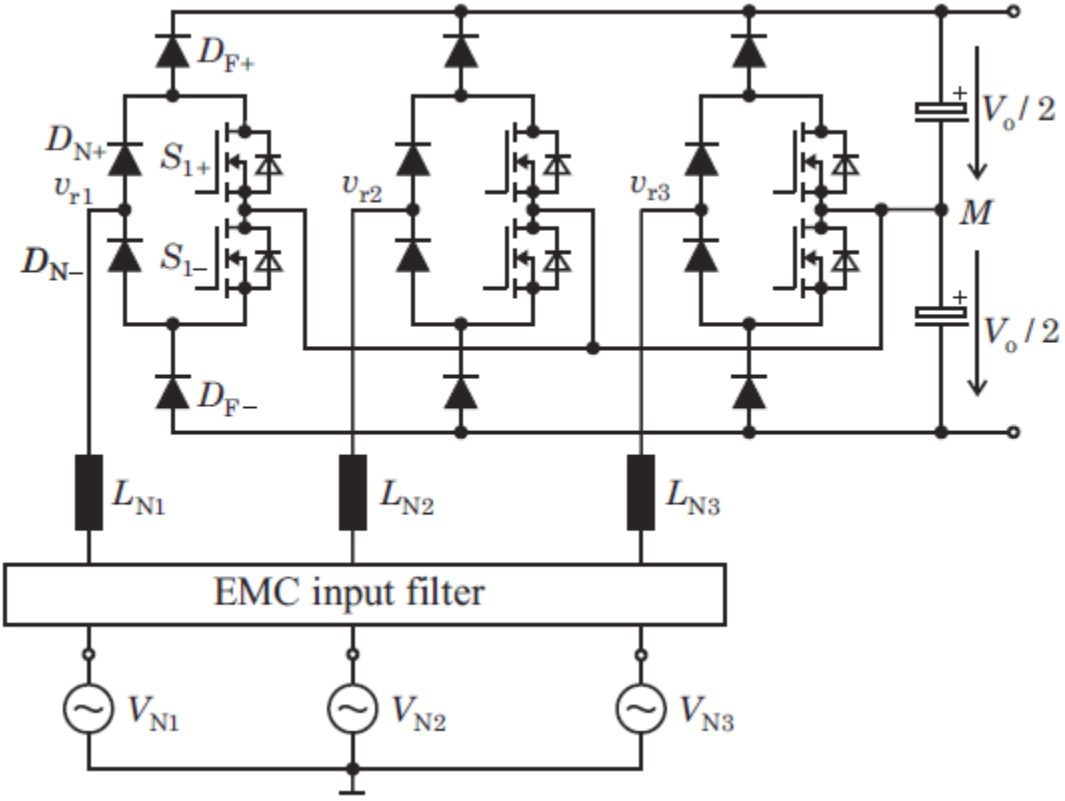


**Fig. 1.9 Six-switch Vienna rectifier**

The main difference between the Three-Switch Vienna rectifier and the Six-Switch Vienna rectifier is the implementation of the key element, the bipolar (voltage), bidirectional (current) switch, in the three-level rectifiers. Two popular structures, having the same function, are shown in Fig. 1.10 (a) and (b). The Three-Switch Vienna rectifier uses the four

diodes bridge and one switch structure given in Fig. 1.10 (a), while the Six-Switch Vienna rectifier uses the two switches structure given in Fig. 1.10 (b).

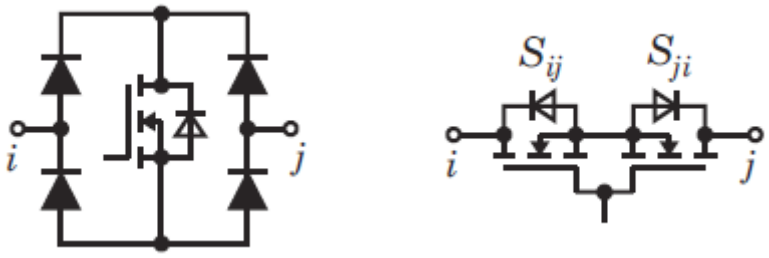


(a) (b)

**Fig. 1.10 Two bipolar bidirectional switch structures**

In report [27], a derivation of unidiractional three-phase rectifier circuits based on conventional bidirectional rectifier topologies, such as the Neutral Point Clamped (NPC), the Flying Capacitor and the converter employing symmetric Cascaded H-Bridges is discussed. A proposed unidirectional rectifier topology based on the NPC converter is shown in Fig. 1.11. In this topology, the conduction losses can be further reduced and high efficiency can be expected.

In conclusion, the three-phase Vienna rectifier topology is an ideal candidate for applicarions requiring high power density, high performance regarding power factor and input current quality. In [28], the Vienna rectifier topology is compared with a 12-pulse passive rectifier system and a conventional six-switch rectifier circuit, and the Vienna rectifier scores well and show several advantages.

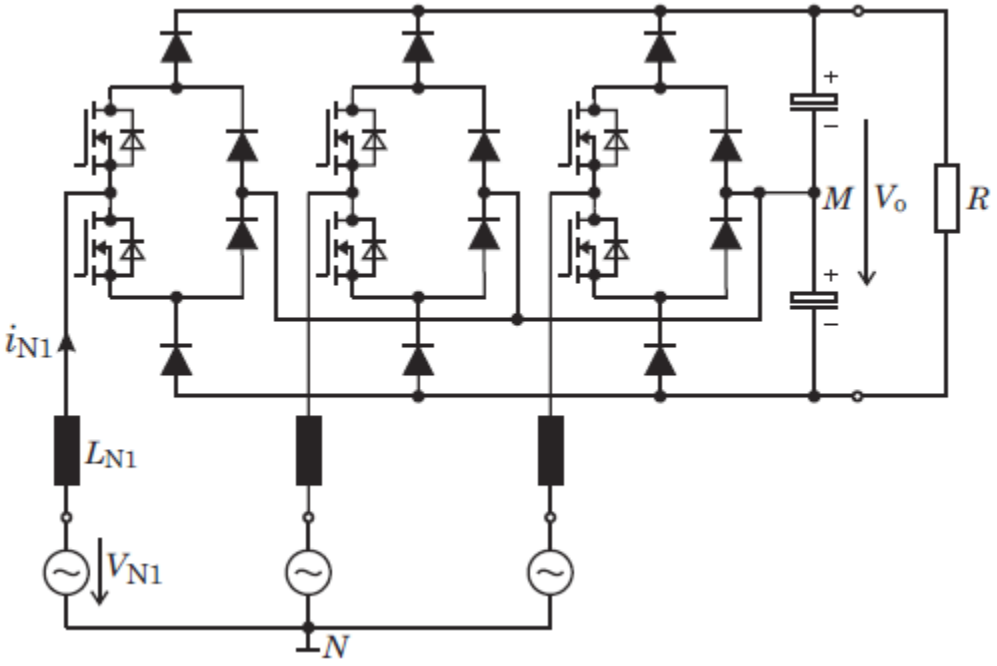


**Fig. 1.11 NPC-converter-based unidirectional rectifier**

## 1.2 Wide Bandgap Semiconductor Power Devices

Silicon (Si) material has been widely used in semiconductor power devices for decades. The technology of silicon power devices has been maturely developed as well. For silicon-based power devices, the limits in terms of power density, operating temperature and switching frequency have almost been reached [29]. However, power converters with higher power density, operating temperature, and switching frequency are very demanding in several application areas, such as mining, military, transportation, renewable energy and etc. A new technological breakthrough based on wide bandgap semiconductor materials, shows advantages to overcome the limits of silicon semiconductor materials. The bandgap characterization of a material pertains to the energy required for an electron to jump from the top of the valence band to the bottom of the conduction band within the semiconductor. The

term "wide bandgap materials" refers to semiconductor materials that typically require energy larger than two or three electron-volts (eV) [30]. Nowadays, two very important wide bandgap materials showing great promise for future are Gallium Nitride (GaN) and Silicon Carbide (SiC). Based on development of wide bandgap materials, breakthrough in semiconductor technology is underway. Wide bandgap semiconductors show several advantages over traditional semiconductors and are gradually changing the market.

### 1.2.1 Material Properties

Table 1.1 [31] shows several material properties of silicon (Si), silicon carbide (SiC) and Gallium Nitride (GaN), including bandgap, critical field, electron mobility, and electron saturation velocity. These material properties have major influence on fundamental performance characteristics of the corresponding devices.

| Material properties | Si | SiC | GaN |
|---|---|---|---|
| Bandgap [eV] | 1.1 | 3.2 | 3.4 |
| Critical field [MV/cm] | 0.3 | 3.0 | 3.5 |
| Electron mobility [$cm^2$/Vsec] | 1450 | 900 | 2000 |
| Electron saturation velocity [$10^6$cm/sec] | 10 | 22 | 25 |

**Table 1.1 Material properties I**

[31]

The bandgaps of SiC and GaN are 3.2 eV and 3.4 eV respectively, which are about three times higher comparing to that of Si (1.1 eV). The bandgap property has major influence on the concentration of intrinsic carriers $n_i$ in a semiconductor device in the form of an exponential function, represented by (1.1) [32]:

$$n_i^2 = N_c N_v \exp\left(\frac{-E_G}{k_B T}\right) \tag{1.1}$$

, where $E_G$ is the bandgap energy, T is the temperature, $N_c$ is related to conduction band density of states, $N_v$ is associated with valence band density of states, and $k_B$ is the Boltzmann constant. The relationship between intrinsic carriers and temperature is also plotted in Fig. 1.12, where characteristics of several materials in different crystal structures are shown.

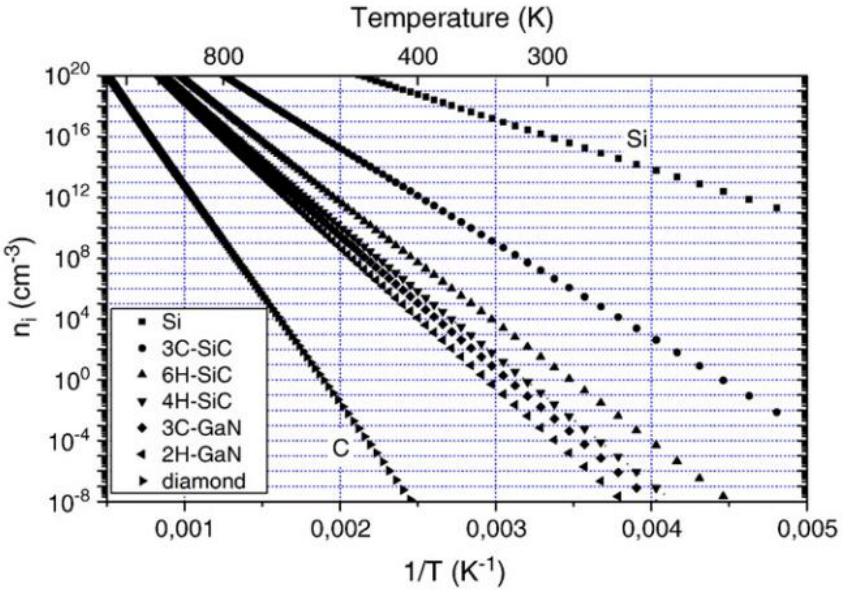


**Fig. 1.12 Concentration of intrinsic carriers in semiconductor vs. temperature**

[33]

Since the p-n junction leakage current is proportional to ni in a quadratic function, it is also determined by the bandgap energy $E_G$ of the material and the operating temperature T. When the operating temperature is high, the p-n junction leakage current increases, thus the device losses increase. The main reason that the operating temperature of normal Si devices is limited is that the leakage current is significant at high temperature. However, for wide

bandgap materials, such as SiC and GaN, the p-n junction leakage current in these materials can remain relatively low at high temperature [34]. It is because they have higher bandgap energy compared with Si, so that the influence on leakage current due to temperature increase can be reduced. As a result, the wide bandgap characteristics allow SiC and GaN power devices to operate under much higher temperature conditions than Si power devices. It is reported that a 4H-SiC JFET can operate at extremely high ambient temperature up to 450℃ [35].

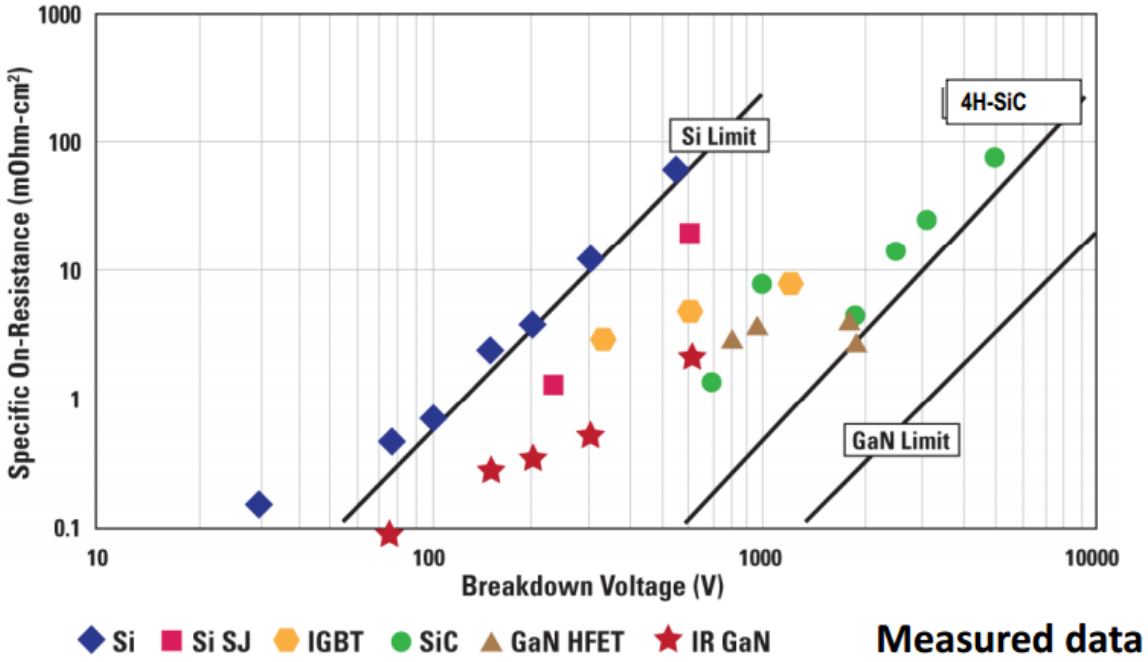


**Fig. 1.13 The specific on-resistance vs. breakdown voltage**

[37]

Besides, SiC and GaN have higher critical field than Si, 11.7 and 10 times higher respectively, as shown in Table 1.1. The higher critical field allows a higher breakdown voltage for identical epitaxial thickness, which means for a certain breakdown voltage, thinner epitaxial layer is needed for materials with higher critical field. As a result, very low on-resistances and very high breakdown voltages can be achieved by SiC and GaN devices

[36]. Fig. 1.13 shows the specific on-resistance vs. breakdown voltage for Si, SiC and GaN devices. This low resistance and high breakdown voltage characteristic is especially significant for high-power and high-efficient applications.

Moreover, the electron mobility and electron saturation velocity are important material parameters as well. They determine the switching performance of power devices by directly affecting the transconductance and output gain [38]. As can be seen from Table 1.1 that GaN has the highest electron mobility and electron saturation velocity, it has great potential to be the best material to make semiconductor devices for high frequency operation [31].

Table 1.2 shows the material properties associated with thermal performance. Higher thermal conductivity means the material is superior in conducting heat more efficiently. Since the thermal conductivity of SiC is higher than Si and GaN, the heat can be easily dissipated in this material and high power density can be achieved. As a result, SiC material has advantages in high power applications.

| Material properties | Si | 4H-SiC | GaN |
|---|---|---|---|
| Thermal conductivity [W/cmK] [3] | 1.5 | 3.8 | 1.3 / 4.1* |
| BFoM [14] | 1 | 500 | 2400 |

*The theoretical value of GaN thermal conductivity [39]

**Table 1.2 Material properties II**

Currently, the thermal conductivity of GaN is only 1.3 W/cmK, which makes GaN material less competitive in high power application. However, the theoretical value of GaN thermal conductivity is estimated as 4.1 W/cmK [39], which is comparable to 4H-SiC. The key limitation for GaN thermal conductivity to reach its theoretical value is the technical difficulty to form high quality defect-free GaN layers [40]. The currently available defect GaN crystal results in lower thermal conductivity. Recently, development and improvement

of GaN process was made to increase GaN thermal conductivity [40], and 2.53 W/cmK thermal conductivity was already achieved [41].

Furthermore, other than thermal conductivity, Baliga's figure of merit (BoFM) is another parameter influencing device thermal performance. Baliga's figure of metir (BoFM) is a measure of the on-resistance of a unipolar device, which dominates the resistive conduction loss of the device. A larger value indicates smaller on-resistance and lower conduction losses. In Table 1.2, the values are calibrated to 1.0 relative to Si. The conduction loss of a SiC and GaN device decreases by a factor of 500 and 2400 respectively when compared with a Si counterpart with identical device size and thermal dissipation area [42].

In conclusion, both silicon carbide (SiC) and gallium nitride (GaN) exhibit great advantages over silicon (Si) semiconductors in terms of power density, operating temperature and switching frequency. By properly applying these wide bandgap materials to power devices and fully taking their advantages, power electronics will be able to operate in extreme high frequency, high temperature and high efficiency conditions. SiC and GaN power devices are promising to dominate the future market of semiconductor power devices.

### 1.2.2 Existing Wide Bandgap Devices

Wide banggap semiconductors, such as SiC and GaN, have been researched for a long time in laboratories. SiC and GaN light-emitting diodes (LEDs) have been well developed and commercially available for a long time. However, SiC and GaN semiconductor power devices just began to present in the market in recent years. In this section, several representative SiC and GaN power devices are introduced.

- **SiC schottky diode**

In general, SiC schottky diode is the most mature wide bandgap semiconductor power device in commercial market. Compared with traditional Si schottky diode, the biggest

advantage of the SiC schottky diode is its extremely high rating voltage of 1700 V [43]. For conventional Si schottky diode, typical rating voltage is 50 V. Although some 200 V Si schottky diodes are available, but they have high reverse leakage current which is sensitive to operating temperature, and the thermal stability is not good. Considering the shortcomings of Si schottky diode in terms of low rating voltage and bad thermal stability, SiC schottky diodes obviously outstand with high rating voltage and good thermal stability. Since 2011, 1700 V SiC schottky diode has become available and its operating temperature can be as high as 200 ℃. Since the rating voltage level and operating temperature level exceeds the reach of Si schottky diode, SiC schottky diode has already taken the market to a large degree.

- **SiC FET**

SiC FETs with the voltage rating in the range of 600 V to 1700 V has become available in the market. Compared with Si FETs, SiC FETs outstand in performance obviously, especially in high rating voltage range. For devices rating at 500 - 900 V, there are a few Si FET products using advanced semiconductor technologies that are comparable to SiC FETs, such as MDmesh by STMicroelectronics and CoolMOS by Infineon. However, for devices rating at 1200 - 1700 V, SiC FETs are dominating the market. At this voltage level, SiC FETs have relatively small on-resistance and allow large rating currents, while Si FETs have very large on-resistance and the current ratings are limited to few amps. Considering products at this voltage level, a variety of choices are available for SiC devices, but the use of Si devices is quite limited. On the other hand, SiC FETs have much higher price compared with Si ones, which limits the wide penetration of SiC devices.

To compare SiC FETs with Si FETs, a SiC FET and a Si FET with identical rating voltage of 1200 V and similar on-resistance of 0.35 Ω are chosen as an example. Detailed comparison of parameters are shown in Table 1.3. Since the two FETs have the same on-resistance, they will have similar conduction loss during operation. However, the performance of the SiC device is 1 - 2 orders of magnitude better then the Si device, indicated by the input capacitance and output capacitance. Considering the body diode reverse recover time and charge, SiC FET has much better performance than Si FET in high

switching frequency operations as well. Moreover, SiC FETs with much lower on-resistance are available in the market, but no such availability for Si FETs.

| | Si | SiC |
|---|---|---|
| Manufacture | IXYS | Rohm |
| Manufacture # | IXFB30N120P | SCT2280KE |
| Rds(on)@25℃ [Ω] | 0.35 | 0.36 |
| Input cap. [pF] | 22500 | 667 |
| Output cap. [pF] | 950 | 27 |
| Body diode reverse recovery time [ns] | 300 | 22 |
| Body diode reverse recovery charge [nC] | 1600 | 21 |

**Table 1.3 Comparison between 1200 V Si and SiC devices**

- **GaN Diode**

Researches directed towards GaN diodes have been taken place in universities and laboratories for a while. However, commercial GaN diodes are not available in the market nowadays. In 2015, Panasonic announced the development of a GaN diode with high operating current (7.6 kA/cm²) and low turn-on voltage (0.8 V) based on a hybrid structure of a low-voltage unit and a high-current-capable unit [51]. Since the GaN diode has achieved simultaneous high-current operations and low threshold voltage, it can handle high current with a small chip area. The capacitance of the chip is also reduced, and lower switching losses and high frequency operation can be achieved. GaN diodes have promising future in the power device market considering its advantages, but technology breakthrough is still needed to bring commercial GaN diodes to the market.

- **GaN FET**

Depletion mode (normally-on) GaN FET devices first started to appear in 2004 by Eudyna Corporation in Japan [44]. In recent years, a large number of researches focusing on high performance GaN transistors have been done, but the progress has never been easy. Due to the thermal mismatch between different materials, there exists a thermal stress between GaN and the substrate when the temperature changes. As a result, GaN is very difficult to grow on the defect-free substrate [45]. Tremendous work has been down to improve the growth of GaN layer on Si substrate [46], sapphire substrate [47] or SiC substrate [48].

GaN has different advantages on different substrate materials. In general, Si material is the most common and commercialized substrate due to its cheap price. But it is difficult to grow GaN on a Si substrate because of the thermal mismatch. In contrary, it is easier to grow GaN on a SiC substrate, since GaN and SiC has a smaller thermal mismatch. Besides, the high thermal conductivity of SiC improves the thermal performance, which is significant in high power density applications. The drawback of SiC as the substrate of GaN is the high cost of the material.

The depletion mode (normally-on) is an inherent behavior of GaN devices with conventional structure. This behavior is due to the strong built-in polarization electric field, which causes two dimensional electron gas (2DEG) in the channel [49]. Since 2DEG cannot be easily depleted at zero gate voltage, GaN devices exhibit normally-on behavior. Generally speaking, normally-on behavior is not desirable for semiconductor devices, especially in voltage source power converter applications. The key reason is that the control unit loses its functionality in several conditions, including start-up, under-voltage transient and etc., which leads to short-circuit problems, device damages, control unit damages, or even input power source damages. In conclusion, normally-on devices require more components and more complicated circuit design to guarantee reliability. Therefore, normally-off devices are more preferred in power electronics applications.

Nowadays, commercialized normally-off GaN devices are available, and the mainstream technologies transferring normally-on behavior to normally-off behavior divided into two major branches. The first is the invention of enhancement mode GaN devices, which have normally-off behavior. This technology breakthrough was made by Efficient Power Conversion Corporation (EPC) that they introduced the first enhancement mode GaN FET on Si substrate. For enhancement mode GaN devices, the 2DEG problem is solved so that the devices exhibit normally-off behavior. Fig. 1.14 shows the lateral structure of an EPC GaN FET. EPC is one of the leading corporations providing advanced commercial enhancement mode GaN FET devices. A wide range of products are available with the voltage ratings from 30 V to 450 V. These devices can be applied up to several kilowatts power converter applications.

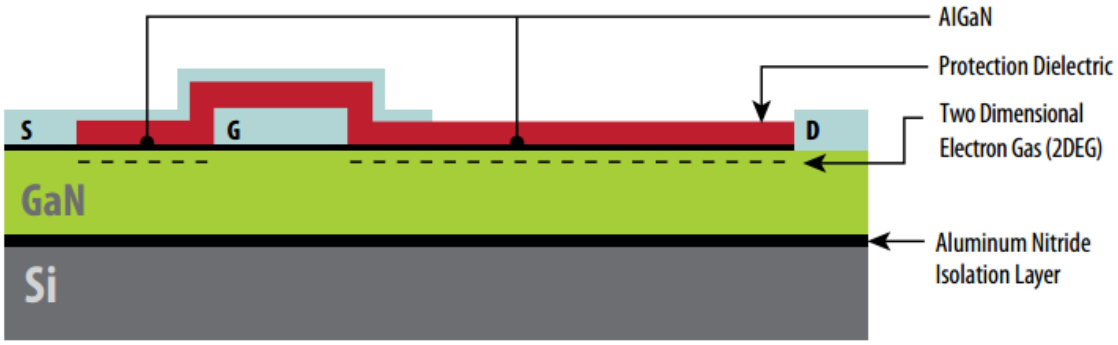


**Fig. 1.14 The structure of EPC GaN FET**

[44]

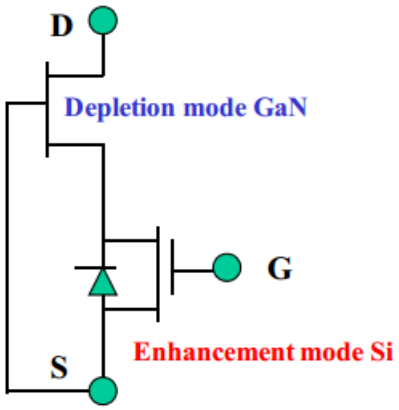


**Fig. 1.15 Illustration of cascode solution**

[50]

Another major solution converts a normally-on GaN device into an equivalent normally-off GaN device by combining an enhancement mode Si device and a depletion mode GaN FET into a cascade switch. Hence, it is referred as "cascode solution". As shown in Fig. 1.15, the gate of the GaN FET is tied to the source of the bottom Si switch, thus the gate voltage of the upper GaN switch is the source to drain voltage of the bottom Si switch, which is a negative value and securely turns off the upper GaN device. As a result, the cascode switch behaves as a normally-off device. In 2014, GaNSystems started to provide 100 V and 650 V cascode GaN devices.

To compare GaN FETs with Si FETs, a GaN FET and a Si FET with identical rating voltage of 200 V and similar rating current of about 20 A are chosen as an example. More comparison of parameters are shown in Table 1.4. It can be seen clearly that the on-resistance of GaN FET is nearly nine times smaller than the on-resistance of Si FET, which means the conduction loss of the GaN device is much smaller than that of the Si device. Compared with the Si device, the GaN device has better parameters in total gate charge, input capacitance, output capacitance and reverse transfer capacitance. Therefore, the switching loss of the GaN device is much smaller than that of the Si device as well. Better performance in high switching frequency operation applications can be expected with the GaN device.

| | Si | GaN |
|---|---|---|
| Manufacture | International Rectifier | EPC |
| Manufacturer # | IRF640N | EPC2010C |
| $V_{DS}$ [V] | 200 | 200 |
| $I_D$ [A] | 18 | 22 |
| Rds(on)@25°C [Ω] | 0.15 | 0.018 |
| Total gate Charge [nC] | 67 | 3.7 |
| Input cap. [pF] | 1160 | 380 |
| Output cap. [pF] | 185 | 240 |
| Reverse Transfer cap. [pF] | 53 | 1.8 |

**Table 1.4 Comparison between 200 V Si and GaN devices**

To summarize, commercial GaN FETs are available in the market. GaN FETs have many advantages over Si FETs, but the device price is currently very high compared to its Si counterparts.

## 1.3 Research Opportunities and Challenges

Theoretical limits of the silicon (Si) based power devices have almost been reached during years of technology improvements, which increases the difficulty in further improving device and system level performance [29]. Wide bandgap semiconductor material such as gallium nitride (GaN) has many advantages including wide band gap, high electron saturation velocity, high critical breakdown electric field, high thermal conductivity, etc. The GaN power devices have low ON-resistance, fast switching speed, nice thermal conductivity, small size and high reliability. Thus GaN power devices can be more suitable for high

frequency, high power density, and high temperature applications [55, 56]. Until recently, the research and applications of GaN power devices are still limited. The enormous benefits and possible applications of GaN devices have not been fully explored yet.

The three-phase three-level three-switch Vienna rectifier is widely used in electric aircraft systems, wind turbine systems and power factor correction systems. It has advantages of low input current harmonics, low blocking voltage stress on the power semiconductor devices, high power density, high efficiency, and high reliability [52]-[54].

However, all Vienna rectifiers were studied based on Si power devices. The Vienna rectifier system can be further improved when the Si power devices are replaced with GaN power devices. Since the Vienna rectifier topology only uses three switches, one in each phase, there is no shoot-through possibility and dead time is thus not necessary in a switching period. As a result, the switching frequency of the switches can be pushed even higher. With GaN FETs, the new system has a lot of potential improvements in terms of the power loss of switching devices, the performance of the rectifier like current harmonics, the size and power density of the rectifier, etc.

This is the first work that the GaN power devices have ever been utilized in the Vienna rectifier. This thesis discusses the advantages and challenges in implementing the Vienna rectifier with GaN FET devices. Based on topology and control discussions, a model of the Vienna rectifier is built and verified by simulation. One Vienna rectifier is designed with GaN FETs and the other one is designed with Si MOSFETs on a similar scale in order to carry out a fair comparison of the two types of devices. Comparative analyses on the power loss reductions of power devices, the performance improvements and size reductions of the Vienna rectifier will be studied based on the two systems.

There are many advantages to establish the Vienna rectifier with GaN FET devices.

The power loss of power devices can be reduced when GaN FET devices are applied. As the On-resistance of GaN FET is small, it has low conduction loss. The switching loss is also low due to short voltage rise and fall time of the GaN FET.

The size of the Vienna rectifier system can be miniaturized and the power density can be improved. As GaN devices can operate at high switching frequency, the value and size of passive components, like inductors and capacitors, in the system can be reduced. Due to low power loss and good thermal conductivity of the devices, heat sinks can be eliminated. As a result, high miniaturization and integration can be realized by using GaN devices in Vienna rectifier , which has promising utilization potentials in integrated modular motor drive systems and other applications with limited space [57].

However, implementing the Vienna rectifier with GaN FET has some challenges as well. For the Vienna rectifier, topology characteristic of single switch per phase makes the control of the rectifier complex and difficult. For the GaN FET, since the commercial devices are newly developed, the device utilization and corresponding driver design are challenging.

# Chapter 2

# Vienna Rectifier Topology & Operation

This chapter will introduce basic concepts of Vienna rectifier. A general topology of three-level rectifiers will be discussed first. Based on it, the typical Vienna rectifier topology and its operation will be demonstrated. Furthermore, the modulation of the Vienna rectifier based on carrier and SVPWM will be illustrated.

## 2.1 General Topology of Three-Level Rectifiers

Typically, a general rectifier system consists of an AC side current filter, a DC side voltage filter, and a rectifying circuit. Respectively, the AC side current filter is usually composed of passive inductive and capacitive components; the DC side voltage filter is often implemented by parallel capacitors; the rectifying circuit is built with fully controlled power electronics switches in various topologies regarding to different types of rectifier systems. Under the assumption that the switches are ideal and driving signals directly control switches' ON/OFF status, the rectifier system can be seen as the DC output is connected to the AC input in a certain form.

### 2.1.1 Single-phase Three-level Rectifying Circuit Topology

The basic classification of the rectifying circuit is based on the voltage level. The term "level" implies the number of the voltage levels that can be achieved during operation on the AC side of the rectifying circuit. For instance, "two-level" demonstrates that there are two possible voltage values on the AC side of the rectifying circuit, while "three-level" indicates three values. The topology of the typical three-level rectifying circuit is shown below, where both the symbolic rectifying circuit (Fig. 2.1 (a)) and its equivalent circuit consisting ideal switches (Fig. 2.1 (b)) can be seen clearly. In the ideal-switch equivalent circuit, the switches are represented by $S_{ij}$. For $S_{ij}=1$, the switch is ON, and for $S_{ij}=0$, the switch is OFF. Since the output of the rectifying system is DC voltage, the output terminals 'p', 'o', and 'n' cannot

connect to each other. Therefore, only one of the three switches shown in Fig. 2.1 (b), $S_{i1}$, $S_{i2}$, and $S_{i3}$, can turn ON at a time. Hence, the three switches, $S_{i1}$, $S_{i2}$, and $S_{i3}$, make a one-pole three-throw switch. This is the operation principle for three-level rectifying circuits.

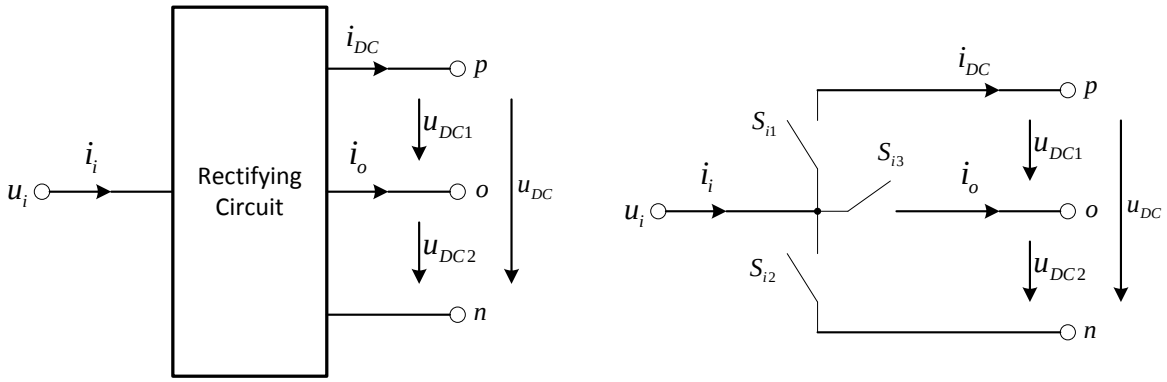


(a) (b)

**Fig. 2.1 (a) Symbolic topology of single-phase three-level rectifying circuit; (b) Equivalent ideal switch topology of single-phase three-level rectifying circuit**

Take point 'o' on the DC side as the voltage reference of the system, and the connection status of the rectifying circuit can be analyzed based on switches' connecting status as follows.

(1) When $S_{i1}=1$, $S_{i2}=0$, and $S_{i3}=0$, which means $S_{i1}$ is ON, and $S_{i2}$ and $S_{i3}$ are OFF, define $S_i=1$. Now $u_{io}=u_{DC1}$, $i_{DC}=i_i$, and $i_o=0$.

(2) When $S_{i1}=0$, $S_{i2}=1$, and $S_{i3}=0$, which means $S_{i2}$ is ON, and $S_{i1}$ and $S_{i3}$ are OFF, define $S_i=-1$. Now $u_{io}=-u_{DC2}$, $i_{DC}=0$, and $i_o=0$.

(3) When $S_{i1}=0$, $S_{i2}=0$, and $S_{i3}=1$, which means $S_{i3}$ is ON, and $S_{i1}$ and $S_{i2}$ are OFF, define $S_i=0$. Now $u_{io}=0$, $i_{DC}=0$, and $i_o=i_i$.

As a result, there are three possible voltages values ($u_{DC1}$, 0, $-u_{DC2}$) on the AC side of the rectifying circuit ($u_{io}$). The AC side voltage $u_{io}$ is a function of the switch status and DC

side voltages (2.1). And the DC side current $i_{DC}$, and the neutral point current $i_o$ are functions of both the switch status and AC input current $i_i$ (2.2)-(2.3).

$$u_{io} = f_v(S_{ij}, u_{DC1}, u_{DC2}) = S_{i1}u_{DC1} - S_{i2}u_{DC2} \tag{2.1}$$

$$i_{DC} = f_{id}(S_{ij}, i_i) = S_{i1}i_i \tag{2.2}$$

$$i_o = f_{io}(S_{ij}, i_i) = S_{i3}i_i \tag{2.3}$$

### 2.1.2 Three-phase Three-level Rectifying Circuit Topology

Based on the topology of the single-phase three-level rectifying circuit, three-phase three-level rectifying circuit topology can be developed. The symbolic topology of three-phase three-level rectifying circuit is shown in Fig. 2.2. Combining Fig. 2.1 (b) and Fig. 2.2, the equivalent ideal switch topology of three-phase three-level rectifying circuit can be derived, as shown in Fig. 2.3. Corresponding equations of three-phase AC side voltages, the DC side current and the neutral point current can also be written as (2.4)-(2.7).

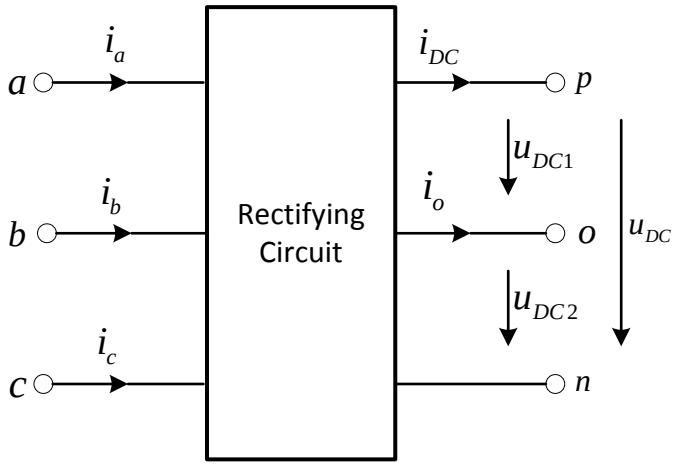


**Fig. 2.2 Symbolic topology of three-phase three-level rectifying circuit**

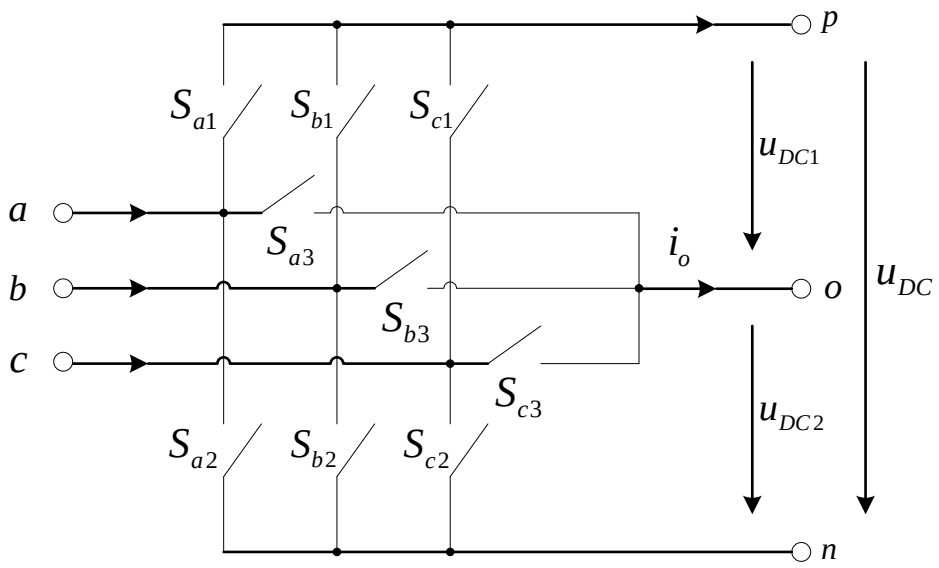


**Fig. 2.3 Equivalent ideal switch topology of three-phase three-level rectifying circuit**

Input AC phase voltages

$$\begin{cases} u_{ao} = S_{a1}u_{DC1} - S_{a2}u_{DC2} \\ u_{bo} = S_{b1}u_{DC1} - S_{b2}u_{DC2} \\ u_{co} = S_{c1}u_{DC1} - S_{c2}u_{DC2} \end{cases} \tag{2.4}$$

Input AC line voltages

$$\begin{cases} u_{ab} = u_{ao} - u_{bo} = (S_{a1} - S_{b1})u_{DC1} - (S_{a2} - S_{b2})u_{DC2} \\ u_{bc} = u_{bo} - u_{co} = (S_{b1} - S_{c1})u_{DC1} - (S_{b2} - S_{c2})u_{DC2} \\ u_{ca} = u_{co} - u_{ao} = (S_{c1} - S_{a1})u_{DC1} - (S_{c2} - S_{a2})u_{DC2} \end{cases} \tag{2.5}$$

$$i_{DC} = S_{a1}i_a + S_{b1}i_b + S_{c1}i_c \tag{2.6}$$

$$i_o = S_{a3}i_a + S_{b3}i_b + S_{c3}i_c \tag{2.7}$$

# 2.2 Vienna Rectifier Topology and Operation

The Vienna rectifier topology was proposed by Professor Johann W. Kolar in 1994. This topology has many outstanding advantages, such as high efficiency, high power density, low voltage stress, sinusoidal input current waveform, small volume of inductive components, and capability to operate under unbalancing voltage conditions. In this section, the implementation of the one-pole three-throw switch with one active power electronics device and four diodes is introduced. Apart from the key switch of the rectifier, the Vienna rectifier power circuit and its operation is discussed as well.

## 2.2.1 Bipolar Bidirectional Switch

The main component in the Vienna rectifier power circuit is the one-pole three-throw switch. This is a bipolar (voltage) bidirectional (current) switch. The position of the throw of this switch determines the connection between AC side and DC side of the rectifier. As shown in Fig. 2.4 (a), a typical implementation of the switch with one power electronics device and four diodes is given. Both the ON/OFF status of the power electronics device and the direction of the AC side current determine the connection status of the switch. Detailed switch connection modes are shown as well. When the power electronics device is OFF and the current flows from the AC side to the switch, terminal 1 and terminal 3 are connected (Fig. 2.4 (b)). When the power electronics device is OFF and the current flows from the switch to the AC side, terminal 1 and terminal 4 are connected (Fig. 2.4 (c)). When the power electronics device is ON and the current flows from the AC side to the switch, terminal 1 inputs the current and terminal 2 outputs it (Fig. 2.4 (d)). When the power electronics device is ON and the current flows from the switch to the AC side, terminal 2 inputs the current and terminal 1 outputs it (Fid. 2.4 (e)).

The one power electronics device and four diodes topology of the one-pole three-throw switch has several advantages. Only one power electronics device is needed in this switch

topology. The control of the switch is easy. There is no shoot-through problem and dead time design is not necessary during operation. However, this topology has some shortcomings: There are always two diodes connecting in each switching mode, so the forward voltage drop is high and the conduction loss on the diodes is high. In this research, GaN device will be utilized in the Vienna rectifier. In order to simplify the control and drive system of the GaN device, the one power electronics device and four diodes topology is selected.

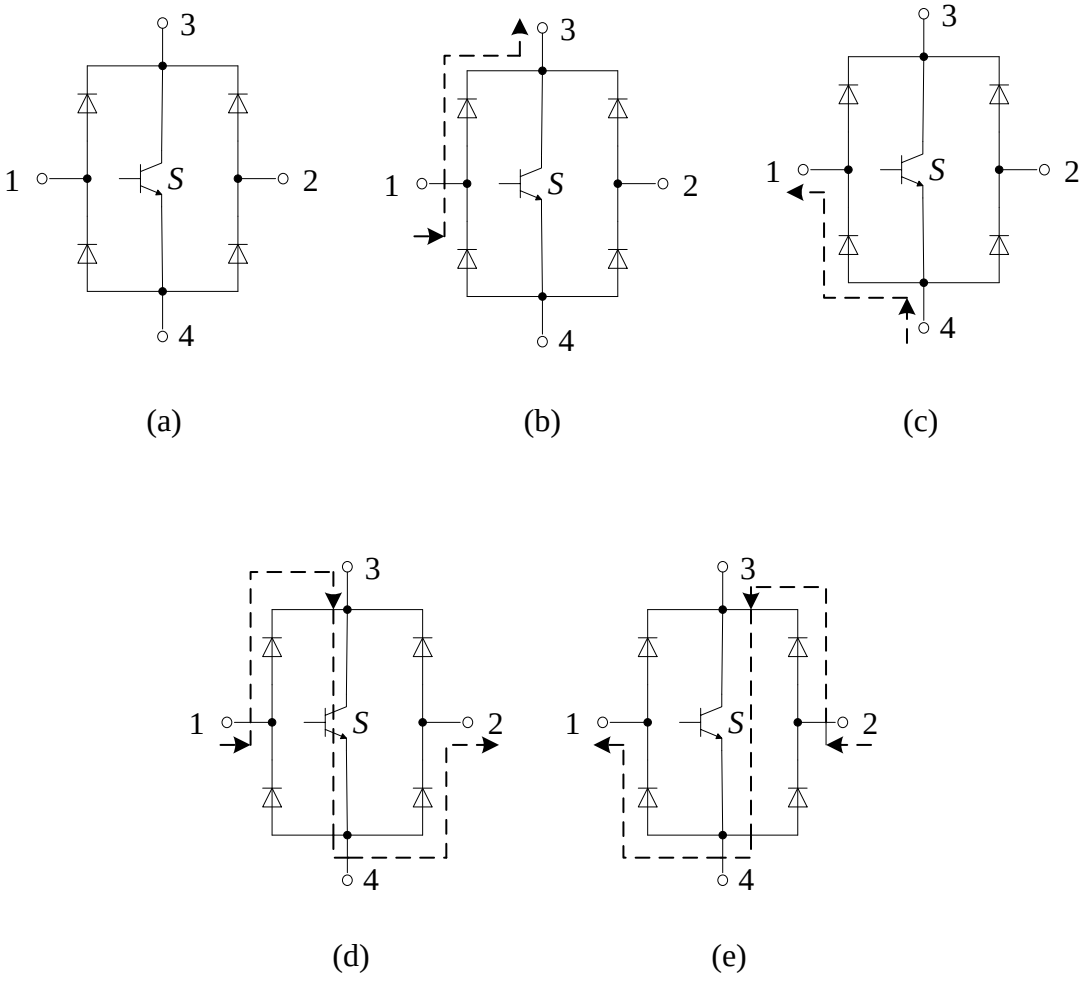


**Fig. 2.4 Switch implementation with one power electronics device and four diodes and its operation modes**

### 2.2.2 Topology of Vienna Rectifier

The topology of Vienna rectifier based on the switch shown in Fig. 2.4 (a) is shown in Fig. 2.5. The Vienna rectifier system consists of three AC side filtering inductors (L and R), three bipolar bidirectional switches, a diode bridge, two DC side filtering capacitors ($C_1$ and $C_2$), and load ($R_L$). The three bidirectional switches are implemented using a single unidirectional switch SWi in combination with a diode bridge, and they are advantageously integrated in the diode bridge ($D_{a+}, D_{a-}, D_{b+}, D_{b-}, D_{c+}, D_{c-}$) of the rectifier system. The output capacitors are split and the bidirectional switches are connected to the output voltage midpoint *o*.

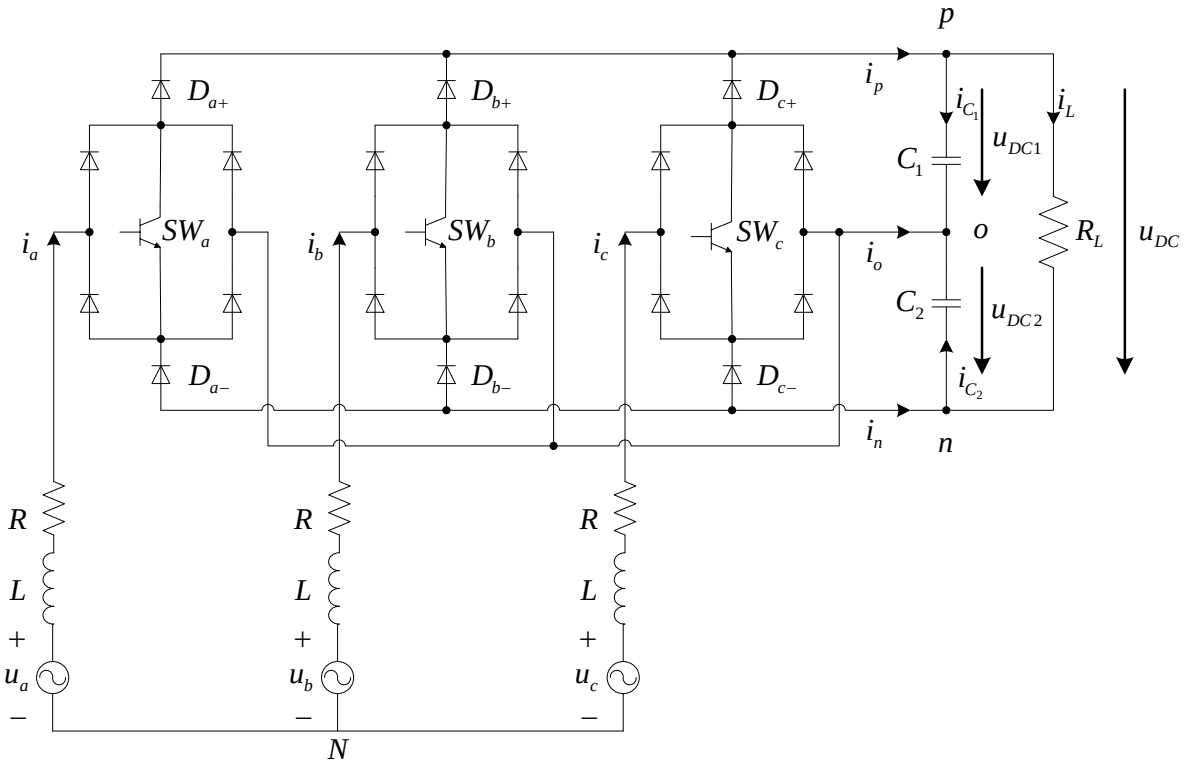


**Fig. 2.5 Topology of Vienna rectifier**

## 2.2.3 Operation of Vienna Rectifier

### 2.2.3.1 Basic Operation of Vienna Rectifier

Based on the Vienna rectifier topology given in Fig. 2.5, the basic operation of the Vienna rectifier can be analyzed. The input of the rectifier system, which is connected to the boost inductor L, can be switched to 0 V (*o* point) by closing switch Si, or depending on the current direction, switched to $+\frac{U_{DC}}{2}$ (*p* point) or $+\frac{U_{DC}}{2}$ (*n* point) by the free-wheeling diodes $D_{i+}$ and $D_{i-}$. Thus, Vienna rectifier shows the three-level rectifier behavior. To summarize, the operation status of the Vienna rectifier is determined by the input current direction of each phase and the switching states of each switch.

Based on the polarity of three phase input voltages, one power frequency (50Hz or 60Hz) period can be divided into six sections, and each section is 60°. In each section, two phase voltages have the same polarity. An example of section classification is given in Table 2.1. In each section, the directions of three-phase input currents are also determined.

| Section 1 | Section 2 | Section 3 | Section 4 | Section 5 | Section 6 |
|---|---|---|---|---|---|
| $u_a > 0$ | $u_a > 0$ | $u_a > 0$ | $u_a < 0$ | $u_a < 0$ | $u_a < 0$ |
| $u_b < 0$ | $u_b < 0$ | $u_b > 0$ | $u_b > 0$ | $u_b > 0$ | $u_b < 0$ |
| $u_c > 0$ | $u_c < 0$ | $u_c < 0$ | $u_c < 0$ | $u_c > 0$ | $u_c < 0$ |

**Table 2.1 Section division based on phase voltage polarity**

Define the switching function of the Vienna rectifier as Si:

$$S_i = \begin{cases} +1 & SW_i \text{ OFF}, i_i > 0 \quad S_{i1} = 1, S_{i2} = 0, S_{i3} = 0 \\ 0 & SW_i \text{ ON}, i = a, b, c \quad S_{i1} = 0, S_{i2} = 0, S_{i3} = 1 \\ -1 & SW_i \text{ OFF}, i_i < 0 \quad S_{i1} = 0, S_{i2} = 1, S_{i3} = 0 \end{cases}$$

The switching function Si is a function of switch ON/OFF status ( $SW_i = 1$, switch is ON; $SW_i = 0$, switch is OFF) and input current direction, as expressed by (2.8).

$$S_i = [1 - SW_i] sign(i_i) \tag{2.8}$$

In different sections, the same switch status $SW_i$ leads to different switching function $S_i$ since the current direction is different. Take section 2 as an instant, the relationship between switching function $S_i$ and switch status $SW_i$ is given in Table 2.2. Besides, the corresponding neutral point current $i_o$ is given under each switch status in section 2 as well, in Table 2.2. The existence of $i_o$ causes voltage unbalance problem between $C_1$ and $C_2$ that $u_{DC1} \neq u_{DC2}$.

| $SW_a$ | $SW_b$ | $SW_c$ | $S_a$ | $S_b$ | $S_c$ | $i_o$ |
|---|---|---|---|---|---|---|
| 1 | 1 | 1 | 0 | 0 | 0 | 0 |
| 1 | 1 | 0 | 0 | 0 | -1 | $-i_c$ |
| 1 | 0 | 1 | 0 | -1 | 0 | $-i_b$ |
| 1 | 0 | 0 | 0 | -1 | -1 | $i_a$ |
| 0 | 1 | 1 | 1 | 0 | 0 | $-i_a$ |
| 0 | 1 | 0 | 1 | 0 | -1 | $i_b$ |
| 0 | 0 | 1 | 1 | -1 | 0 | $i_c$ |
| 0 | 0 | 0 | 1 | -1 | -1 | 0 |

**Table 2.2 Switching states in Section 2** ($u_a > 0$ , $u_b < 0$ , $u_c < 0$)

The operation of Vienna rectifier in other sections is very similar to that in Section 2. By controlling the turn-on and turn-off of switches ($SW_i$), the input current can be regulated to follow current demand, and the output voltage can be regulated steady as well.

### 2.2.3.2 Voltage Space Vector of Vienna Rectifier

The Vienna rectifier has three phases and each phase has three switching function values (referring to switching function definition), thus there are 27 theoretical switching states for the rectifier system. However, based on the specific topology of Vienna rectifier, switching function ( $S_a$ , $S_b$ , $S_c$ ) does not have (+1, +1, +1) and (-1, -1, -1). As a result, there are only 25 switching stateses of the system.

Voltage space vectors of the Vienna rectifier can be found based on the 25 switching stateses of the system. Under stable operation conditions, the voltages on two separate DC capacitors can be assumed to be the same ( $u_{DC1} = u_{DC2} = \frac{u_{DC}}{2}$ ). Then the rectifier input voltages between the inputs of the rectifier and the neutral point *o* are

$$\begin{bmatrix} u_{ao} & u_{bo} & u_{co} \end{bmatrix} = \frac{u_{DC}}{2} \begin{bmatrix} S_a & S_b & S_c \end{bmatrix} \tag{2.9}$$

The phase voltages between the inputs of the rectifier and the mains neutral point N are

$$\begin{aligned} u_{aN} &= u_{ao} - u_{No} \\ u_{bN} &= u_{bo} - u_{No} \\ u_{cN} &= u_{co} - u_{No} \end{aligned} \tag{2.10}$$

Since the sum of the three-phase mains voltages is zero

$$\sum_{i=a}^{c} u_{iN} = 0 \tag{2.11}$$

The voltage between neutral point *o* and mains neutral point N can be calculated

$$u_{No} = \frac{u_{DC}}{6} \sum_{i=a}^{c} S_i \tag{2.12}$$

Therefore, the voltage space vectors of the Vienna rectifier can be calculated by

$$\vec{u}_r = \frac{2}{3}(u_{aN} + \alpha u_{bN} + \alpha^2 u_{cN}) = \frac{2}{3}(u_{ao} + \alpha u_{bo} + \alpha^2 u_{co}) = \frac{1}{3}u_{DC}(S_a + \alpha S_b + \alpha^2 S_c) \qquad (2.13)$$

where $\alpha = e^{j\frac{2}{3}\pi}$.

Based on Equations (2.8)-(2.13) and the 25 switching states of the Vienna rectifier, 19 different voltage space vectors, including 18 non-zero vectors and 1 zero vector, can be obtained. Among the 18 non-zero vectors, there are 6 long vectors with the norm of $\frac{2}{3}u_{DC}$, 6 medium vectors with the norm of $\frac{1}{\sqrt{3}}u_{DC}$, and 6 short vectors with the norm of $\frac{1}{3}u_{DC}$.

Table 2.3 shows the list of the voltage space vectors of the Vienna rectifier, and Fig. 2.6 shows the space vector diagram.

**Table 2.3 Voltage space vectors of Vienna rectifier**

| Current direction | | | Switch ON/OFF | | | Switching states | Phase rectifier input voltage | | | Space vector norm |
|---|---|---|---|---|---|---|---|---|---|---|
| $i_a$ | $i_b$ | $i_c$ | $SW_a$ | $SW_b$ | $SW_c$ | [ $S_a$ $S_b$ $S_c$ ] | $u_{aN}$ | $u_{bN}$ | $u_{cN}$ | |
| + | - | - | 0 | 0 | 0 | [1, -1, -1] | $\frac{2}{3}u_{DC}$ | $-\frac{1}{3}u_{DC}$ | $-\frac{1}{3}u_{DC}$ | $\frac{2}{3}u_{DC}$ |
| + | - | - | 0 | 0 | 1 | [1, -1, 0] | $\frac{1}{2}u_{DC}$ | $-\frac{1}{2}u_{DC}$ | 0 | $\frac{1}{\sqrt{3}}u_{DC}$ |
| + | - | - | 0 | 1 | 0 | [1, 0, -1] | $\frac{1}{2}u_{DC}$ | 0 | $-\frac{1}{2}u_{DC}$ | $\frac{1}{\sqrt{3}}u_{DC}$ |
| + | - | - | 0 | 1 | 1 | [1, 0, 0] | $\frac{1}{3}u_{DC}$ | $-\frac{1}{6}u_{DC}$ | $-\frac{1}{6}u_{DC}$ | $\frac{1}{3}u_{DC}$ |

| | | | | | | | | | | |
|---|---|---|---|---|---|---|---|---|---|---|
| + | - | - | 1 | 0 | 0 | [0, -1, -1] | $\frac{1}{3}u_{DC}$ | $-\frac{1}{6}u_{DC}$ | $-\frac{1}{6}u_{DC}$ | $\frac{1}{3}u_{DC}$ |
| + | - | - | 1 | 0 | 1 | [0, -1, 0] | $\frac{1}{6}u_{DC}$ | $-\frac{1}{3}u_{DC}$ | $\frac{1}{6}u_{DC}$ | $\frac{1}{3}u_{DC}$ |
| + | - | - | 1 | 1 | 0 | [0, 0, -1] | $\frac{1}{6}u_{DC}$ | $\frac{1}{6}u_{DC}$ | $-\frac{1}{3}u_{DC}$ | $\frac{1}{3}u_{DC}$ |
| + | - | - | 1 | 1 | 1 | [0, 0, 0] | 0 | 0 | 0 | 0 |
| + | + | - | 0 | 0 | 0 | [1, 1, -1] | $\frac{1}{3}u_{DC}$ | $\frac{1}{3}u_{DC}$ | $-\frac{2}{3}u_{DC}$ | $\frac{2}{3}u_{DC}$ |
| + | + | - | 0 | 0 | 1 | [1, 1, 0] | $\frac{1}{6}u_{DC}$ | $\frac{1}{6}u_{DC}$ | $-\frac{1}{3}u_{DC}$ | $\frac{1}{3}u_{DC}$ |
| + | + | - | 0 | 1 | 0 | [1, 0, -1] | $\frac{1}{2}u_{DC}$ | 0 | $-\frac{1}{2}u_{DC}$ | $\frac{1}{\sqrt{3}}u_{DC}$ |
| + | + | - | 0 | 1 | 1 | [1, 0, 0] | $\frac{1}{3}u_{DC}$ | $-\frac{1}{6}u_{DC}$ | $-\frac{1}{6}u_{DC}$ | $\frac{1}{3}u_{DC}$ |
| + | + | - | 1 | 0 | 0 | [0, 1, -1] | 0 | $\frac{1}{2}u_{DC}$ | $-\frac{1}{2}u_{DC}$ | $\frac{1}{\sqrt{3}}u_{DC}$ |
| + | + | - | 1 | 0 | 1 | [0, 1, 0] | $-\frac{1}{6}u_{DC}$ | $\frac{1}{3}u_{DC}$ | $-\frac{1}{6}u_{DC}$ | $\frac{1}{3}u_{DC}$ |
| + | + | - | 1 | 1 | 0 | [0, 0, -1] | $\frac{1}{6}u_{DC}$ | $\frac{1}{6}u_{DC}$ | $-\frac{1}{3}u_{DC}$ | $\frac{1}{3}u_{DC}$ |
| + | + | - | 1 | 1 | 1 | [0, 0, 0] | 0 | 0 | 0 | 0 |
| - | + | - | 0 | 0 | 0 | [-1, 1, -1] | $-\frac{1}{3}u_{DC}$ | $\frac{2}{3}u_{DC}$ | $-\frac{1}{3}u_{DC}$ | $\frac{2}{3}u_{DC}$ |
| - | + | - | 0 | 0 | 1 | [-1, 1, 0] | $-\frac{1}{2}u_{DC}$ | $\frac{1}{2}u_{DC}$ | 0 | $\frac{1}{\sqrt{3}}u_{DC}$ |
| - | + | - | 0 | 1 | 0 | [-1, 0, -1] | $-\frac{1}{6}u_{DC}$ | $\frac{1}{3}u_{DC}$ | $-\frac{1}{6}u_{DC}$ | $\frac{1}{3}u_{DC}$ |
| - | + | - | 0 | 1 | 1 | [-1, 0, 0] | $-\frac{1}{3}u_{DC}$ | $\frac{1}{6}u_{DC}$ | $\frac{1}{6}u_{DC}$ | $\frac{1}{3}u_{DC}$ |

| | | | | | | | | | | |
|---|---|---|---|---|---|---|---|---|---|---|
| - | + | - | 1 | 0 | 0 | [0, 1, -1] | 0 | $\frac{1}{2}u_{DC}$ | $-\frac{1}{2}u_{DC}$ | $\frac{1}{\sqrt{3}}u_{DC}$ |
| - | + | - | 1 | 0 | 1 | [0, 1, 0] | $-\frac{1}{6}u_{DC}$ | $\frac{1}{3}u_{DC}$ | $-\frac{1}{6}u_{DC}$ | $\frac{1}{3}u_{DC}$ |
| - | + | - | 1 | 1 | 0 | [0, 0, -1] | $\frac{1}{6}u_{DC}$ | $\frac{1}{6}u_{DC}$ | $-\frac{1}{3}u_{DC}$ | $\frac{1}{3}u_{DC}$ |
| - | + | - | 1 | 1 | 1 | [0, 0, 0] | 0 | 0 | 0 | 0 |
| - | + | + | 0 | 0 | 0 | [-1, 1, 1] | $-\frac{2}{3}u_{DC}$ | $\frac{1}{3}u_{DC}$ | $\frac{1}{3}u_{DC}$ | $\frac{2}{3}u_{DC}$ |
| - | + | + | 0 | 0 | 1 | [-1, 1, 0] | $-\frac{1}{2}u_{DC}$ | $\frac{1}{2}u_{DC}$ | 0 | $\frac{1}{\sqrt{3}}u_{DC}$ |
| - | + | + | 0 | 1 | 0 | [-1, 0, 1] | $-\frac{1}{2}u_{DC}$ | 0 | $\frac{1}{2}u_{DC}$ | $\frac{1}{\sqrt{3}}u_{DC}$ |
| - | + | + | 0 | 1 | 1 | [-1, 0, 0] | $-\frac{1}{3}u_{DC}$ | $\frac{1}{6}u_{DC}$ | $\frac{1}{6}u_{DC}$ | $\frac{1}{3}u_{DC}$ |
| - | + | + | 1 | 0 | 0 | [0, 1, 1] | $-\frac{1}{3}u_{DC}$ | $\frac{1}{6}u_{DC}$ | $\frac{1}{6}u_{DC}$ | $\frac{1}{3}u_{DC}$ |
| - | + | + | 1 | 0 | 1 | [0, 1, 0] | $-\frac{1}{6}u_{DC}$ | $\frac{1}{3}u_{DC}$ | $-\frac{1}{6}u_{DC}$ | $\frac{1}{3}u_{DC}$ |
| - | + | + | 1 | 1 | 0 | [0, 0, 1] | $-\frac{1}{6}u_{DC}$ | $-\frac{1}{6}u_{DC}$ | $\frac{1}{3}u_{DC}$ | $\frac{1}{3}u_{DC}$ |
| - | + | + | 1 | 1 | 1 | [0, 0, 0] | 0 | 0 | 0 | 0 |
| - | - | + | 0 | 0 | 0 | [-1, -1, 1] | $\frac{1}{3}u_{DC}$ | $-\frac{2}{3}u_{DC}$ | $\frac{1}{3}u_{DC}$ | $\frac{2}{3}u_{DC}$ |
| - | - | + | 0 | 0 | 1 | [-1, -1, 0] | $-\frac{1}{6}u_{DC}$ | $-\frac{1}{6}u_{DC}$ | $\frac{1}{3}u_{DC}$ | $\frac{1}{3}u_{DC}$ |
| - | - | + | 0 | 1 | 0 | [-1, 0, 1] | $-\frac{1}{2}u_{DC}$ | 0 | $\frac{1}{2}u_{DC}$ | $\frac{1}{\sqrt{3}}u_{DC}$ |
| - | - | + | 0 | 1 | 1 | [-1, 0, 0] | $-\frac{1}{3}u_{DC}$ | $\frac{1}{6}u_{DC}$ | $\frac{1}{6}u_{DC}$ | $\frac{1}{3}u_{DC}$ |

| | | | | | | | | | | |
|---|---|---|---|---|---|---|---|---|---|---|
| - | - | + | 1 | 0 | 0 | [0, -1, 1] | 0 | $-\frac{1}{2}u_{DC}$ | $\frac{1}{2}u_{DC}$ | $\frac{1}{\sqrt{3}}u_{DC}$ |
| - | - | + | 1 | 0 | 1 | [0, -1, 0] | $\frac{1}{6}u_{DC}$ | $-\frac{1}{3}u_{DC}$ | $\frac{1}{6}u_{DC}$ | $\frac{1}{3}u_{DC}$ |
| - | - | + | 1 | 1 | 0 | [0, 0, 1] | $-\frac{1}{6}u_{DC}$ | $-\frac{1}{6}u_{DC}$ | $\frac{1}{3}u_{DC}$ | $\frac{1}{3}u_{DC}$ |
| - | - | + | 1 | 1 | 1 | [0, 0, 0] | 0 | 0 | 0 | 0 |
| + | - | + | 0 | 0 | 0 | [1, -1, 1] | $\frac{1}{3}u_{DC}$ | $-\frac{2}{3}u_{DC}$ | $\frac{1}{3}u_{DC}$ | $\frac{2}{3}u_{DC}$ |
| + | - | + | 0 | 0 | 1 | [1, -1, 0] | $\frac{1}{2}u_{DC}$ | $-\frac{1}{2}u_{DC}$ | 0 | $\frac{1}{\sqrt{3}}u_{DC}$ |
| + | - | + | 0 | 1 | 0 | [1, 0, 1] | $\frac{1}{6}u_{DC}$ | $-\frac{1}{3}u_{DC}$ | $\frac{1}{6}u_{DC}$ | $\frac{1}{3}u_{DC}$ |
| + | - | + | 0 | 1 | 1 | [1, 0, 0] | $\frac{1}{3}u_{DC}$ | $-\frac{1}{6}u_{DC}$ | $-\frac{1}{6}u_{DC}$ | $\frac{1}{3}u_{DC}$ |
| + | - | + | 1 | 0 | 0 | [0, -1, 1] | 0 | $-\frac{1}{2}u_{DC}$ | $\frac{1}{2}u_{DC}$ | $\frac{1}{\sqrt{3}}u_{DC}$ |
| + | - | + | 1 | 0 | 1 | [0, -1, 0] | $\frac{1}{6}u_{DC}$ | $-\frac{1}{3}u_{DC}$ | $\frac{1}{6}u_{DC}$ | $\frac{1}{3}u_{DC}$ |
| + | - | + | 1 | 1 | 0 | [0, 0, 1] | $-\frac{1}{6}u_{DC}$ | $-\frac{1}{6}u_{DC}$ | $\frac{1}{3}u_{DC}$ | $\frac{1}{3}u_{DC}$ |
| + | - | + | 1 | 1 | 1 | [0, 0, 0] | 0 | 0 | 0 | 0 |

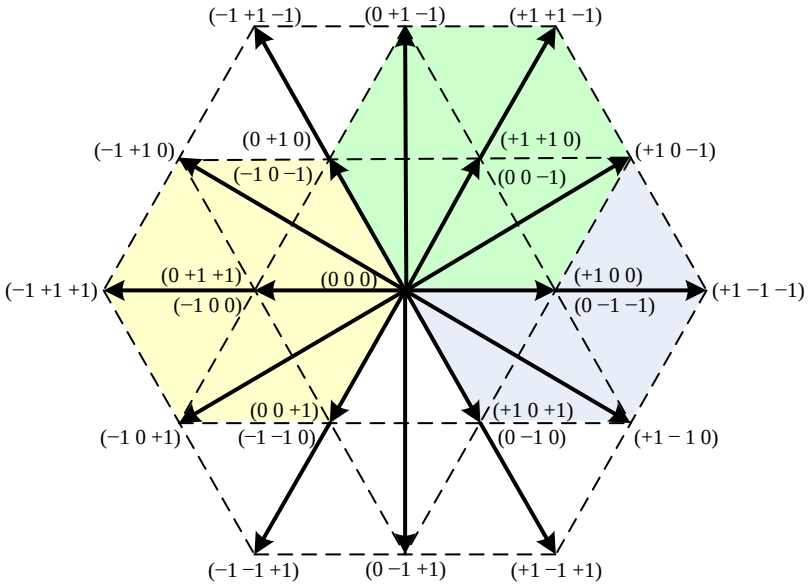


**Fig. 2 6 Voltage space vector of Vienna rectifier**

By selecting proper voltage space vectors and creating optimal switching sequences, space vector modulation can be achieved to modulate the Vienna rectifier. Detailed modulation analysis is discussed in the following section.

## 2.3 Modulation of Vienna Rectifier

A modulator is essential in the rectifier system to generate proper PWM signals (optimal switching sequence) to drive power electronics switches based on the specific modulation index $m_i$ given by the system controller. With proper modulation, the input currents and output voltage can follow corresponding demands which are represented by the modulation index $m_i$. Two typical modulation methods of the Vienna rectifier is introduced as follows: The first is space vector PWM (SVPWM) modulation, and the other is carrier based PWM modulation.

### 2.3.1 Space Vector PWM (SVPWM) Based Modulation

Since the Vienna rectifier has plenty of voltage space vectors, as shown in Fig. 2.6, space vector PWM (SVPWM) can be used to modulate the rectifier. However, considering the inherent limitations of the input current direction on the voltage space vectors, only 7 vectors in a certain section of the space vector diagram are achievable at a time, e.g. the dark area shown in Fig. 2.6. This feature distinguishes the Vienna rectifier SVPWM modulation from the general SVPWM modulation. A typical control flowchart of the Vienna rectifier SVPWM is shown in Fig. 2.7.

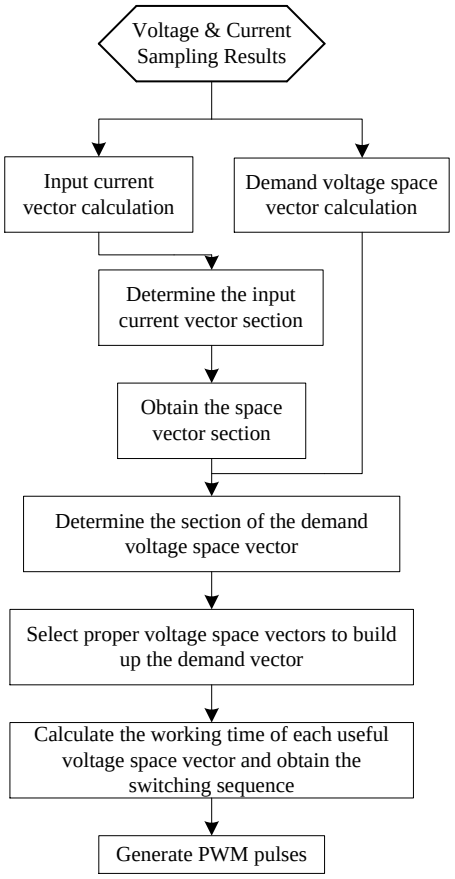


**Fig. 2.7 Control flowchart of the Vienna Rectifier SVPWM**

It can be concluded from Fig. 2.7 that the first step of SVPWM in the Vienna rectifier is determining the input current space vector and its position. Based on the current section, the section where the voltage demand space vector belongs to need to be calculated. Since there are only 7 available voltage space vectors at a time due to the inherent limitations of the Vienna rectifier, the demand voltage space vector locating can only be done within one current section (Table 2.1). Several times of calculation and judgments are necessary to obtain correct section of the demand voltage space vector and determine effective voltage space vectors in the three-level space vector diagram. Another SVPWM method introduced in reference [58] transfers the three-level space vector diagram into two-level space vector diagram by coordinate transformation, thus the demand voltage space vector can be built in the two-level space vector diagram. Then the modulation results are transferred back to three-level space vector diagram with inverse coordinate transformation. In this method, fewer calculation and judgments are needed to determine the section of the demand voltage space vector and corresponding effective voltage space vectors at the cost of coordinate transformation.

### 2.3.2 PWM Carrier Based Modulation

Though a SVPWM modulation can be applied to implement the optimal switching sequence, it requires high efforts of computation. Therefore, its relatively long computation time makes SVPWM not suitable for systems operating under very high switching frequencies. A pulse width modulation using a well-designed carrier signal intrinsically achieves the optimal switching sequence is invented in [59]. This allows the reduction of the processing demand.

In practical operation, the modulator generates proper PWM signals to drive power electronic devices in three phases based on modulation index $m_i^*$. The magnitude of the modulation index $m_i^*$ is determined by the rectifier system controller, while the polarity of

the modulation index $m_i^*$ corresponds to the direction of the phase input current, as expressed by (2.14).

$$m_i^* = m_i sign(i_i) \tag{2.14}$$

where $m_i$ is the magnitude of the modulation index, which is always a value between 0 and 1 and is the output of the rectifier system controller.

The duty cycle can be expressed as a function of the modulation index as (2.15)

$$\delta_i = \begin{cases} 1 - m_i^* & m_i^* > 0 \\ 1 + m_i^* & m_i^* < 0 \end{cases} \tag{2.15}$$

where the duty ratio is value between 0 and 1.

The proposed three-phase modulator using two unipolar, 180°-phase shifted triangular carrier signals is shown in Fig. 2.8(a). Dependent on the input current direction either the switch signal $SW_i^+$ or $SW_i^-$ has to be operated. According to Fig. 2.8(a) the modulation signal generated by the current controller is directly used for pulse-width modulation of $SW_i^+$ and the inverted modulation signal is used for $SW_i^-$. And the final switch signal $SW_i$ is the logic AND of $SW_i^+$ and $SW_i^-$.

The modulator output of each phase is high if the triangular carrier signal exceeds the modulation index signal $m_i^*$ or $-m_i^*$ (Fig. 2.8(b)). As the carrier signals for the PWM corresponding to different current directions are 180° out of phase, inverse pulse-patterns are generated inherently. In Fig. 2.8 (b), a specific modulation example in the current section ($i_a > 0$, $i_b < 0$, $i_c < 0$) is shown. The optimal switching sequence (011)-(010)-(000)-(100)-(000)-(010)-(011) is in consistency with the result obtained from the SVPWM modulation method.

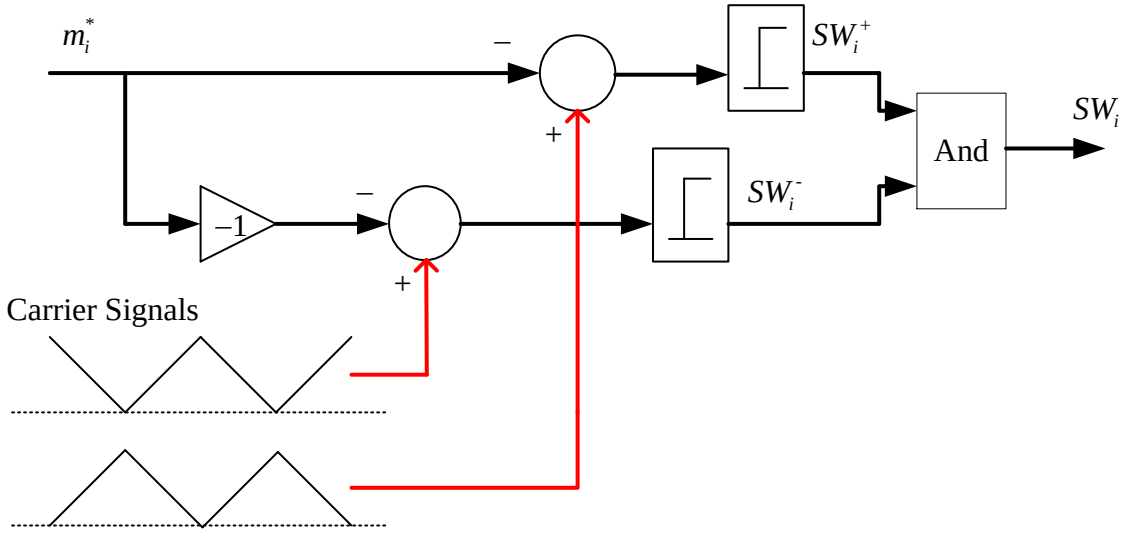
$m_i^*$
−
+
$SW_i^+$
And
$SW_i$
−1
−
+
$SW_i^-$
Carrier Signals

(a)

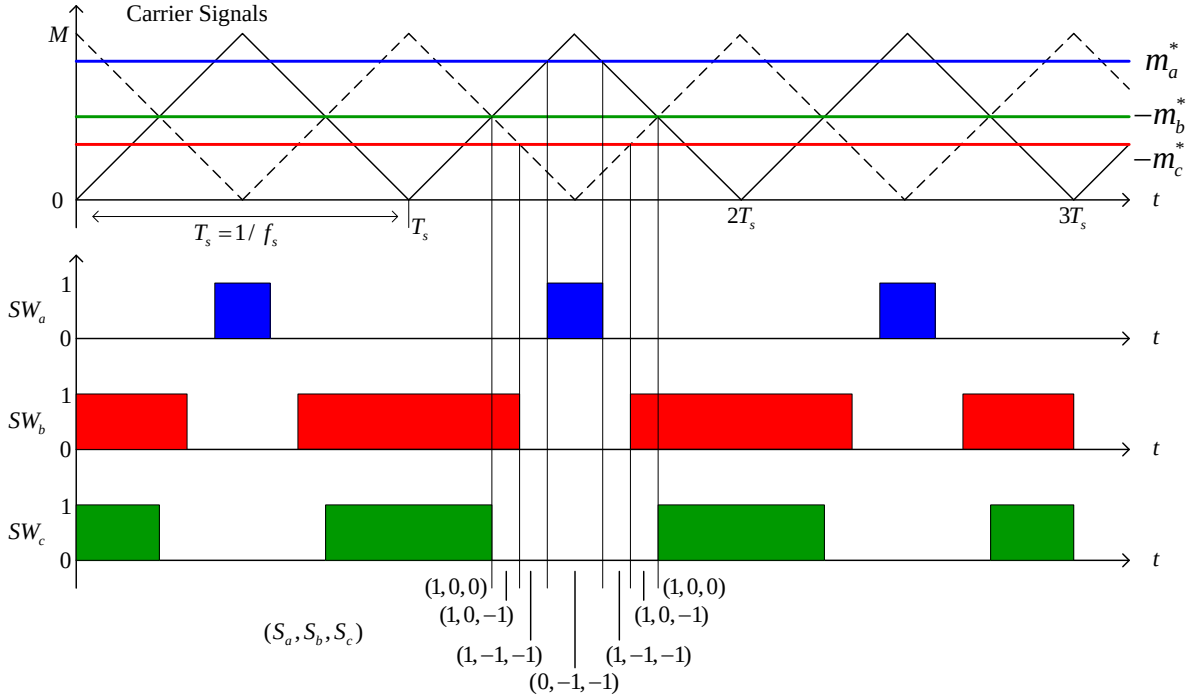
Carrier Signals
M
0
$m_a^*$
$-m_b^*$
$-m_c^*$
t
$T_s = 1/f_s$
$T_s$
$2T_s$
$3T_s$
$SW_a$
$SW_b$
$SW_c$
1
0
(1,0,0)
(1,0,−1)
(1,−1,−1)
(0,−1,−1)
$(S_a, S_b, S_c)$

(b)

**Fig. 2.8 (a)Architecture of the modulator of the Vienna rectifier system; (b) Pulse-width modulation using two 180°-phase-shifted triangular carrier signals at $\phi_N = 10°$ in ($i_a > 0, i_b < 0$ , $i_c < 0$ ) section**

In conclusion, both the SVPWM modulation method and the proper carrier based modulation method have the same capability to generate the optimal switching sequence. However, the SVPWM is more complex and processing time consuming because several calculation and judgments are essential. On the other hand, the proper carrier based modulation is simple and fast. Therefore, in this thesis, the proper carrier based modulation method is selected.

# *Chapter 3*

# *Control of the Vienna Rectifier*

To design a controller for the active three-phase rectifier, an appropriate model of the rectifier system is required. In this chapter, a model for control of the three-phase three-level rectifier system using state space averaging is introduced, and the model transformation among different reference frames is described. Based on this model, a basic controller structure including the inner-loop current controller, the outer-loop DC voltage controller, and the voltage balance controller is demonstrated [61]. Detailed design of each specific controller is indicated respectively as well. Other than the basic controller's structure based on the instantaneous current control, a Direct Power Control (DPC) structure is also introduced at the end of this chapter.

## 3.1 Mathematical Model of Vienna Rectifier System

In general, the mathematical model of the Vienna rectifier system can be established using the state-space averaging technique in continuous current mode. The averaging process is applied on two time intervals: the switching period for average current evaluation, and the mains period for average voltage computation. Neglecting the possible input EMI filter, the Vienna rectifier system exhibits five energy storage elements (three boost inductors and two output capacitors), thus a fifth order model is expected.

### 3.1.1 Model in Three-Phase Stationary (ABC) Reference Frame

Based on the Vienna rectifier topology shown in Fig. 2.5 and analysis of its operation principles given in Chapter 2, the mathematical model of the Vienna rectifier under the steady-state and balanced load operating conditions in the basic three-phase stationary (ABC) reference frame can be derived (3.1).

$$\begin{bmatrix} L\frac{di_a}{dt} \\ L\frac{di_b}{dt} \\ L\frac{di_c}{dt} \\ C_1\frac{du_{DC1}}{dt} \\ C_2\frac{du_{DC2}}{dt} \end{bmatrix} = \begin{bmatrix} -R & 0 & 0 & -\frac{2}{3}S_{a1}+\frac{1}{3}S_{b1}+\frac{1}{3}S_{c1} & \frac{2}{3}S_{a2}-\frac{1}{3}S_{b2}-\frac{1}{3}S_{c2} \\ 0 & -R & 0 & \frac{1}{3}S_{a1}-\frac{2}{3}S_{b1}+\frac{1}{3}S_{c1} & -\frac{1}{3}S_{a2}+\frac{2}{3}S_{b2}-\frac{1}{3}S_{c2} \\ 0 & 0 & -R & \frac{1}{3}S_{a1}+\frac{1}{3}S_{b1}-\frac{2}{3}S_{c1} & -\frac{1}{3}S_{a2}-\frac{1}{3}S_{b2}+\frac{2}{3}S_{c2} \\ S_{a1} & S_{b1} & S_{c1} & -\frac{1}{R_L} & -\frac{1}{R_L} \\ -S_{a2} & -S_{b2} & -S_{c2} & -\frac{1}{R_L} & -\frac{1}{R_L} \end{bmatrix} \begin{bmatrix} i_a \\ i_b \\ i_c \\ u_{DC1} \\ u_{DC2} \end{bmatrix} + \begin{bmatrix} u_{aN} \\ u_{bN} \\ u_{cN} \\ 0 \\ 0 \end{bmatrix} \tag{3.1}$$

where the $S_{i1}$ and $S_{i2}$ were defined as the ideal switches connecting to positive output potential point '*p*' and negative output potential point '*n*' respectively in Section 2.1.2. The relationship between $S_{i1}$ and $S_{i2}$ and the switching function $S_i$ was given in Section 2.2.3.

### 3.1.2 Model in Two-Phase Stationary (αβ) Reference Frame

Frame transformation from the three-phase stationary ABC reference frame to the two-phase stationary αβ reference frame can be achieved by Clark transforming matrix $T_{ABC-\alpha\beta}$.

$$T_{ABC-\alpha\beta} = \sqrt{\frac{2}{3}}\begin{bmatrix} 1 & -\frac{1}{2} & -\frac{1}{2} \\ 0 & -\frac{\sqrt{3}}{2} & -\frac{\sqrt{3}}{2} \end{bmatrix} \tag{3.2}$$

Define

$$\begin{bmatrix} u_\alpha \\ u_\beta \end{bmatrix} = T_{ABC-\alpha\beta} \begin{bmatrix} u_{aN} \\ u_{bN} \\ u_{cN} \end{bmatrix}$$

$$\begin{bmatrix} i_\alpha \\ i_\beta \end{bmatrix} = T_{ABC-\alpha\beta} \begin{bmatrix} i_a \\ i_b \\ i_c \end{bmatrix}$$

$$\begin{bmatrix} S_{\alpha 1} \\ S_{\beta 1} \end{bmatrix} = T_{ABC-\alpha\beta} \begin{bmatrix} S_{a1} \\ S_{b1} \\ S_{c1} \end{bmatrix} \tag{3.3}$$

$$\begin{bmatrix} S_{\alpha 2} \\ S_{\beta 2} \end{bmatrix} = T_{ABC-\alpha\beta} \begin{bmatrix} S_{a2} \\ S_{b2} \\ S_{c2} \end{bmatrix}$$

and the mathematical model of the Vienna rectifier under the steady-state and balanced load operating conditions in the two-phase stationary (αβ) reference frame can be obtained (3.4).

$$\begin{bmatrix} L\frac{di_\alpha}{dt} \\ L\frac{di_\beta}{dt} \\ C_1\frac{du_{DC1}}{dt} \\ C_1\frac{du_{DC1}}{dt} \end{bmatrix} = \begin{bmatrix} -R & 0 & -S_{\alpha 1} & S_{\alpha 2} \\ 0 & -R & -S_{\beta 1} & S_{\beta 2} \\ S_{\alpha 1} & S_{\beta 1} & -\frac{1}{R_L} & -\frac{1}{R_L} \\ -S_{\alpha 2} & -S_{\beta 2} & -\frac{1}{R_L} & -\frac{1}{R_L} \end{bmatrix} \begin{bmatrix} i_\alpha \\ i_\beta \\ u_{DC1} \\ u_{DC2} \end{bmatrix} + \begin{bmatrix} u_\alpha \\ u_\beta \\ 0 \\ 0 \end{bmatrix} \tag{3.4}$$

### 3.1.3 Model in Two-Phase Rotating (dq) Reference Frame

Furthermore, based on the model in the two-phase stationary (αβ) reference frame, the model in the two-phase rotating (dq) reference frame can be formed with Park transformation matrixes. In the rotating reference frame, all AC terms, such as rectifier input

currents and voltages, are transformed to DC terms, which largely simplifies the analysis process of the AC system. The Park transformation matrixes are given in (3.5) and the terms in the dq frame are defined in (3.7). The model of the Vienna rectifier under the steady-state and balanced load operating conditions in the two-phase rotating (dq) reference frame is shown in (3.7), where θ is the position of the rotating reference frame $\theta = \omega t$, and $\omega$ is the angular speed of the reference frame, which equals to the angular frequency of the power grid $\omega = 2\pi f_{grid}$.

$$T_{\alpha\beta-dq} = \begin{bmatrix} \cos\theta & \sin\theta \\ -\sin\theta & \cos\theta \end{bmatrix} \tag{3.5}$$

$$\begin{bmatrix} u_d \\ u_q \end{bmatrix} = T_{\alpha\beta-dq} \begin{bmatrix} u_\alpha \\ u_\beta \end{bmatrix}$$

$$\begin{bmatrix} i_d \\ i_q \end{bmatrix} = T_{\alpha\beta-dq} \begin{bmatrix} i_\alpha \\ i_\beta \end{bmatrix}$$

$$\begin{bmatrix} S_{d1} \\ S_{q1} \end{bmatrix} = T_{\alpha\beta-dq} \begin{bmatrix} S_{\alpha1} \\ S_{\beta1} \end{bmatrix} \tag{3.6}$$

$$\begin{bmatrix} S_{d2} \\ S_{q2} \end{bmatrix} = T_{\alpha\beta-dq} \begin{bmatrix} S_{\alpha2} \\ S_{\beta2} \end{bmatrix}$$

$$\begin{bmatrix} L\frac{di_d}{dt} \\ L\frac{di_q}{dt} \\ C_1\frac{du_{DC1}}{dt} \\ C_1\frac{du_{DC1}}{dt} \end{bmatrix} = \begin{bmatrix} -R & \omega L & -S_{d1} & S_{d2} \\ -\omega L & -R & -S_{q1} & S_{q2} \\ S_{d1} & S_{q1} & -\frac{1}{R_L} & -\frac{1}{R_L} \\ -S_{d2} & -S_{q2} & -\frac{1}{R_L} & -\frac{1}{R_L} \end{bmatrix} \begin{bmatrix} i_d \\ i_q \\ u_{DC1} \\ u_{DC2} \end{bmatrix} + \begin{bmatrix} u_d \\ u_q \\ 0 \\ 0 \end{bmatrix} \tag{3.7}$$

## 3.2 Controller Structure

As the general model of the Vienna rectifier for control is obtained, the controller of the Vienna rectifier can be designed based on the model. In [61], a controller structure was proposed after the analysis of the basic operation of the rectifier system. The model of the AC-side of the rectifier system and the model of the DC-side of the rectifier system can be seen as decoupled to a certain degree. The decoupling of the output voltage controller from the input current controller is justifiable by the different dynamic behaviors of both sides. The dynamic behavior of the input current control loop is related to the switching frequency $f_s$ (relatively high frequency, usually kilo-Hertz to mega-Hertz) while that of the output voltage control loop is associated with the mains frequency $f_N$ (much lower than $f_s$, usually 50 Hz or 60 Hz). Typically, the large output capacitors are the decoupling elements of the two control loops. As a result, a cascade control structure can be used in the Vienna rectifier system.

A basic cascade control structure is shown in Fig. 3.1 where a phase-oriented modulation strategy is assumed in combination with superimposed output voltage and voltage balance controllers. A three-phase current controller $K_I(s)$ is required to ensure sinusoidal input currents which are in phase with the mains phase voltages or leading/lagging the mains voltages by a limited amount. An output voltage controller $K_V(s)$ has to be employed to regulate the output voltage constantly. Since the output capacitor is split into two parts, a voltage balance controller $K_S(s)$ is essential to balance the corresponding output voltages $u_{DC1}$ and $u_{DC2}$. Otherwise, the system is not stable and cannot achieve designed performance. The design of the corresponding controllers is summarized in the following sections.

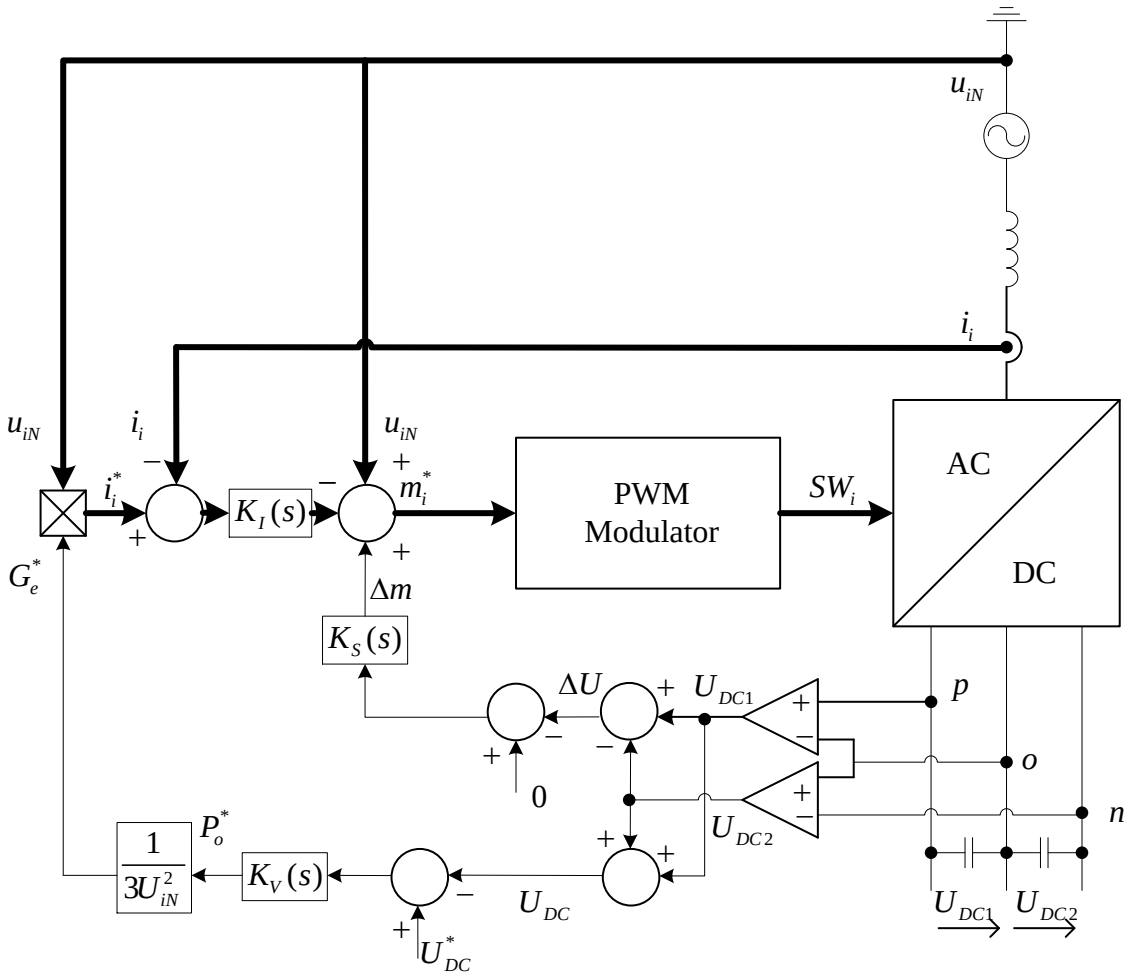


**Fig. 3.1 Basic controller structure of the Vienna Rectifier system. (Signal paths being equal to all three phases are shown in double lines)**

# 3.3 Current Controller

In the following a very simple linear model for current controller design is derived which describes the main behavior of the rectifier system. As already mentioned average mode control is used, which means that all signals are averaged over one switching period. The input of the current controller $K_I(s)$ is the difference between two currents. One is the reference phase current, which has sinusoidal waveform and is in phase with the phase

voltage. Another is the measured phase current. The deviation between the measured phase current and the reference phase current generates corresponding PWM pulse driving signal, which can be expressed by modulation index or duty cycle. Therefore, the output of the current controller is the PWM pulse signal that makes the practical phase current following the reference phase current.

Under the assumptions that the output voltages on output capacitors are balanced and the common mode voltage $u_{oN}$ between DC side neutral point and mains neutral point can be neglected, the operation of the phases is decoupled. Therefore, (3.8) can be written using the duty cycle $\delta_i(t)$.

$$u_{iN}(t) - L_i \frac{di_i(t)}{dt} = \frac{u_{DC}(t)}{2}(1-\delta_i(t)) \tag{3.8}$$

This equation is nonlinear since the output voltage is multiplied by the duty cycle and time-varying as the sinusoidal mains voltage $u_{iN}(t)$ is included. The output voltage $u_{DC}(t)$ is controlled to a constant value by the output voltage controller and as the dynamic of the voltage control loop is much slower than the dynamic of the current control loop, a constant output voltage $u_{DC}(t)=U_{DC}$ can be assumed. This assumption eliminates the nonlinearity in (3.8). To eliminate the time variance of (3.8), a proper feed-forward signal $\delta_{ff,i}(t)$ is applied, as shown in (3.9). Note that an ideal input voltage feed-forward signal is assumed which generates the duty cycle according the sinusoidal mains voltages $u_{iN}(t)$ and that the current controller only has to deal with the deviations from the reference current.

$$\begin{aligned} \delta_{res,i}(t) &= \delta_{ff,i}(t) + \delta_i(t) \\ \delta_{ff,i}(t) &= 1 - \frac{u_{iN}(t)}{U_{DC}/2} \end{aligned} \tag{3.9}$$

Since the nonlinearity and time variance is eliminated, after the Laplace transform, a very simple linear model of the rectifier system is obtained (3.10). In this model, some details,

such as the impedance of the mains, the characteristics of the EMI-filter or the delay times of the switches are not considered for the sake of simplicity.

$$G(s) = \frac{i_i(s)}{\delta_i(s)} = \frac{U_{DC}}{2L_i s} \tag{3.10}$$

A state block diagram of the simplified current controller is shown in Fig. 3.2. In the state block diagram, $G(s)$ is the derived simple model of the Vienna rectifier, $K_I(s)$ is the current controller, and $M_I(s)$ is the transfer function of the current measurement considering the bandwidth limitation of the current sensor.

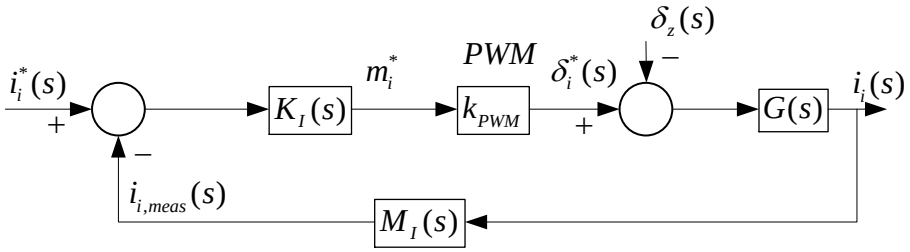


**Fig. 3.2 State block diagram of the current controller**

A simple proportional controller (P controller) can be used to implement the function of $K_I(s)$.

$$K_I(s) = K_{P,i} \tag{3.11}$$

Besides, a P + lag controller is also a good choice to $K_I(s)$.

$$K_I(s) = K_{P,i}\frac{1+sT_D}{1+sT_1} \tag{3.11}$$

In this work, the P controller is selected for the sake of simplicity.

# 3.4 DC Output Voltage Controller

The DC output voltage controller $K_V(s)$ of the Vienna rectifier is used to regulate the DC output voltage of the rectifier system to a specified value. The input of the DC output voltage controller $K_V(s)$ is the difference between the reference output voltage and the measured output voltage. The final output of the voltage controller $K_V(s)$ is the reference currents, which are used as demand in the current controller $K_I(s)$. As a result, the DC output voltage controller $K_V(s)$ is the outer-loop while the current controller $K_I(s)$ is the inner-loop, which matches the controller structure shown in Fig. 3.1.

Previously, only the AC side of the rectifier system has been modeled to design the current controller to control the AC currents. In order to control the DC output voltage $u_{DC}$ of the rectifier, an appropriate model of the DC side of the rectifier system has been derived as shown in Fig. 3.3, and the results are summarized as follows.

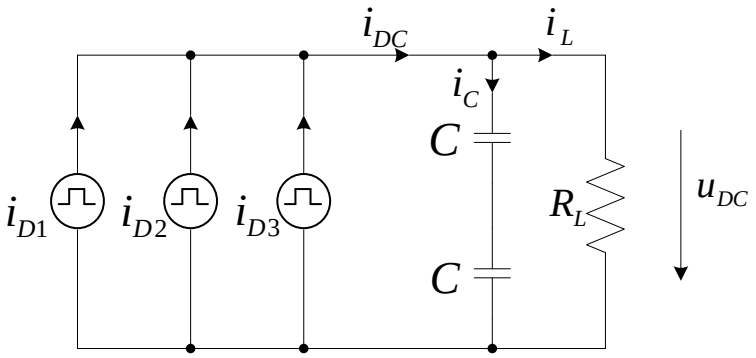


**Fig. 3.3 Model of the DC side of the Vienne Rectifier with a resistive load**

The rectifier system has to obey the rule of power conversation, so that the output power $p_o$ equals to the input power $p_{in}$ minus the rectifier system power losses $p_{loss}$ (3.12).

$$p_o = p_{in} - p_{loss} \tag{3.12}$$

The output power and the input power of the rectifier system can be expressed respectively by (3.13) and (3.14).

$$p_o = i_{DC,avg} u_{DC,avg} \approx i_{DC} u_{DC} \tag{3.13}$$

where $i_{DC}$ is the DC side current and $u_{DC}$ is the output voltage.

$$p_{in} = 3U_{iN} I_i \cos(\varphi_i) \tag{3.14}$$

where $U_{iN}$ is the RMS value of the phase voltage and $I_i$ is the RMS value of the phase current on the AC side.

The efficiency of the rectifier $\eta$ can be defined by (3.15).

$$\eta = \frac{p_o}{p_{in}} = \frac{i_{DC} u_{DC}}{3U_{iN} I_i \cos(\varphi_i)} \tag{3.15}$$

Under the assumption that the rectifier system has unity power factor $\cos(\varphi_i) = 1$ and negligence of the energy stored in the boost inductors, the power conversation rule of the system can be expressed as (3.16).

$$i_{DC,avg} u_{DC} = 3\eta U_{iN} I_i \tag{3.16}$$

This nonlinear equation can be linearized around the operating point $U_{DC_0}$ , $U_{iN_0}$ , $I_{DC_0}$ and $I_{i_0}$ using

$$\begin{aligned} u_{DC} &= U_{DC_0} + \tilde{u}_{DC} \\ u_{iN} &= U_{iN_0} + \tilde{u}_{iN} \\ i_{DC,avg} &= I_{DC_0} + \tilde{i}_{DC} \\ i_i &= I_{i_0} + \tilde{i}_i \end{aligned} \tag{3.17}$$

The variation of the DC current $\tilde{i}_{DC}$ is influenced by the variations of the AC currents $\tilde{i}_i$, the AC voltages $\tilde{u}_{iN}$, and the DC voltage $\tilde{u}_{DC}$ (3.18).

$$\tilde{i}_{DC} = \frac{3\eta U_{iN_0}}{U_{DC_0}} \tilde{i}_i + \frac{3\eta I_{i_0}}{U_{DC_0}} \tilde{u}_{iN} - \frac{I_{DC_0}}{U_{DC_0}} \tilde{u}_{DC} \tag{3.18}$$

Hence, the small signal model between the AC input currents and the DC output current is found (3.19). This relationship proves that the DC output currents are proportional to the AC input currents.

$$k_{p1} = \frac{\tilde{i}_{DC}}{\tilde{i}_i} = \frac{3\eta U_{iN_0}}{U_{DC_0}} \tag{3.19}$$

The output of the DC voltage controller $K_V(s)$ is equivalent to the demanded output power $P_o^*$. Using the RMS values of the mains voltages, a conductance $G_e^* = \frac{P_o^*}{3U_{iN}^2}$ can be calculated. And the instantaneous reference currents can be generated based on the conductance and the instantaneous phase voltages (3.20).

$$i_i^* = G_e^* u_{iN} = \frac{P_o^*}{3U_{iN}^2} u_{iN} \tag{3.20}$$

The small signal model can be built by linearizing equation (3.20) around an operating point $P_{o_0}^*$, $u_{iN_0}$, and $I_{i_0}^*$ using

$$\begin{aligned} p_o^* &= P_{o_0}^* + \tilde{p}_o^* \\ u_{iN} &= U_{iN_0} + \tilde{u}_{iN} \\ i_i^* &= I_{i_0}^* + \tilde{i}_i^* \end{aligned} \tag{3.21}$$

which results in

$$\tilde{i}_i^* = \frac{1}{3U_{iN_0}} \tilde{p}_o^* + \left( \frac{P_{o_0}^*}{3U_{iN_0}^2} - \frac{2I_{i_0}^*}{U_{iN_0}} \right) \tilde{u}_{iN} \tag{3.18}$$

Thus, the relationship between the demanded output power and the reference input currents is obtained.

$$k_{p2} = \frac{\tilde{i}_i^*}{\tilde{p}_o^*} = \frac{1}{3U_{iN_0}} \tag{3.23}$$

In the case of a constant resistive load, the load side of the rectifier system can be modeled by

$$H_{load}(s) = \frac{R_L}{1 + sR_L C} \tag{3.24}$$

Based small signal models (3.19), (3.23) and (3.24), the state block diagram of the DC output voltage controller can be drawn, as shown in Fig. 3.4. In the state block diagram, $K_V(s)$ represents the DC output voltage controller, $T_I(s)$ represents the closed loop transfer function of the current controller, and $M_V(s)$ represents the transfer function of the voltage measurement circuit considering the bandwidth limitations of the voltage sensors.

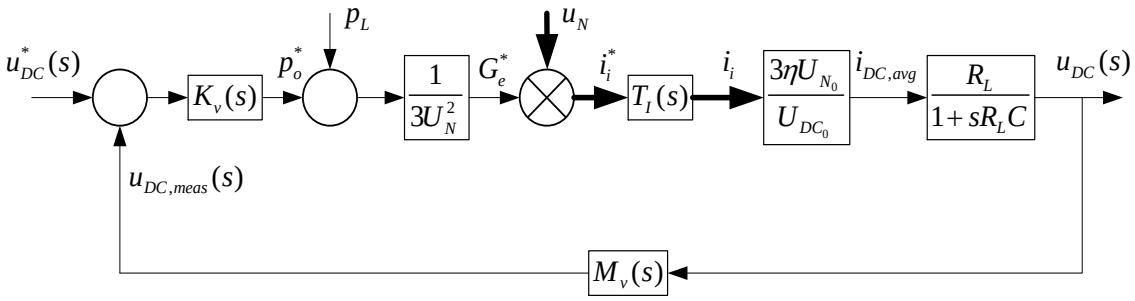


**Fig. 3.4 State block diagram of the DC output voltage controller**

In order to prevent steady state DC output voltage control errors, a PI-type controller is usually applied.

$$K_V(s) = K_{P,v} + \frac{K_{I,v}}{s} \tag{3.25}$$

In conclusion, the DC output voltage control is achieved in the following process. Firstly, the DC output voltage demand determines the required output power (under the condition of constant resistive load). Secondly, the required output power generates the reference AC input currents. Thirdly, the current controller guarantees that the AC input currents follow corresponding reference currents well. Then, the DC output current is proportional to the AC input currents. Finally, the DC output voltage is influenced by the DC output current because of the constant resistive load.

# 3.5 Voltage Balance Controller

As discussed in [62] an unbalanced output voltage $\Delta U$

$$\Delta U = \frac{1}{2}(u_{DC1} - u_{DC2}) \tag{3.26}$$

which could result from unequal leakage currents of the output capacitors or from an asymmetrical load of the two rectifier outputs, results in an asymmetrical distribution of the switching actions which finally yields to increased input current distortions.

The average neutral point current $i_{o,avg}$ can be formed by averaging the neutral point current $i_o$ over a switching period

$$i_{o,avg} = \delta_a i_a + \delta_b i_b + \delta_c i_c \tag{3.27}$$

This neutral point current causes unbalanced output voltages according to

$$i_o = 2C\frac{d\Delta U}{dt} \tag{3.28}$$

where two output capacitors have the same value of C.

Due to the modulation of the rectifier, a third harmonic neutral point current is generated. As a result, the third harmonic neutral point current leads to a third harmonic output voltage unbalance. It can be minimized by injecting a proper third harmonic signal, but is still present.

According to [63], if average mode current control in conjunction with a pulse-width modulation is applied, the output voltage unbalance $\Delta U$ always exists stably. It is verified by Fig. 3.5 where the corresponding modulation indexes $m_i$ are plotted for $\phi_N = 10°$ in the ($i_a > 0$, $i_b < 0$, $i_c < 0$) current section when the output voltage unbalance $\Delta U$ is considered. The voltage unbalance can be presented by (3.29)

$$U_{DC1} = \frac{U_{DC}}{2} + \Delta U$$
$$U_{DC2} = \frac{U_{DC}}{2} - \Delta U \tag{3.29}$$

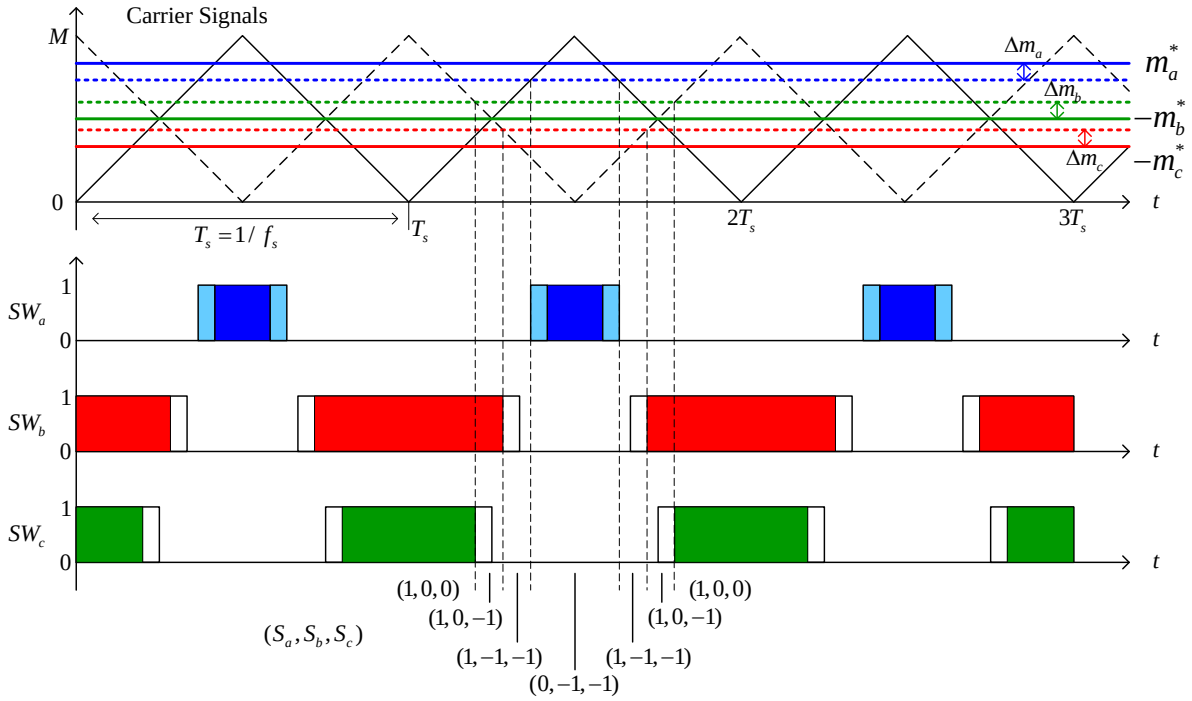


**Fig. 3.5 Pulse-width modulation and switching sequence illustrating the self stability of an unbalanced output voltage**

According to (3.8) and (2.15), the values of the output voltages $U_{DC1}$ and $U_{DC2}$ directly influence the values of corresponding duty cycle $\delta_i$ and modulation index $m_i$. To be more specific, the effects of the output voltage unbalance in the condition of $\phi_N = 10°$, as shown in Fig. 3.5, are analyzed in details as follows. The increased output voltage $U_{DC1}$ causes the decrease input current in phase a. Accordingly, the current controller increases the duty cycle of phase a, which is conducted by decreasing the modulation index of phase a by $\Delta m_a$. On

the other hand, phase b and phase c generate a relatively low output voltage $U_{DC2}$. Hence, duty cycles of phase b and phase c are reduced by increasing the corresponding modulation index by $\Delta m_b$ and $\Delta m_c$ respectively. The resulting modulation indexes, as altered by the current controllers, are plotted in Fig. 3.5 by dashed lines and the changes in optimal switching sequence and operating time are shown as well. The optimized switching sequence is unchanged, but compared to a balanced output voltage condition, the duration of switching state $(S_a, S_b, S_c) = (0, -1, -1)$ is enlarged, the duration of switching state $(S_a, S_b, S_c) = (1, 0, 0)$ is reduced, and the duration of other switching states is kept unchanged. The two switching states $(S_a, S_b, S_c) = (0, -1, -1)$ and $(S_a, S_b, S_c) = (1, 0, 0)$ are redundant concerning the differential mode input currents, but they lead to neutral point currents with opposite directions as shown in Fig. 3.6 (a) and (b). As shown in Fig. 3.6 (a), switching state $(S_a, S_b, S_c) = (1, 0, 0)$ results in a negative neutral point current which charges $C_1$ and discharges $C_2$. For switching state $(S_a, S_b, S_c) = (0, -1, -1)$, as shown in Fig. 3.6 (b), it yields a positive neutral point current which discharges $C_1$ and charges $C_2$. The asymmetric distribution of the two redundant switching states caused by the current controllers counteract the voltage unbalance $\Delta U$ by discharging $C_1$ and charging $C_2$. Therefore, it automatically stabilizes the output voltage unbalance. However, though the output voltage unbalance is stable, it cannot be reduced to zero without active control.

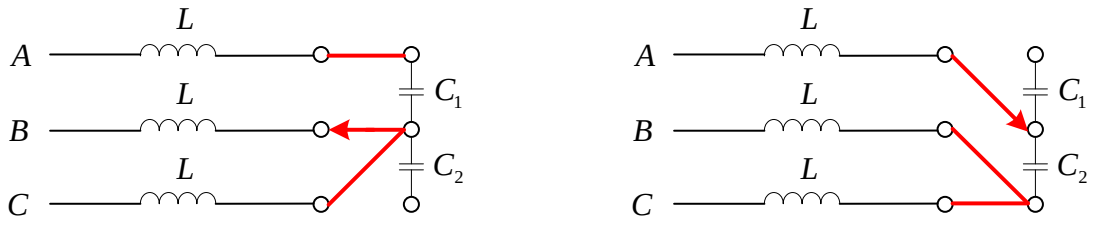

**Fig. 3.6 (a) Vienna rectifier connection and neutral point current direction for the switching state $(S_a, S_b, S_c) = (0, -1, -1)$ for $\phi_N = 10°$; (b) Vienna rectifier connection and neutral point current direction for the switching state $(S_a, S_b, S_c) = (1, 0, 0)$ for $\phi_N = 10°$**

Therefore, an output voltage balance controller is required to actively balance the two output voltages. The redundant switching states with different directions of the neutral point current $i_o$ are used for active balancing. Active balancing can be achieved by adding a variable DC component $\Delta m$ to all three modulation index $m_a$, $m_b$ and $m_c$.

$$\begin{aligned} m_a &= m_{a,old} + \Delta m \\ m_b &= m_{b,old} + \Delta m \\ m_c &= m_{c,old} + \Delta m \end{aligned} \tag{3.30}$$

The resulting modulation signals, switching states and switching sequence are illustrated in Fig. 3.7. Since the DC component $\Delta m$ inversely changes the relative on time of the redundant switching states, it can be used for active output voltage balancing. In this specific case, if the output voltage unbalance is $U_{DC1} > U_{DC2}$, $C_1$ needs discharging and $C_2$ needs charging. Setting $\Delta m$ with a proper negative value would decrease the unbalanced voltage $\Delta U$. In contrary, if the output voltage unbalance is $U_{DC1} < U_{DC2}$, $C_1$ would be charged and $C_2$ would be discharged when a positive $\Delta m$ is selected.

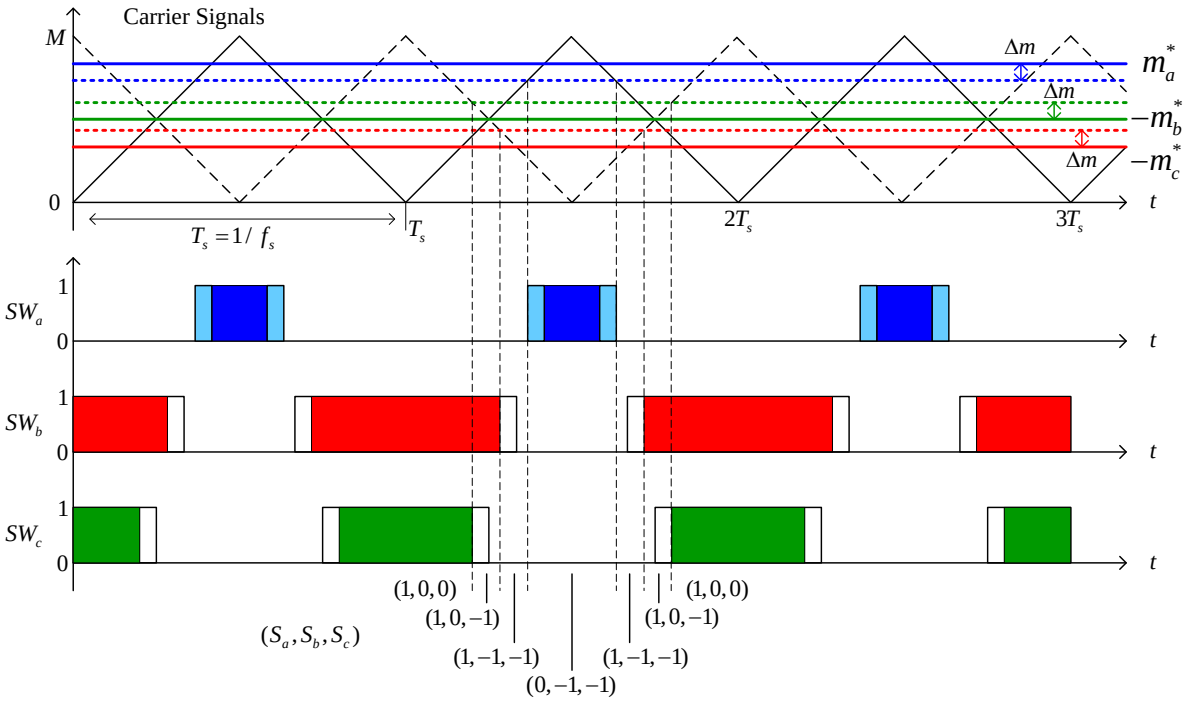


**Fig. 3.7 Influence of a DC component $\Delta m$ added to all three modulation indexes on the switching sequence of the rectifier system for $\phi_N = 10°$**

As a result, the input of the voltage balance controller $K_S(s)$ is the unbalanced output voltage, while the output of $K_S(s)$ is a variable DC component $\Delta m$ which can reduce the unbalanced output voltage by affecting all three phase modulation indexes. The implementation of the voltage balance controller $K_S(s)$ can be a PI controller.

$$K_S(s) = K_{P,s} + \frac{K_{I,s}}{s} \tag{3.31}$$

# 3.6 Direct Power Controller (DPC)

From the perspective of the power of a rectifier system, when the AC mains voltage is constant, if the instantaneous power (active power and reactive power) of the rectifier system can be controlled with in a specific range, then the instantaneous current (active current and reactive current) of the rectifier system can be consequently controlled. This control strategy is named as Direct Power Control (DPC). In general, a DPC control system consists of a DC voltage control outer-loop and a instantaneous power control inner-loop. By selecting corresponding switching states in the switch table to generate required rectifier input voltages based on AC voltages and instantaneous power of the rectifier system, high quality rectifying can be achieved. Comparing with traditional current controllers, DPC has advantages such as high power factor, low THD, high efficiency, easy algorithm, simple system structure, and good dynamics corresponding to load changes. As a result, DPC has promising potential to be applied in the three-phase/level/switch Vienna rectifier system.

Since the DPC directly controls the instantaneous active power and the instantaneous reactive power of the rectifier system, the key point of this control strategy is the accurate observation of the instantaneous active/reactive power. Instantaneous power theory is the theoretical base of the DPC. In 1980's, the instantaneous power theory was proposed by H. Akagi [64], and in 1990's, a PWM converter closed-loop control evolved the instantaneous power was proposed and further developed by T. Ohnishi, T. Noguchi, etc. [65].

The instantaneous active power is defined as the scalar product of the instantaneous voltage vector $\vec{u}$ and the instantaneous current vector $\vec{i}$. The instantaneous reactive power is defined as the vector product of the instantaneous voltage vector $\vec{u}$ and the instantaneous current vector $\vec{i}$. In the three-phase stationary ABC reference frame, the definition of the instantaneous active power and reactive power are given as (3.32).

$$\begin{aligned} p &= \vec{u}\cdot\vec{i} = u_a i_a + u_b i_b + u_c i_c = |\vec{u}||\vec{i}|\cos\varphi = |\vec{u}||\vec{i}_p| \\ \vec{q} &= \vec{u}\times\vec{i} = u_a^* i_a + u_b^* i_b + u_c^* i_c = |\vec{u}||\vec{i}|\sin\varphi\vec{k} = |\vec{u}||\vec{i}_q|\vec{k} \end{aligned} \tag{3.32}$$

where $p$ is the instantaneous active power of the AC mains, $q$ is the instantaneous reactive power of the AC mains, $u_i$ is the AC mains voltages, $i_i$ is the AC mains currents, $u_a^*$, $u_a^*$, and $u_a^*$ are $\begin{pmatrix} u_a^* \\ u_b^* \\ u_c^* \end{pmatrix} = \frac{1}{\sqrt{3}}\begin{pmatrix} u_c - u_b \\ u_a - u_c \\ u_b - u_a \end{pmatrix} = \frac{1}{\sqrt{3}}\begin{pmatrix} u_{cb} \\ u_{ac} \\ u_{ba} \end{pmatrix}$, $\vec{k}$ is a unit vector perpendicular to the surface of $\vec{u}$ and $\vec{i}$.

Equations in (3.32) can also be written in the matrix form, as shown in (3.33).

$$\begin{pmatrix} p \\ q \end{pmatrix} = \begin{pmatrix} u_a & u_b & u_c \\ u_a^* & u_b^* & u_c^* \end{pmatrix}\begin{pmatrix} i_a \\ i_b \\ i_c \end{pmatrix} \tag{3.33}$$

In the two-phase stationary αβ reference frame, the instantaneous active power $p$ and the instantaneous reactive power $q$ can be calculated by (3.34).

$$\begin{pmatrix} p \\ q \end{pmatrix} = \begin{pmatrix} u_\alpha & u_\beta \\ u_\beta & -u_\alpha \end{pmatrix}\begin{pmatrix} i_\alpha \\ i_\beta \end{pmatrix} \tag{3.34}$$

In the two-phase rotating dq reference frame, the instantaneous active power $p$ and the instantaneous reactive power $q$ can be calculated by (3.35).

$$\begin{pmatrix} p \\ q \end{pmatrix} = \begin{pmatrix} u_d & u_q \\ u_q & -u_d \end{pmatrix}\begin{pmatrix} i_d \\ i_q \end{pmatrix} \tag{3.35}$$

Align the d-axis with the AC mains voltage vector $\vec{u}$, then $u_q$=0. Thus, substitute $u_q$=0 into (3.35), (3.36) can be gained.

$$\begin{pmatrix} p \\ q \end{pmatrix} = \begin{pmatrix} u_d & 0 \\ 0 & -u_d \end{pmatrix} \begin{pmatrix} i_d \\ i_q \end{pmatrix} \tag{3.36}$$

Based on the model of the Vienna rectifier in the two-phase rotating dq reference frame, given by (3.37), which is another form of (3.7),

$$\begin{aligned} L\frac{di_d}{dt} &= e_d - u_d - Ri_d + \omega L i_q \\ L\frac{di_q}{dt} &= e_q - u_q - Ri_q - \omega L i_d \end{aligned} \tag{3.37}$$

where $e_d$ and $e_q$ are mains voltages, $u_d$ and $u_q$ are rectifier input voltages, $i_d$ and $i_q$ are mains currents.

Multiply $e_d$ to (3.37) to get (3.38)

$$\begin{aligned} L\frac{di_d e_d}{dt} &= e_d(e_d - u_d - Ri_d + \omega L i_q) \\ L\frac{di_q e_d}{dt} &= e_d(e_q - u_q - Ri_q - \omega L i_d) \end{aligned} \tag{3.38}$$

Define $L_{new} = L / e_d$ and $R_{new} = R / e_d$, and substitute (3.36) into (3.38), hence (3.39) can be obtained.

$$\begin{aligned} L_{new}\frac{dp}{dt} &= e_d - u_d - R_{new} p - \omega L_{new} q \\ L_{new}\frac{dq}{dt} &= e_q + R_{new} q + \omega L_{new} p \end{aligned} \tag{3.39}$$

Equation (3.39) presents the essence of the DPC controller. The state block diagram of DPC controller is shown in Fig. 3.8. It can be seen clearly that there are two control loops in the DCP system. The first loop is the outer DC voltage control loop, where the sampled DC output voltage $U_{DC}$ is compared with the demanded DC reference voltage $U_{DC}^*$, and the voltage error is used to generate the d-axis current command $i_d^*$ through a PI controller. The

instantaneous active power command $p^*$ is the product of the d-axis current command $i_d^*$ and the DC output voltage $U_{DC}$. The reactive power command $q^*$ is zero in the condition of unit power factor.

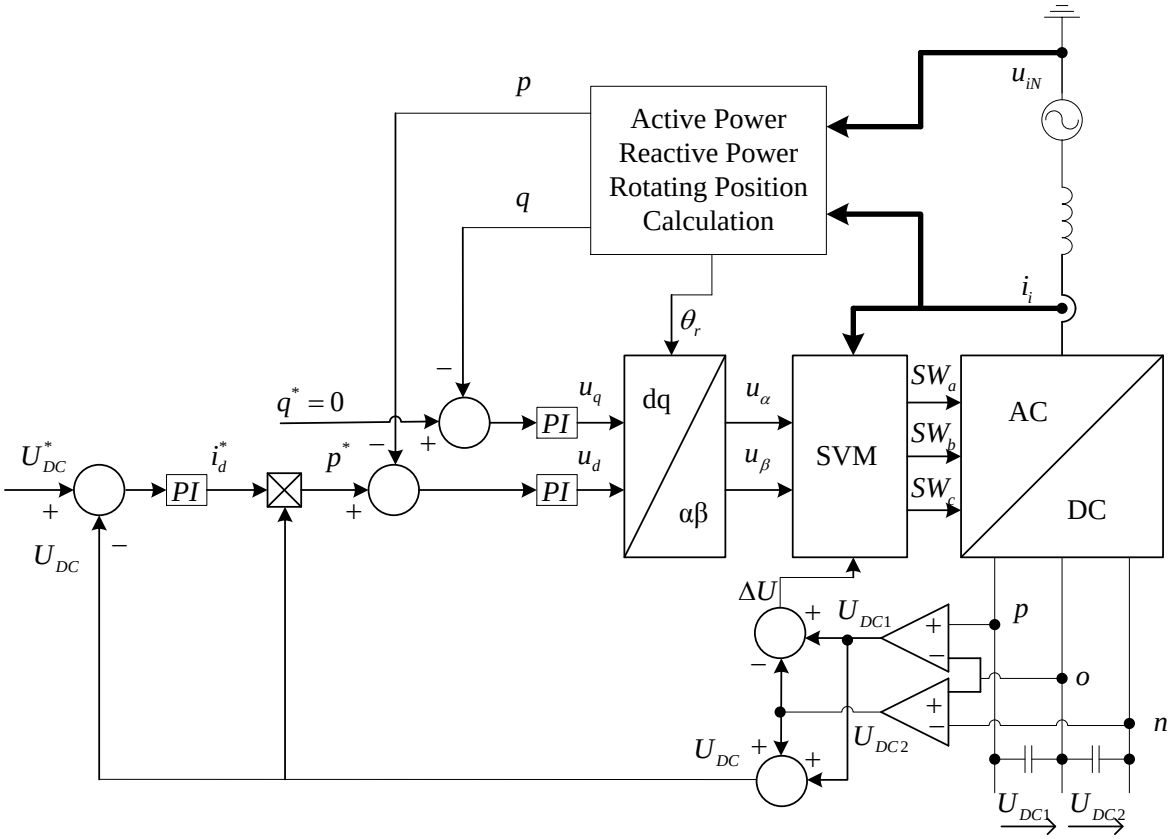


**Fig. 3.8 DPC controller structure of the Vienna rectifier system. (Signal paths being equal to all three phases are shown in double lines)**

The second loop is the inner instantaneous power control loop, where the instantaneous active power *p* and reactive power *q*, which are calculated based on sampled AC mains voltages and currents, are compared with active power command $p^*$ and reactive power command $q^*$ respectively. The power errors are used to generate desired rectifier input voltages ( $u_d$ , $u_q$ ) via PI controllers. Once the rectifier input voltages are selected,

corresponding switching states can be chosen by the switch table in the Space Vector Modulator (SVM). Therefore, the rectifier is controlled to perform with specific DC output voltage and power (AC currents) requirements.

Design of the outer DC voltage loop in the DPC system is similar to the output voltage controller design discussed in section 3.4, so that it would not be repeated again. Design of the inner power loop in the DPC system will be illustrated in the following.

As can be seen in (3.39), the d-axis and q-axis in the DPC system are cross-coupled, which increases difficulty in designing the controller. In order to simplify the controller design and improve control performance, feed-forward decouple control strategy is employed in the DPC system. When PI controllers are used in the inner power control loop of DPC system, the control function can be expressed as (3.40)

$$\begin{aligned} u_d &= -\left(K_p + \frac{K_i}{s}\right)\left(p^* - p\right) - \omega L_{new} q + e_d \\ u_q &= \left(K_p + \frac{K_i}{s}\right)\left(q^* - q\right) - \omega L_{new} p \end{aligned} \tag{3.40}$$

where $K_p$ is the gain of the proportional controller and $K_i$ is the gain of the integrating controller.

Substitute (3.40) into (3.39) to get (3.41). Therefore, the active power $p$ and the reactive power $q$ are decoupled and can be controlled independently.

$$\begin{aligned} L_{new}\frac{dp}{dt} &= \left(K_p + \frac{K_i}{s}\right)p^* - \left(R_{new} + \left(K_p + \frac{K_i}{s}\right)\right)p \\ L_{new}\frac{dq}{dt} &= \left(K_p + \frac{K_i}{s}\right)q^* + \left(R_{new} - \left(K_p + \frac{K_i}{s}\right)\right)q \end{aligned} \tag{3.41}$$

The state block diagram of the decoupled power control loops is shown in Fig. 3.9.

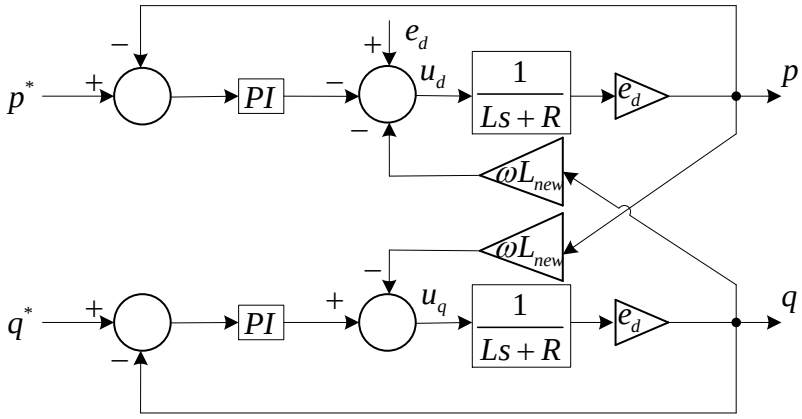


**Fig. 3.9 State block diagram of decoupled power control loops in the DPC system**

The state block diagram of the simplified active power control loop is shown in Fig. 3.10, where $T_i = \frac{K_p}{K_i}$ and $T_s$ is related to sampling period.

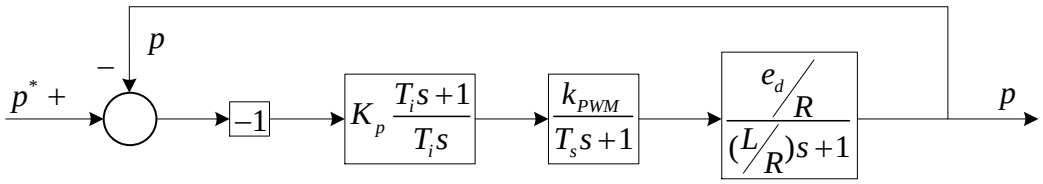


**Fig. 3.10 State block diagram of simplified active power control loop in the DPC system**

By adjusting gains of the PI controllers, the DPC control of the Vienna rectifier can be achieved easily based on the feed-forward decouple.

# *Chapter 4*

# *Simulation of the Vienna Rectifier*

In this chapter, the simulation of the Vienna rectifier system is discussed. In the first part, how to build the simulation model of the Vienna rectifier system is built in MATLAB / Simulink is introduced. The simulation model mainly consists of the power circuit, the modulator and the control circuit. In the second part, the simulation results of the Vienna rectifier system are shown and analyzed.

## 4.1 Simulation Model of the Vienna Rectifier

In this work, simulation of the Vienna rectifier system was done in MATLAB / Simulink. The simulation model of the Vienna rectifier system can be divided into three main subsystems, the power circuit subsystem, the modulator subsystem, and the control circuit subsystem. The general structure of the simulation model of the Vienna rectifier system is shown in Fig. 4.1. It can be concluded from Fig. 4.1 that at a specific operating point, the voltages and currents signals can be sampled in the power circuit and be used as inputs to the control circuit. The control circuit processes the sampled signals and provide appropriate modulation index following the commands as the output. Based on the modulation index, the modulator generates proper pulses to drive the switches in the power circuit so that the power circuit can follow the specific commands given by the controller.

In the following sections, detailed information about building the power circuit simulation subsystem, the modulator simulation subsystem, and the control circuit simulation subsystem will be demonstrated consequently.

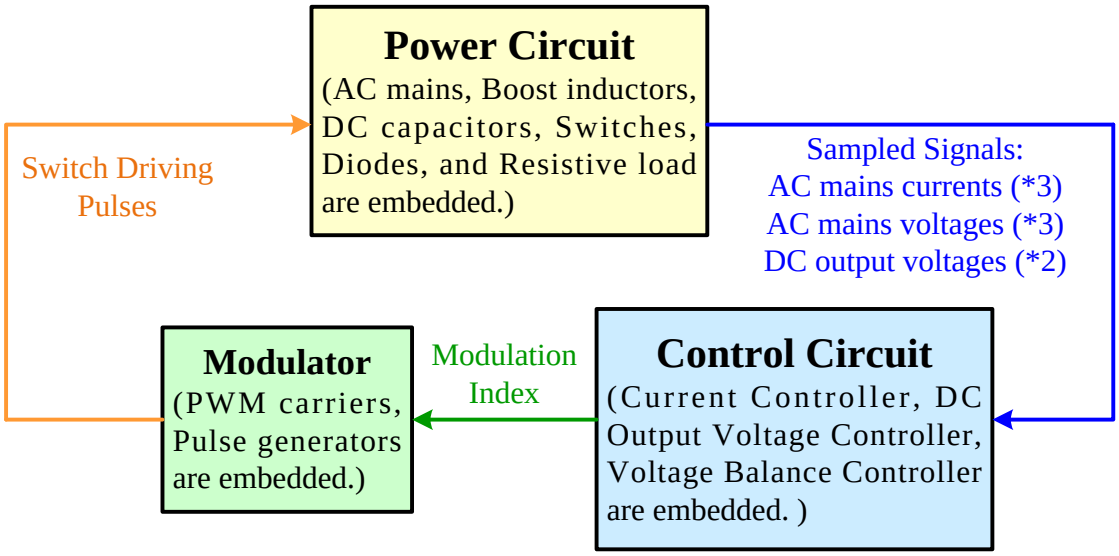


**Fig. 4.1 Structure of the simulation model of the Vienna rectifier system**

## 4.1.1 Power Circuit Simulation Model

### 4.1.1.1 Build Power Circuit Model in MATLAB / Simulink

The power circuit model of the Vienna rectifier system is mainly composed of the AC mains, AC side boost inductors, switches and diode bridges, DC side capacitors, resistive load, current sensors and voltage sensors. The power circuit simulation model has exactly the same topology with the Vienna rectifier topology given in Fig. 2.5. Fig. 4.2 (a) shows the power circuit model of the Vienna rectifier system in MATLAB / Simulink. From left to right, the AC mains, AC side boost inductors, AC line-to-line voltage sensors, AC phase current sensors, rectifying subsystem consists of one switch and six diodes of each phase which connecting AC side and DC side, DC side capacitors, DC voltage sensors and resistive load can be seen in consequence in Fig. 4.2 (a). The rectifying circuit of each phase leg is exactly the same for all

three phases, and it can be expressed by a subsystem with two input terminals and three output terminals, as shown in Fig. 4.2 (b). The first input of the rectifying subsystem is the AC rectifier input voltage of the phase leg, and the second input is the pulse to drive the switch in the phase leg and control rectifying performance. The three output terminals represent the positive point, neutral point, and negative point of the DC voltage.

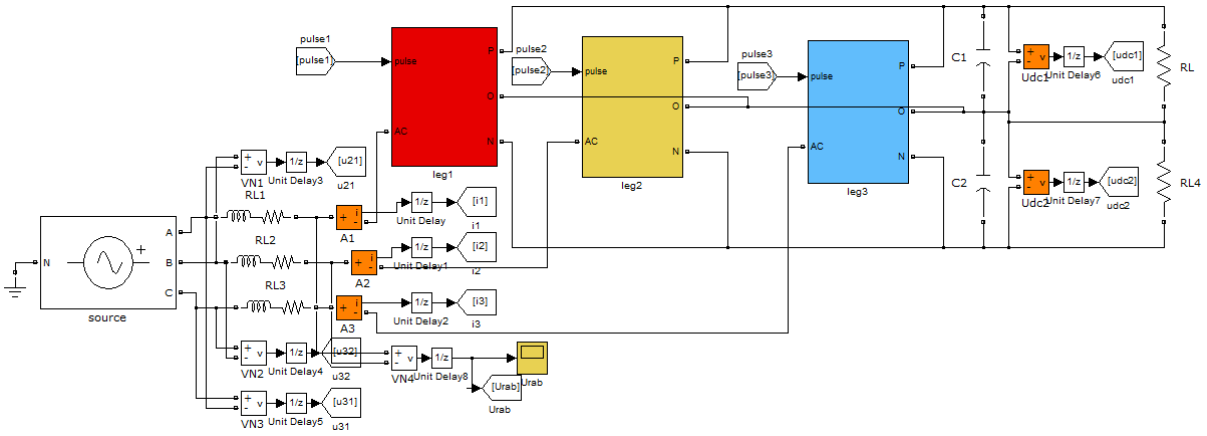


(a)

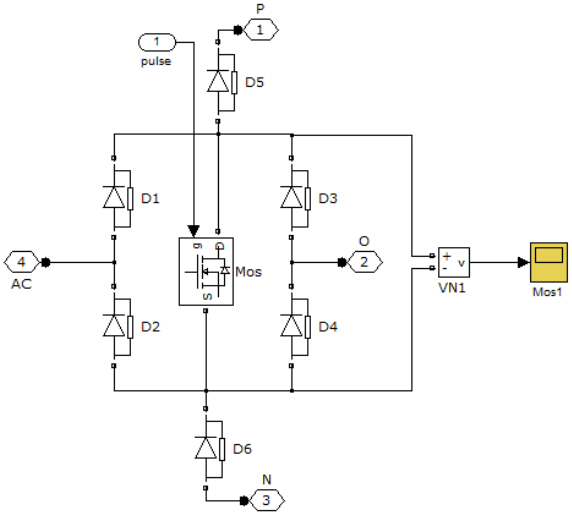


(b)

**Fig. 4.2 (a) Simulation model of the power circuit of the Vienna rectifier system; (b) Detailed simulation model of the rectifying subsystem in the power circuit**

#### 4.1.1.2 Parameter Design of the Power Circuit

The parameters of components in the power circuit are specified in Table 4.1. The simulation and the hardware prototype of the Vienna rectifier system have the same parameters.

| | |
|---|---|
| AC mains voltage (phase peak voltage) | $U_{ph-pk} = 20$ V |
| DC command voltage | $U_{DC} = 50$ V |
| Resistive load | $R_L = 110$ Ω |
| Boost inductor | $L = 2$ mH |
| DC capacitor | $C = 500$ μF |
| AC mains frequency | $f_N = 50$ Hz |
| Switching frequency | $f_s = 100$ kHz |
| Simulation type | Discrete |
| Sample time | $10^{-8}$ s |

**Table 4.1 Parameters of the power circuit of the Vienna rectifier system**

### 4.1.2 Control Circuit Simulation Model

The control circuit model of the Vienna rectifier system mainly includes an inner-loop current controller, an outer-loop DC voltage controller, and an independent voltage balancing controller. As mentioned previously, the control circuit processes the sampled signals provided by the power circuit, like comparing sampled signals with commands, generating control signals based on errors via controllers, etc. In consequence, proper commands and modulation index are generated by the control circuit of the Vienna rectifier. The general structure of the control circuit model of the Vienna rectifier is shown in Fig. 4.3. There are three current controllers (one for each phase), one DC voltage controller, and one voltage balancing controller. The inputs of the DC voltage controller are the sampled DC output voltage and the DC voltage command (reference), and the output of the DC voltage controller is the magnitude reference of the AC currents. The inputs of the voltage balancing controller are the DC voltages on two DC capacitors, and the output of the voltage balancing controller is a variable DC value added to the modulation index to reduce the unbalanced voltage of the rectifier system to zero. The inputs of the current controller are the AC current reference generated by the DC voltage controller, the modulation index adjustment generated by the voltage balancing controller, the sampled AC mains voltage and current of the phase. The output of the current controller is the modulation index, which can be used to provide corresponding pulses to control switches in the modulator.

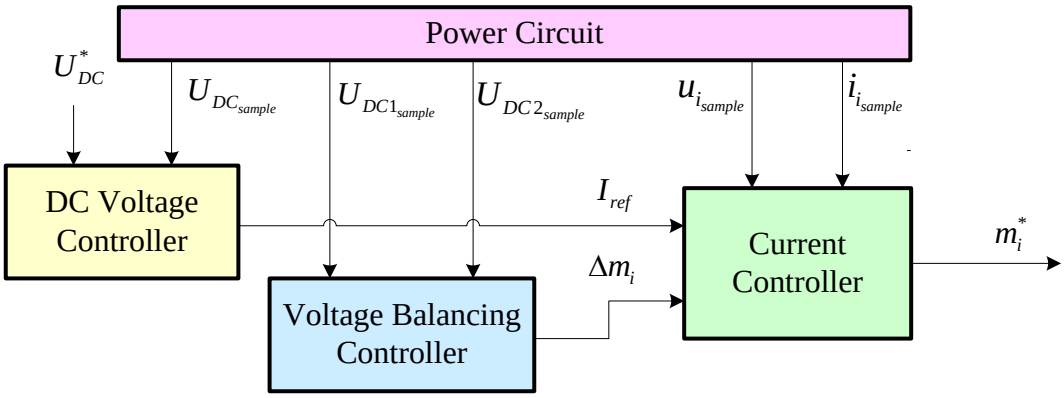


**Fig. 4.3 Structure of the simulation model of the control circuit**

Note that only line-to-line AC mains voltages can be measured in three-phase systems. Therefore, the sensed line-to-line AC mains voltages need line-to-phase transforming into phase AC mains voltages.

In this work, two forms of the current control are simulated. One is the current controller based on the instantaneous current control theory. Another is the current controller based on the direct power control theory.

#### 4.1.2.1 Instantaneous Current Controller

The function of the current controller based on the instantaneous current control theory (introduced in section 3.3) is carried out by programming in MATLAB / Simulink. The state block diagram of the current controller subsystem is given in Fig. 4.4 (a), while the MATLAB function of the current controller is given in Fig. 4.4 (b).

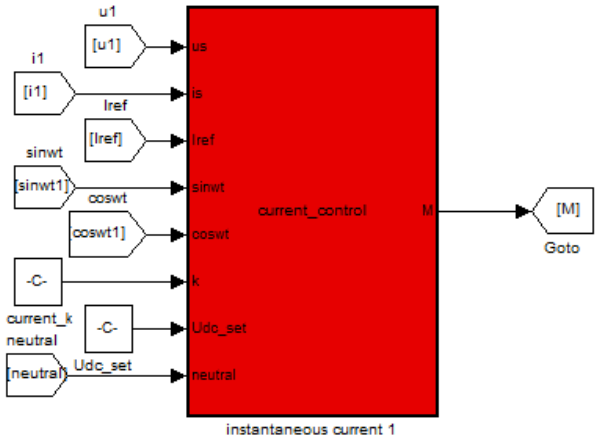


(a)

```
function M =current_control(us, is, Iref, sinwt, coswt, k, Udc_set, neutral)
w=50*2*pi;
L=500e-6;
M=us-w*L*Iref*coswt-k*(Iref*sinwt-is);
M=M/Udc_set-neutral;
if M>1
M=1;
end
if M<-1
M=-1;
end
end
```

(b)

**Fig. 4.4 (a) State block diagram of the instantaneous current controller; (b) Function of the instantaneous current controller**

#### 4.1.2.2 DPC Based Current Controller

The current controller based on the direct power control theory (introduced in section 3.6) is carried out by building state block diagram models and programming in MATLAB / Simulink. The state block diagram of the current controller subsystem is given in Fig. 4.5.

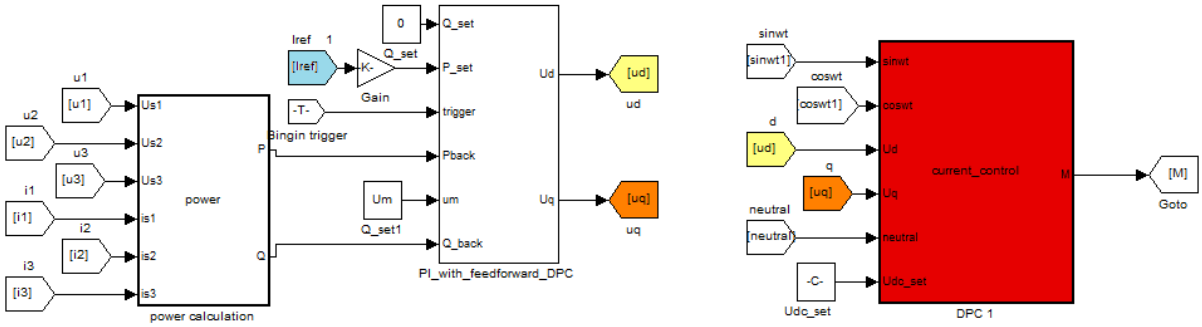


**Fig. 4.5 State block diagram of the DPC based current controller**

As shown in Fig. 4.5, the DPC based current controller consists of three main functional sections, shown from left to right respectively: the power calculation section, the DPC PI control with feed-forward section, and the modulation index generating section. In the power calculation section, instantaneous active power $P$ and reactive power $Q$ of the rectifier are calculated based on sampled AC mains voltages and currents. In the DPC PI control with feed-forward section, DPC with feed-forward decouple is conducted. Based on the comparison between active power command $P_{\_set}$ (determined by the AC current reference gained from the DC voltage controller) and calculated active power $P$ as well as reactive power command $Q_{\_set} = 0$ and calculated reactive power $Q$, the desired d-axis and q-axis rectifier input voltages ($u_d$ and $u_q$) can be obtained via the DPC PI control with feed-forward section ((3.39)-(3.41)). The modulation index generating section generates required modulation index with the inputs of the d-axis rectifier input voltage $u_d$, the q-axis rectifier input voltage $u_q$, the modulation index adjustment provided by the voltage balancing controller. The function of the modulation index generating section is shown in Fig. 4.6, which has similar structure with the instantaneous current controller.

```
function M =current_control(sinwt, coswt, Ud, Uq, neutral, Udc_set)
w=50*2*pi;
M=Ud*sinwt+Uq*coswt;
M=M/Udc_set-neutral;
if M>1
M=1;
end
if M<-1
M=-1;
end
end
```

**Fig. 4.6 Function of the modulation index generating section in the DPC based current controller**

#### 4.1.2.3 DC Voltage Controller

The DC voltage controller is implemented by a PI controller based on theoretical analysis given in section 3.4. Since the resistive load in the rectifier system is fixed, the DC current is proportional to the DC voltage. As proved in section 3.4, the AC currents have proportional relationship with the DC current, which results in the fact that AC currents are proportional to DC voltage. To summarize, the DC voltage controller provides the AC current reference based on DC voltage command.

In Fig. 4.7, the state block diagram of the DC voltage controller is shown. The DC voltage controller is simple that the error between the DC voltage command and the sampled DC voltage determines the AC current reference to control the DC voltage to follow its command. The PI controller is expressed in (3.25).

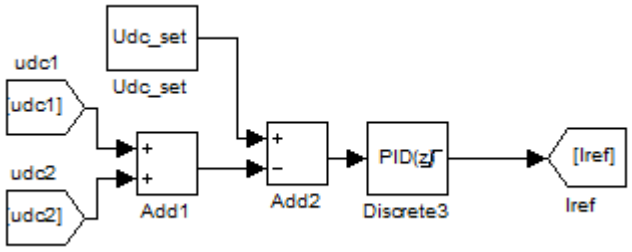


**Fig. 4.7 State block diagram of the DC voltage controller**

#### 4.1.2.4 Voltage Balancing Controller

The voltage balancing controller is carried out based on a PI controller, which can be written as (3.31). As indicated in section 3.5, the voltage balancing controller aims to reduce the unbalanced output voltages on the two capacitors by adding a variable DC component to the modulation index to change the charging/discharging time of the two capacitors. The state block diagram of the voltage balancing controller can be seen in Fig. 4.8.

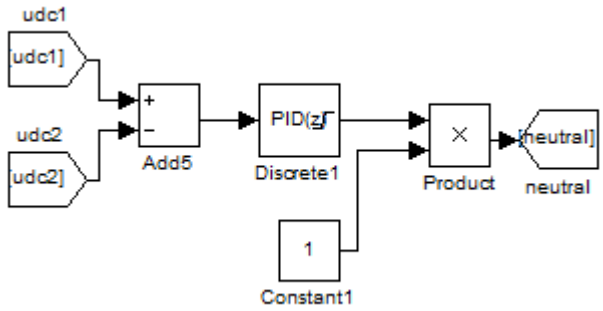


**Fig. 4.8 State block diagram of the voltage balancing controller**

### 4.1.3 Modulator Simulation Model

In this work, the modulator of the Vienna rectifier system is implemented with the carrier based PWM modulation method demonstrated in section 2.3.2. Fig. 2.8 shows the modulation structure and concepts. The state block diagram of the modulator simulation model is shown in Fig. 4.9 (a). The state block diagram of the PWM generator subsystem in the modulator model is shown in Fig. 4.9 (b).

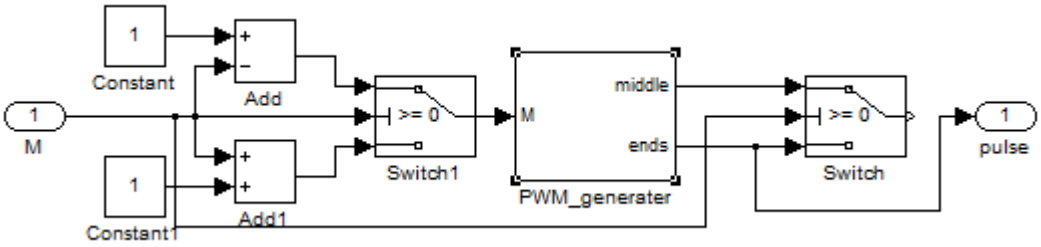


(a)

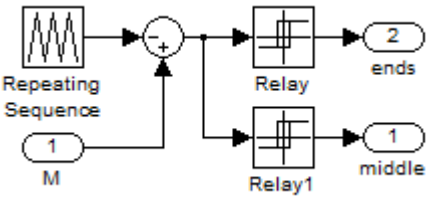


(b)

**Fig. 4.9 (a) State block diagram of the modulator based on the carrier based PWM modulation; (b) State block diagram of the PWM generator in the modulator**

It can be concluded from Fig. 4.9 (a) and (b) that when the modulation index is injected into the modulator, its polarity will be determined and corresponding effective modulation function will be obtained. And then, proper pulse signal, which will be used to drive the switch in each phase, can be generated accordingly. To summarize, the simulation model of the modulator is in consistency with the theoretical analysis of the modulation discussed in section 2.3.2.

### 4.1.4 Summary of the Vienna Rectifier Simulation Model

Based on models of several subsystems, the complete simulation model of the Vienna rectifier system can be established by combining and connecting the subsystems correctly. Fig. 4.10 (a) shows the model of the Vienna rectifier system utilizing the instantaneous current control method, while Fig. 4.10 (b) illustrates the model of the Vienna rectifier systm employing the direct power control method. In conclusion, the simulation models of the Vienna rectifier system built in MATLAB / Simulink correlate to the structure given in Fig. 4.1 very well. Accurate simulation results can be expected from the simulation models.

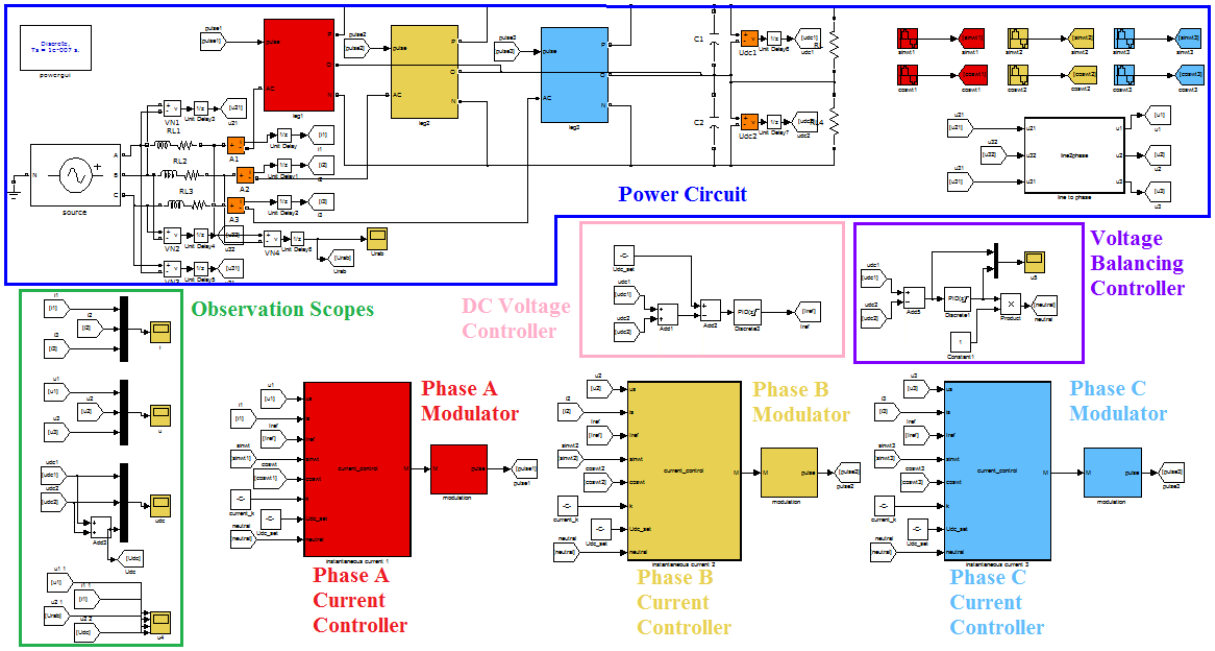

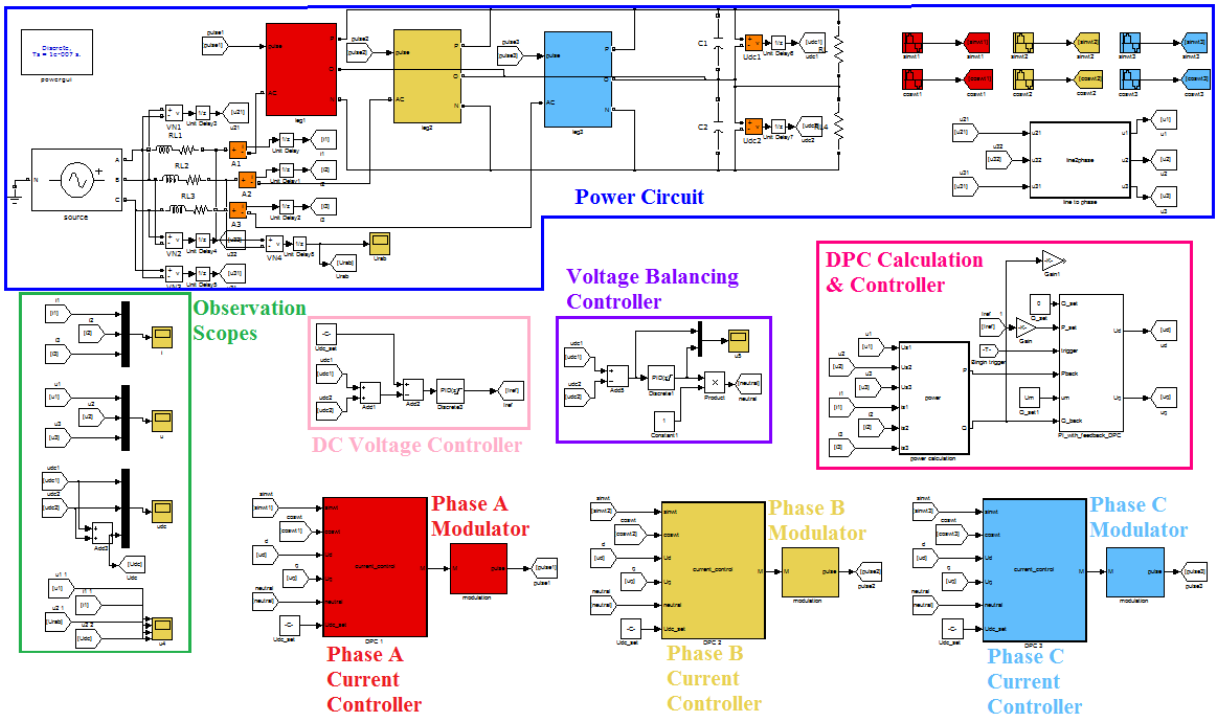


**Fig. 4.10 (a) State block diagram of the Vienna rectifier system simulation model with the instantaneous current control strategy; (b) State block diagram of the Vienna rectifier system simulation model with the direct power control strategy**

# 4.2 Simulation Results of the Vienna Rectifier

Based on the established simulation model, the Vienna rectifier system is simulated in MATLAB / Simulink under different circumstances. Analysis and discussion are also given based on the simulation results.

## 4.2.1 Simulation Results of the Vienna Rectifier Based on Instantaneous Current Control (ICC)

For the Vienna rectifier system utilizing the instantaneous current control (ICC), various simulations are carried out in different operating conditions. To start with, the simulation is

conducted in rated operating condition, which means the parameters of the power circuit of the Vienna rectifier are the same as given in Table 4.1. To be more specific, the switching frequency of the system is 100 kHz, and the resistive load is of 110 Ω. After adjusting gain of the P-type current controller ($K_{P,i}=10$), gains of the PI-type DC voltage controller ($K_{P,v}=3$, $K_{I,v}=0.2$), and gains of the PI-type voltage balancing controller ($K_{P,s}=2$, $K_{I,s}=0.5$), the simulation results of the ICC based Vienna rectifier system are acquired.

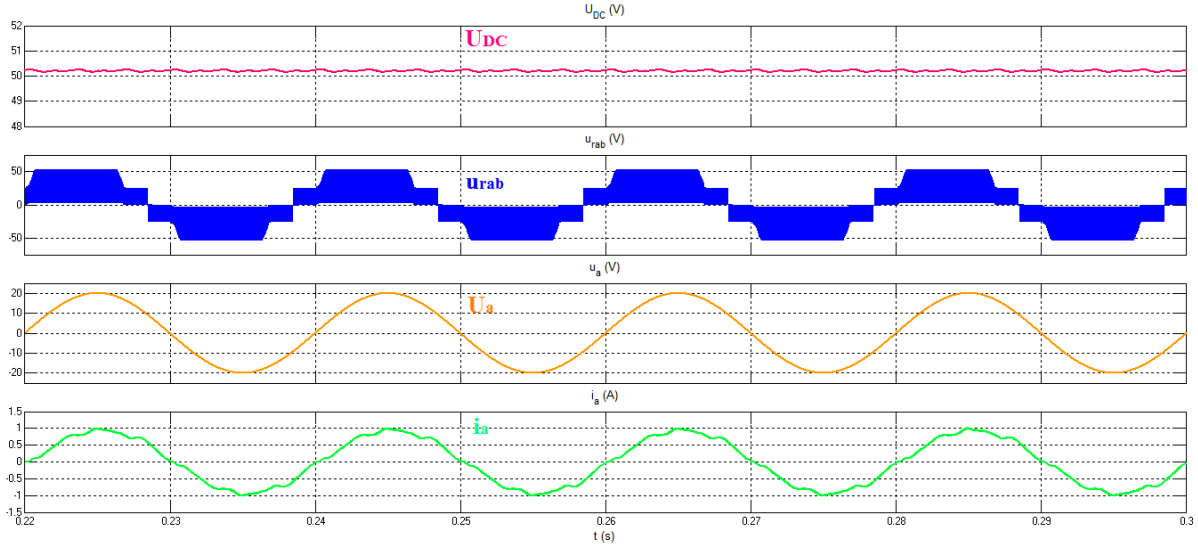


**Fig. 4.11 Simulation results of the ICC based Vienna rectifier system in the rated operating condition with $f_s=100$ kHz, and $R_L=110$ Ω**

Fig. 4.11 shows the four voltage/current waveforms of the ICC based Vienna rectifier in steady state in the rated operating condition. The first waveform is the DC output voltage $U_{DC}$, the second waveform is the line-to-line rectifier input voltage $u_{rab}$, the third waveform is the phase voltage of phase $a$ $u_a$, and the fourth waveform is the phase current of phase $a$ $i_a$. All the simulation results in this work will be presented in the same formula with all four waveforms.

It can be concluded from Fig. 4.11 that the current in phase $a$ $i_a$ is in phase with the voltage of phase $a$ $u_a$, which means the rectifier system has high power factor. Moreover, the current quality is high since it includes little harmonics and the shape of the current is nearly sinusoidal. FFT analysis is done on the current waveform and the THD of the current is 6.92%. More details of the FFT analysis results can be seen in Fig. 4.12. The DC output voltage is regulated to the command value with small low-frequency ripples (at frequency of $6f_N$) due to topology inherent features. In conclusion, the simulation model for the ICC based Vienna rectifier system is built successfully, and the simulation results of the Vienna rectifier are in consistency with previous theoretical analysis.

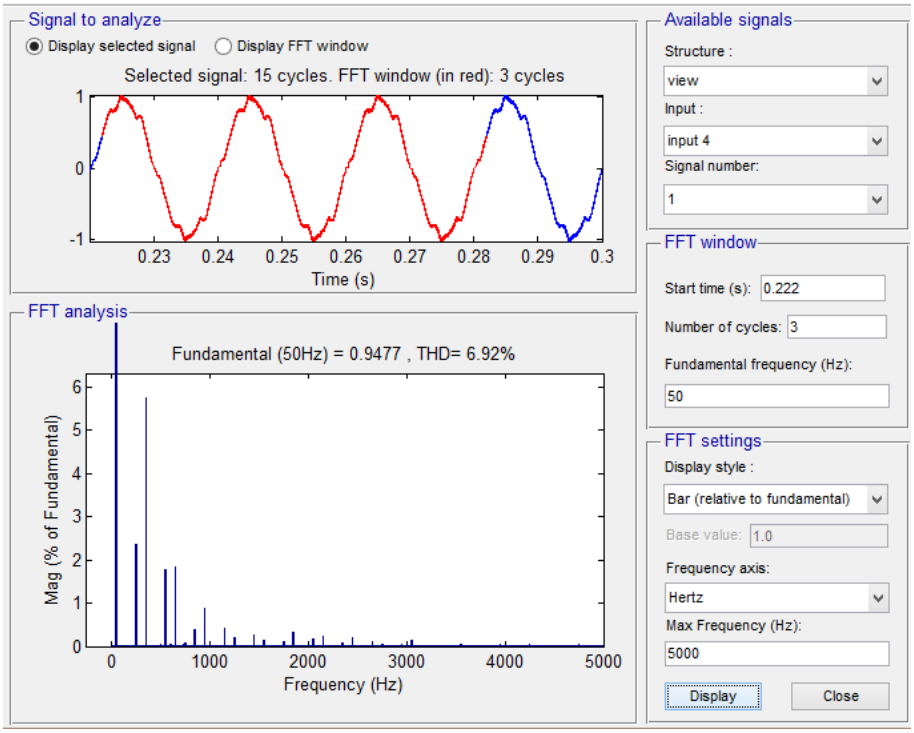


**Fig. 4.12 FFT analysis results of the ICC based Vienna rectifier in the rated operating condition with $f_s = 100$ kHz, and $R_L = 110$ Ω**

Furthermore, in order to study the influence of the switching frequency $f_s$ on the performance of the Vienna rectifier system, more simulations are carried out under various

circumstances with different switching frequencies. Compared with the rated switching frequency $f_{s\_rated} = 100$ kHz, simulations are also done with low frequency at $f_{s\_low} = 10$ kHz and high frequency $f_{s\_high} = 500$ kHz. The simulation results under low/high frequency operating conditions are shown in Fig. 4.13 and Fig. 4.14 respectively. Note that the power circuit parameters and controller parameters in the low frequency condition are set exactly the same as the rated frequency condition. However, in the high frequency condition, the current controller gain $K_{P,i}$ is changed to 20, while the rest parameters are kept unchanged.

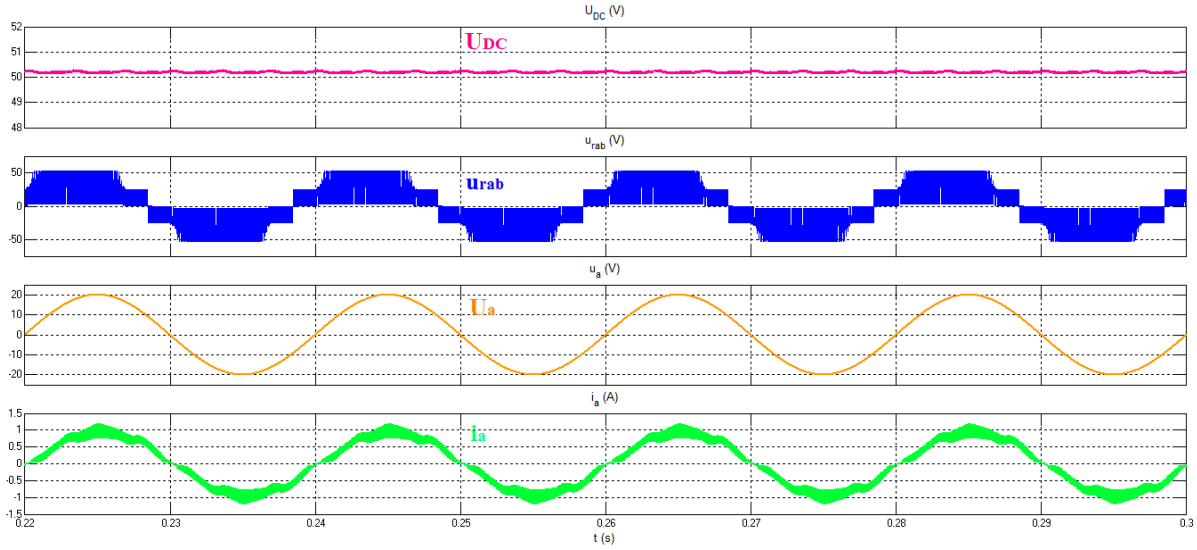


**Fig. 4.13 Simulation results of the ICC based Vienna rectifier system in the low frequency operating condition with $f_{s\_low} = 10$ kHz**

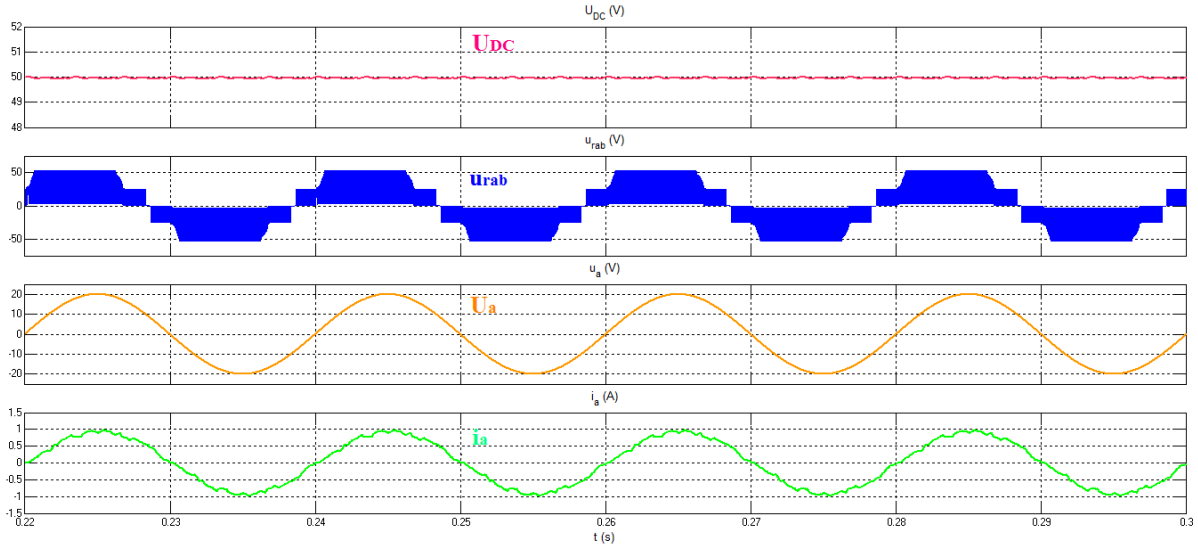


**Fig. 4.14 Simulation results of the ICC based Vienna rectifier system in the high frequency operating condition with $f_{s\_high} = 500$ kHz**

It can be seen clearly by comparing Fig. 4.1, Fig. 4.13 and Fig. 4.14 that increasing the switching frequency improves the performance of the Vienna rectifier system. Firstly, the amplitude of the current ripples at switching frequency is closely related to the switching frequency of the system. When the switching frequency is low, the current ripples are high and the current quality is low. In contrary, when the switching frequency is high, the current ripples are low and the current quality is high. This conclusion is also proved by the FFT analysis results. For the current in low frequency operating condition, the THD is 13.44%. However, for the current in high frequency operating condition, the THD is only 5.74%. Secondly, with higher switching frequency, the amplitude of the DC voltage ripples is reduced. As a result, by increasing the switching frequency, the performance of the Vienna rectifier system is better in terms of the AC current and DC voltage waveforms.

Since high frequency operation is preferred in the Vienna rectifier system, GaN devices are the top choice because they have tremendous advantages over traditional Si devices in high frequency applications.

### 4.2.2 Simulation Results of the Vienna Rectifier Based on Direct Power Control (DPC)

For the Vienna rectifier system using the direct power control (DPC), simulation in the rated operating condition is conducted. For DPC, it shares the same DC voltage controller and voltage balancing controller with ICC. Corresponding controlling gains are set as $K_{P,v}=3$, $K_{I,v}=0.2$, $K_{P,s}=2$, $K_{I,s}=0.5$. However, for DPC, there is no direct current control loop $K_{P,i}$, instead the power control loop dominated by $K_{P,P}$, $K_{I,P}$, $K_{P,Q}$, and $K_{I,Q}$ replaces the current control loop. Here, the parameters of the active/reactive controller are selected as $K_{P,P}=25$, $K_{I,P}=45$, $K_{P,Q}=25$, $K_{I,Q}=45$.

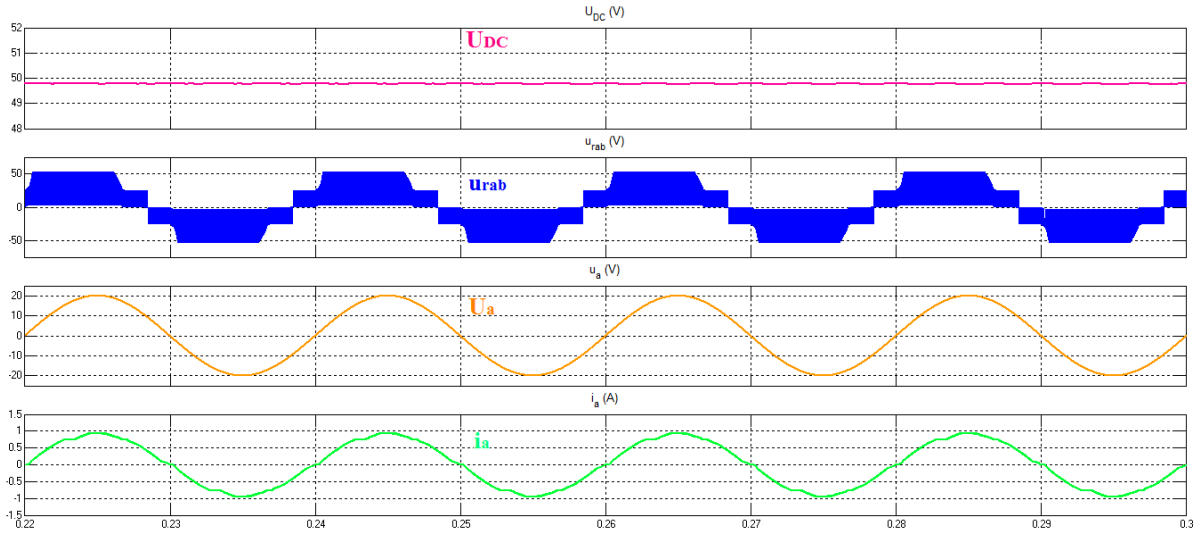


**Fig. 4.15 Simulation results of the DPC based Vienna rectifier system in the rated operating condition with $f_s=100$ kHz, and $R_L=110$ Ω**

Fig. 4.15 shows the simulation results of the DPC based Vienna rectifier system in the rated operating condition. Besides, FFT analysis on the current is shown in Fig. 4.16. The THD in the current is only 4.29%.

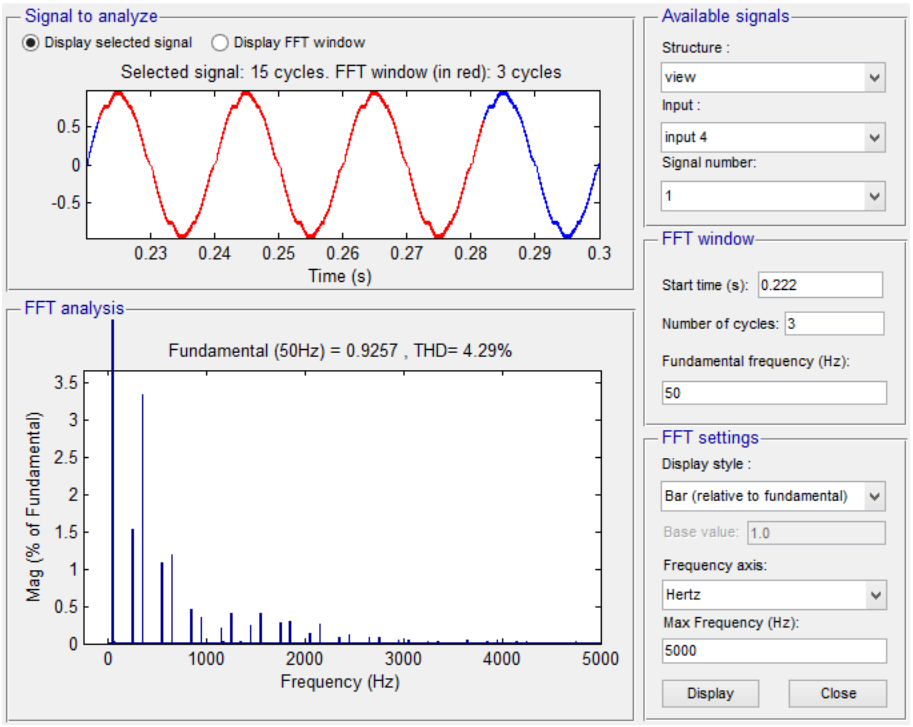


**Fig. 4.16 FFT analysis results of the DPC based Vienna rectifier in the rated operating condition with $f_s = 100$ kHz, and $R_L = 110$ Ω**

Since the results illustrated in Fig. 4.12 and Fig. 4.15 are carried out under the same operating condition, the difference in the steady state performance of the ICC based and DPC based Vienna rectifier system can be indicated. In general, the DPC based Vienna rectifier system has advantages over the ICC based Vienna rectifier system in the steady state. The DC output voltage of the DPC system is regulated better with smaller ripples. The AC current quality of the DPC system is higher with relatively low THD value.

### 4.2.3 Simulation Results of the Vienna Rectifier with Load Change

In addition to steady state performance, dynamic performance of the ICC and DPC based Vienna rectifier systems also needs study.

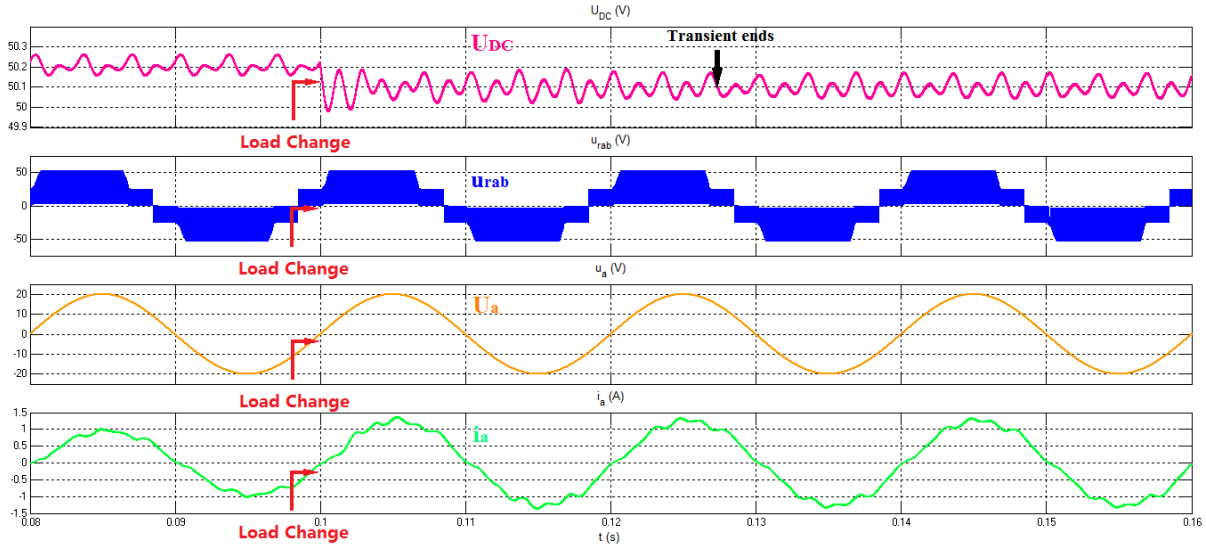


**Fig. 4.17 Simulation results of the ICC based Vienna rectifier system when the resistive load $R_L$ changes from 110 Ω to 80 Ω at 0.1 s**

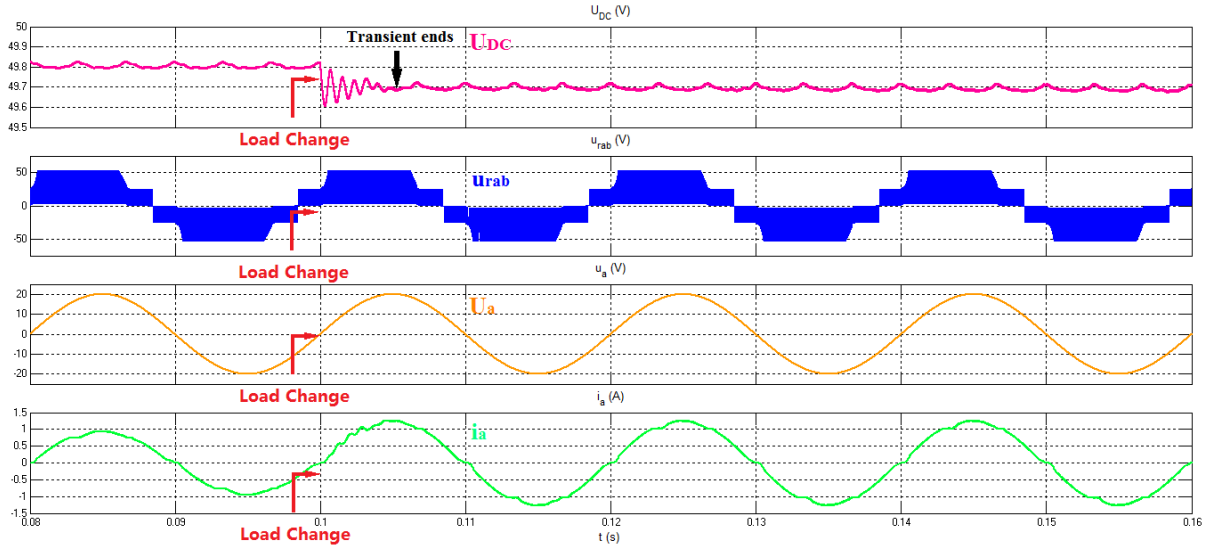


**Fig. 4.18 Simulation results of the DPC based Vienna rectifier system when the resistive load $R_L$ changes from 110 Ω to 80 Ω at 0.1 s**

Specific simulations for ICC and DPC based Vienna rectifier systems are designed under a load change condition, where the resistive load changes from 110 Ω to 80 Ω. The simulation

results of the ICC based and DPC based Vienna rectifier systems are shown in Fig. 4.17 and Fig. 4.18 respectively. Based on comparison of Fig. 4.17 and Fig. 4.18, it can be concluded that the DPC based Vienna rectifier system still has advantages over the ICC based Vienna rectifier system in dynamic performance. When the load changes, the time of the transient status in the DPC based system is about 0.006 s, which is much shorter than the 0.026 s of the transient status in the ICC based system. Therefore, the DPC based Vienna rectifier system has better capability to rapidly respond to disturbance and command changes and it has better dynamic performance.

### 4.2.4 Summary of Simulation Results of Vienna Rectifier

The simulation results of the Vienna rectifier verifies that the theoretical analysis of the Vienna rectifier system, including the power circuit, modulation method, control strategies, is correct, since all simulation results correlate with theoretical analysis results well.

The ICC based Vienna rectifier system can successfully achieve desired performance with regulated DC output voltage and sinusoidal AC currents. The power factor of the system is good and the THD of the current is acceptable.

The switching frequency is a key element influencing the performance of the Vienna rectifier system. The higher the switching frequency, the better DC output voltage regulation and smaller AC current distortion.

The DPC based Vienna rectifier system has outstanding performance in both the steady state operation and transient state operation. Direct power control strategy has promising potential in applications in the Vienna rectifier system.

# Chapter 5

# Experiments of the Vienna Rectifier

Practical experiments are always essential to prove the theoretical analysis results and simulation results of a power electronics system. In this chapter, the experiments are carried out on two prototypes of the GaN FET and Si MOSFET based Vienna rectifier systems with each type of the power devices on a similar scale. Therefore, comparative analysis of the Vienna rectifier based on different devices can be conducted. The selected GaN FET and Si MOSFET devices have the same rating voltage (200 V) and similar rating current (around 20 A), and more parameters are compared in Table 5.1

| | Si | GaN |
|---|---|---|
| Manufacture | International Rectifier | EPC |
| Manufacture # | IRF640N | EPC2010C |
| $V_{DS}$ [V] | 200 | 200 |
| $I_D$ [A] | 18 | 22 |
| Rds(on)@25℃ [Ω] | 0.15 | 0.018 |
| Total gate Charge [nC] | 67 | 3.7 |
| Input cap. [pF] | 1160 | 380 |
| Output cap. [pF] | 185 | 240 |
| Reverse Transfer cap. [pF] | 53 | 1.8 |

**Table 5.1 Parameters of the selected Si MOSFET and GaN FET devices**

In this chapter, the hardware design and software design of prototypes of the GaN FET and Si MOSFET based Vienna rectifier systems are demonstrated. Experiment results of the two prototypes are shown and analyzed as well.

# 5.1 The Hardware Design of the Vienna Rectifier

For the two prototypes of the Vienna rectifier systems based on GaN FET and Si MOSFET respectively, the most parts of the systems, other than the switching devices and corresponding driver circuit, are the same. In other words, the two prototypes share the power circuit, sensing circuit, DSP control circuit and power supplier, but the switching devices and the driver circuit are different.

To start with, the general structure of the hardware design of the Vienna rectifier system can be illustrated by Fig. 5.1. In the figure, the yellow sections are high power level sections and double lines represent high-power electrical connections and energy flows. On the other hand, the other colorful sections are low power level sections and single lines indicate low-power digital connections and signal flows.

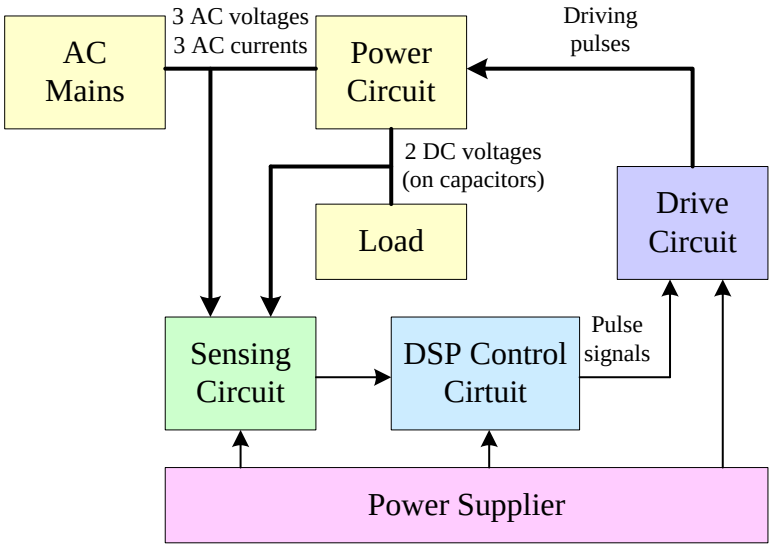


**Fig. 5.1 Structure of the hardware design of the Vienna rectifier system**

Based on the given structure, the hardware design of the two prototypes of the Vienna rectifier can divided into several functional sections, such as the power circuit, the driver

circuit, the sensing circuit, the DSP control circuit, and the power supplier, and will be introduced in detail respectively.

### 5.1.1 The Power Circuit Hardware Design

In the power circuit hardware design, a key step is to select proper passive components, diodes and switching devices. Based on the power circuit specification given in Table 4.1, components selection can be determined. The AC boost inductor has the value of 2 mH with the saturation current of about 10 A (DC) to guarantee that the inductor works in continuous conducting mode and is not saturated during operation. The DC capacitor has the value of about 500 μF, which consists one 470 μF electrolytic capacitor and several 10 μF ceramic capacitors in parallel. The rating voltage of these capacitors is 100 V (DC). For diodes, SS 510 Schottky diode from HY Electronic Corp. are selected, with 100 V reversed voltage and 5 A forward current. For switching devices, GaN FET EPC2010C is employed in the GaN FET based system while Si MOSFET IRF640N is utilized in the Si MOSFET based system. The resistive load is a power load of 110 Ω, 500 W. Considering the DC capacitors need time to charge and reach designed voltage level, a three-phase transformer is used as the AC mains to provide adjustable voltages.

### 5.1.2 The Driver circuit Hardware Design

#### 5.1.2.1 The Driver Circuit Hardware Design of the Si MOSFET

The output pulse signals of the DSP controller have the voltage level of 3 V with low energy, however, the required gate voltage signals to drive the Si MOSFET have the voltage level of 15 V with high energy. As a result, a driver circuit, which has the function as a power amplifier, is needed to amplify low-power digital pulse signals to high-power electrical pulse signals to drive the Si MOSFET. For the conventional Si

MOSFET, the semiconductor switch and its driver circuit are not always necessarily integrated together. Thus, the Si MOSFETs are connected in the power circuit and corresponding driver circuits provide gate signals to the switches.

The schematic of the driver circuit PCB board for Si MOSFET is shown in Fig. 5.2. There are two main chips in each driver circuit. One is the MOSFET driver chip IR 2110s, which isolates the low-power digital side and high-power electrical side and transfers the 0~3 V low-power pulse signals on the first side to the 0~15 V high-power pulse signals on the second side. Another is the isolated power supply chip MORNSUN QA04, which offers the isolated +15 V voltage to the second side of the driver chip IR 2110s.

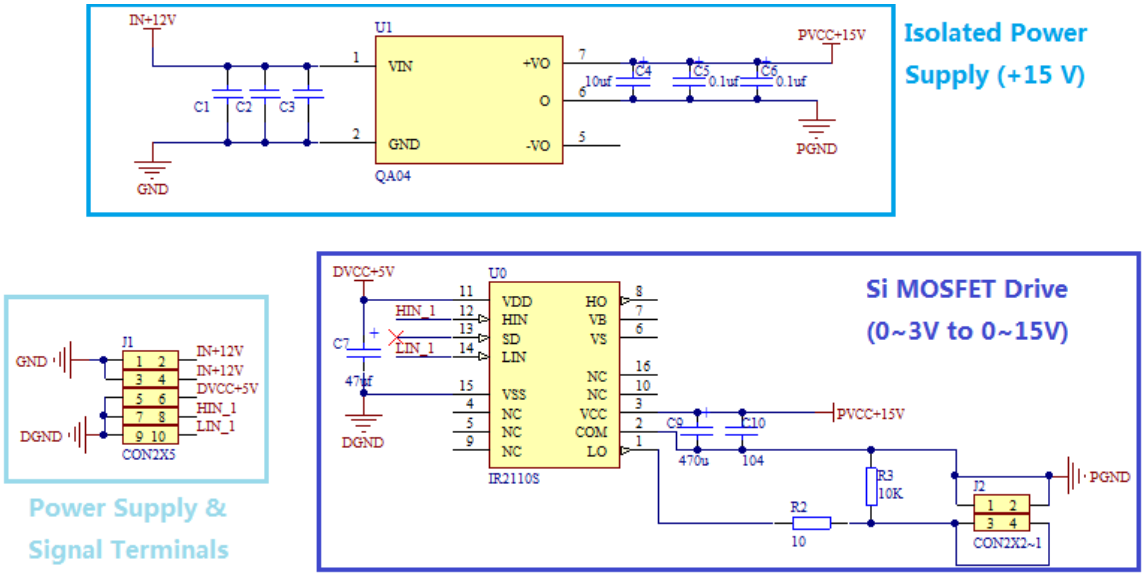


**Fig. 5.2 Schematic of the driver circuit in the Si MOSFET based Vienna rectifier system**

### 5.1.2.2 The Driver circuit Hardware Design of the GaN FET

For the GaN FET, the appropriate gate voltage to drive the device is around 5 V. Therefore, a driver circuit is still essential to transfer low-power pulse signals generated

by the DSP controller to high-power pulse signals, which can drive the GaN FET. Take the extremely small size of the GaN device and the sensitivity of the distortion of driving signals due to parasitic inductors and parasitic capacitors in practical circuit into account, the driver circuit of GaN FET and the GaN FET device itself should be integrated and carefully designed. Hence, the GaN FET and its driver circuit are designed on one PCB board which is placed in the power circuit directly. Fig. 5.3 shows the schematic of the driver circuit PCB board for GaN FET.

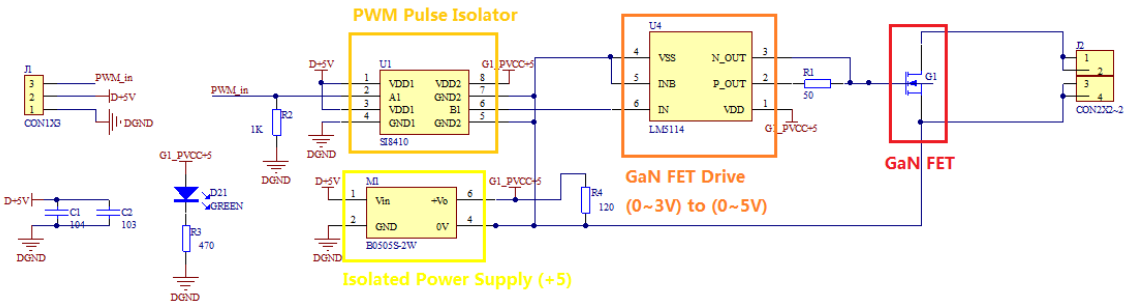


**Fig. 5.3 Schematic of the driver circuit with GaN FET in the GaN FET based Vienna rectifier system**

The driver circuit for the GaN FET consists of one isolated power supply, one PWM signal isolator, one drive chip and one GaN FET device. This circuit is ready to be used in one phase of the power circuit as the switch. The isolated power supply chip is B5050s-2W from MORNSUN, which supplies isolated +5 V. The PWM signal isolator chip is Si8410. The main function of the PWM signal isolator is isolating the GaN FET drive chip from the DSP controller, which reduces disturbances and noises for the GaN FET drive. The GaN FET drive chip is LM5114 from TI with a single driver. Since there is only one semiconductor switch in each phase in the Vienna rectifier topology, the single driver chip is suitable. A photo of a real driver circuit for the GaN FET is shown in Fig. 5.4. The blue device on the upper left corner of the PCB board is a GaN FET. The size of the GaN FET device is very small, and considering the current it can conduct and the

voltage it can block, the power density of the GaN FET device is really high. At the same time, the total volume of the complete driver circuit of the GaN FET is relatively small compared with that of the Si MOSFET.

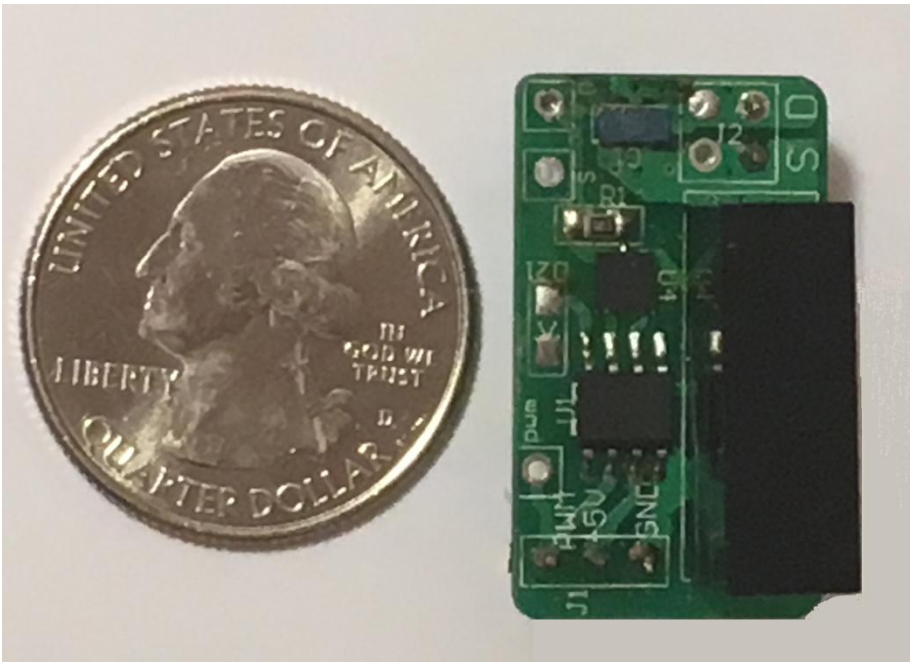


**Fig. 5.4 Photo of a real driver circuit for the GaN FET**

### 5.1.3 The Sensing Circuit Hardware Design

According to Fig. 5.1, the Vienna rectifier system requires eight sensors. Among them, three are AC voltage sensors, two are DC voltage sensors, and three are AC current sensors. These sensors measure crucial instantaneous information of the power circuit and provide it to the controller. The sensing circuit is an important part of the Vienna rectifier system. The accuracy of the sensing results largely influences the effectiveness of the control and the performance of the whole system. Detailed design information of the three types of sensing circuits are demonstrated as follows.

#### 5.1.3.1 The AC Voltage Sensing Circuit Hardware Design

Voltage transducer LV25-P from LEM is selected to measure the AC line-to-line voltages. This voltage transducer can measure DC voltage, AC voltage and pulse voltage, with a galvanic isolation between the primary circuit (high-voltage) and secondary circuit (electronic circuit). The nominal RMS current of the primary side is 10 mA and the nominal RMS current of the secondary side is 25 mA. By selecting proper external resistance in the primary circuit ( $R_4$ and $R_{4\_2}$ as shown in Fig. 5.5), the voltage transducer can measure voltages with amplitude in the range of 10 V to 500 V, because in order to measure the voltage, a current proportional to the voltage must pass the primary circuit. By setting value of the external resistors in the secondary circuit ( $R_{20}$ and $R_{21}$ as shown in Fig. 5.5), the ratio between the output and the input of the voltage transducer can be determined. As the output signal of the sensing circuit is the input signal of the DSP controller, the voltage range of the signal should be limited within 0 V to 3 V, otherwise it will damage the DSP controller. Besides, there is no DC offset of the output of the voltage transducer, which means when the input voltage is 0 V, the output voltage is 0 V. However, since the voltage transducer is used to measure AC voltage in this application, the DC offset of the sensor output need to be added so that the bipolar voltage can be represented in the range of 0 V to 3 V. In order to add DC offset to the output signal of the voltage transducer, operational amplifiers are needed.

The schematic of the AC voltage sensing circuit in the Vienna rectifier system is given in Fig. 5.5. An amplifier chip LM6142, with two operational amplifiers embedded, is employed to add DC offset to the output of the voltage transducer to make the sensing circuit generate accurate and effective signal within the range limitation.

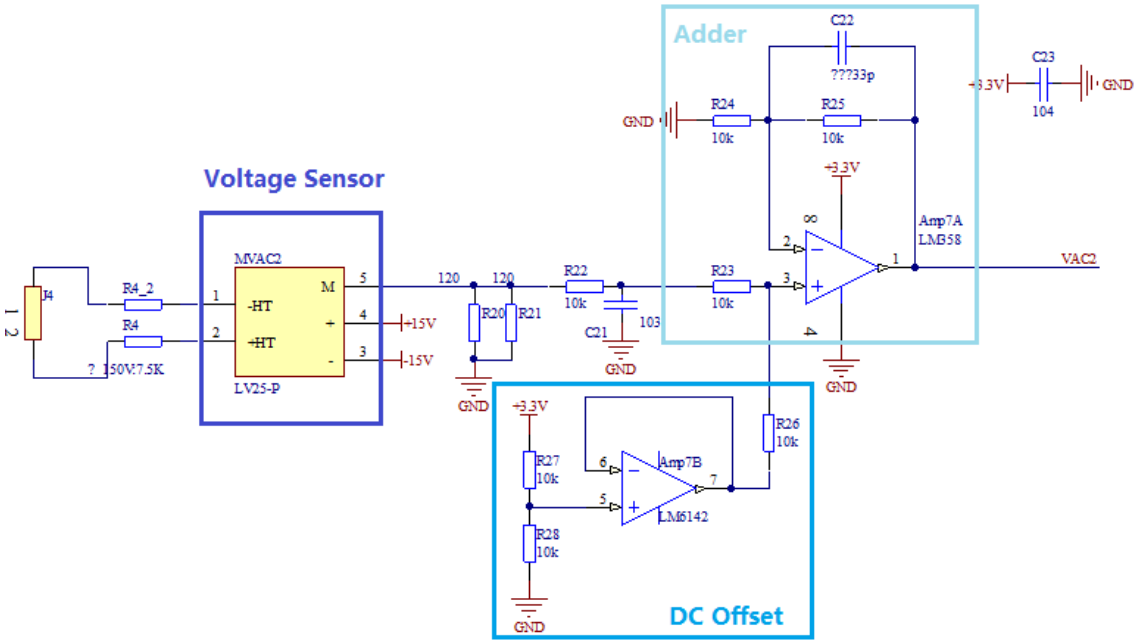


**Fig. 5.5 Schematic of the AC voltage sensing circuit in the Vienna rectifier system**

### 5.1.3.2 The DC Voltage Sensing Circuit Hardware Design

In the DC voltage sensing circuit, the same voltage transducer LV25-P, as used in the AC voltage sensing circuit, is utilized. Since in this application, the voltage transducer only needs to measure unipolar voltage, the DC offset and adder in the AC voltage sensing circuit are no longer necessary. By choosing value of the external resistor in the primary circuit ($R_1$ and $R_{1\_1}$ as shown in Fig. 5.6), the measuring range of the voltage transducer is determined. By selecting value of the external resistor in the secondary circuit ($R_5$ and $R_6$ as shown in Fig. 5.6), the voltage ratio between the input and output of the voltage transducer is set. As the schematic of the DC sensing circuit shown in Fig. 5.6, an amplifier is still employed and playing the role of a voltage follower. It helps reduce noise in the signal and provide isolation between the sensing circuit and DSP controller.

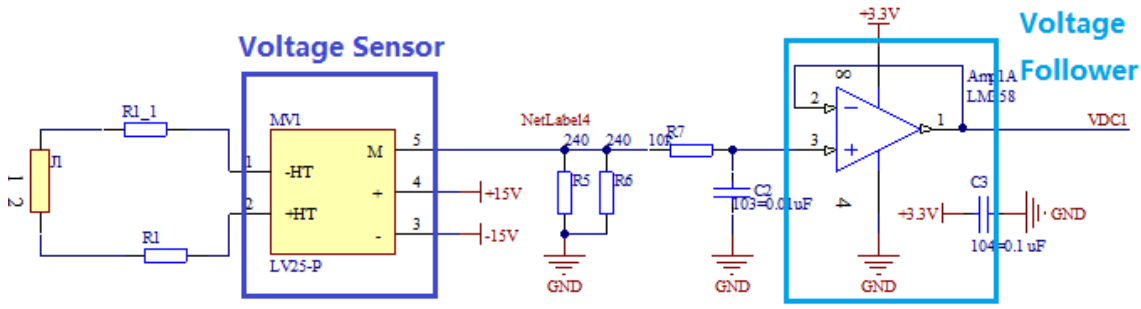


**Fig. 5.6 Schematic of the DC voltage sensing circuit in the Vienna rectifier system**

### 5.1.3.3 The AC Current Sensing Circuit Hardware Design

Hall-effect based linear current sensor ACS712-05B from Allergo Microsystem Inc. is selected in this work to measure AC currents. The optimized range of the objective current is ±5 A, and the typical output sensitivity is 185 mV/A. The original DC offset of the current sensor is 2.5V. Therefore, DC offset adjustment is necessary to make the output signal of the current sensing circuit meet the requirement of the DSP controller. Fig. 5.7 shows the schematic of the AC current sensing circuit in the Vienna rectifier.

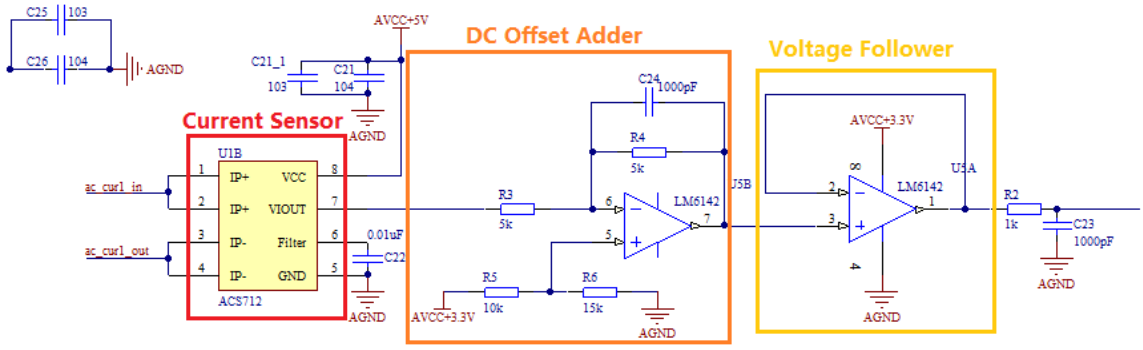


**Fig. 5.7 Schematic of the AC current sensing circuit in the Vienna rectifier system**

### 5.1.4 The DSP Control Circuit Hardware Design

DSP TMS320F28335 from TI is selected as the microcontroller in the Vienna rectifier system. A DSP development board embedding a DSP TMS320F28335 chip and fundamental function sections is employed in the Vienna rectifier system. The DSP development board makes the applications of the DSP in the system easy. A photo of the DSP development board is shown in Fig. 5.8.

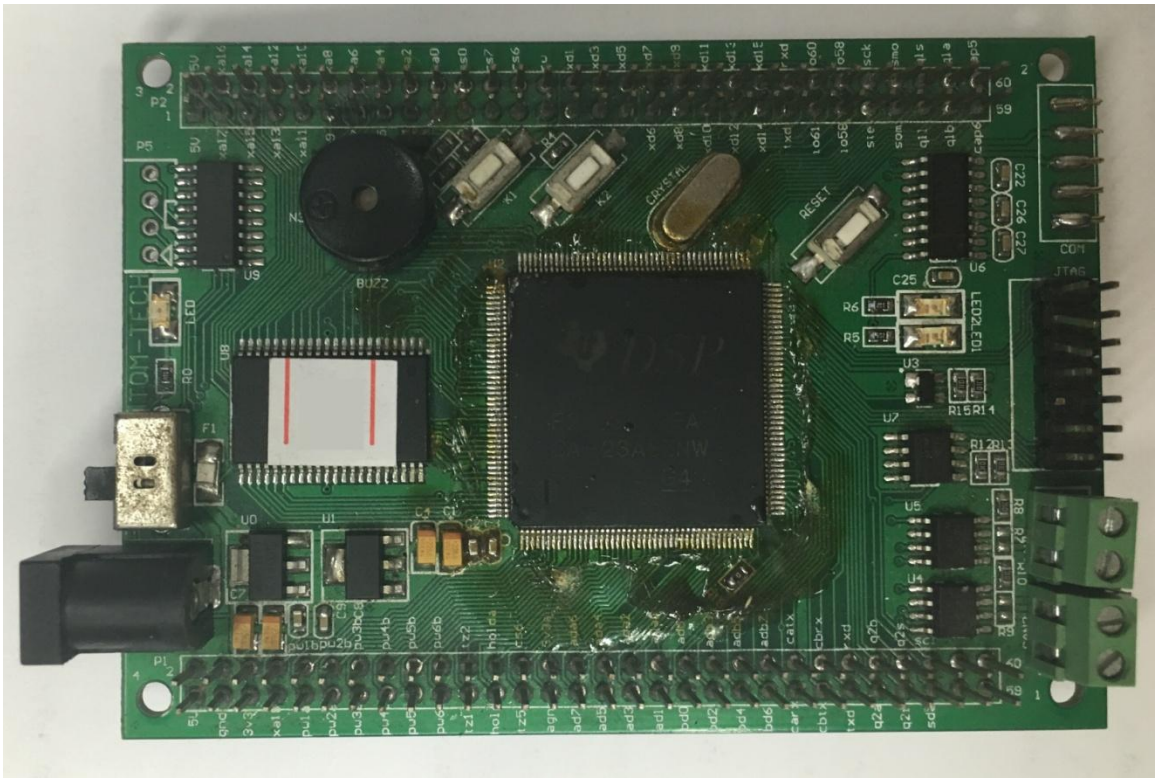


**Fig. 5.8 Photo of the DSP development board**

### 5.1.5 The Power Supplier Hardware Design

The power supplying system is a significant part of every power electronics system that it provides the electronic power and enables devices to work. In the Vienna rectifier

system, several power suppliers are supporting the sensing circuit, the DSP controlling circuit, and the driver circuit. Table 5.2 shows the power supply chips applied in the Vienna rectifier system and their characteristics.

| System | Chip | Input | Output | Isolation | Object |
|---|---|---|---|---|---|
| Si MOSFET Based System | WRB0505-6W | 4.5 ~ 9 $V_{DC}$ | 5$V_{DC}$/1200mA | Yes | DSP control circuit<br>Voltage sensing circuit |
| | WRB0505-6W | 4.5 ~ 9 $V_{DC}$ | 5$V_{DC}$/1200mA | Yes | Current sensing circuit |
| | WRA0512-6W | 4.5 ~ 9 $V_{DC}$ | ±12$V_{DC}$/250mA | Yes | Voltage sensing circuit |
| | External DC Power Supply | 12$V_{DC}$ | 12$V_{DC}$/2A | Yes | Driver circuit |
| GaN FET Based System | WRB0505-6W | 4.5 ~ 9 $V_{DC}$ | 5$V_{DC}$/1200mA | Yes | DSP control circuit<br>Driver circuit |
| | WRA0512-6W | 4.5 ~ 9 $V_{DC}$ | ±12$V_{DC}$/250m | Yes | Voltage sensing circuit |
| | L7805CV | 7 ~ 35 $V_{DC}$ | + 5 $V_{DC}$/1.5A | Yes | Voltage sensing circuit<br>Current sensing circuit<br>D/A circuit |
| | L7905CV | -7 ~ -35 $V_{DC}$ | −5 $V_{DC}$/1.5A | Yes | D/A circuit |

**Table 5.2 Power supplying chips and their characteristics**

### 5.1.6 The Prototypes of the Vienna Rectifier Systems

With design introduction given in previous sections, the two prototypes of the Vienna rectifier system based on the GaN FET devices and Si MOSFET devices can be built. Fig. 5.9 and Fig. 5.10 show the photos of the final prototypes of the Si MOSFET based and GaN FET based Vienna rectifier systems respectively.

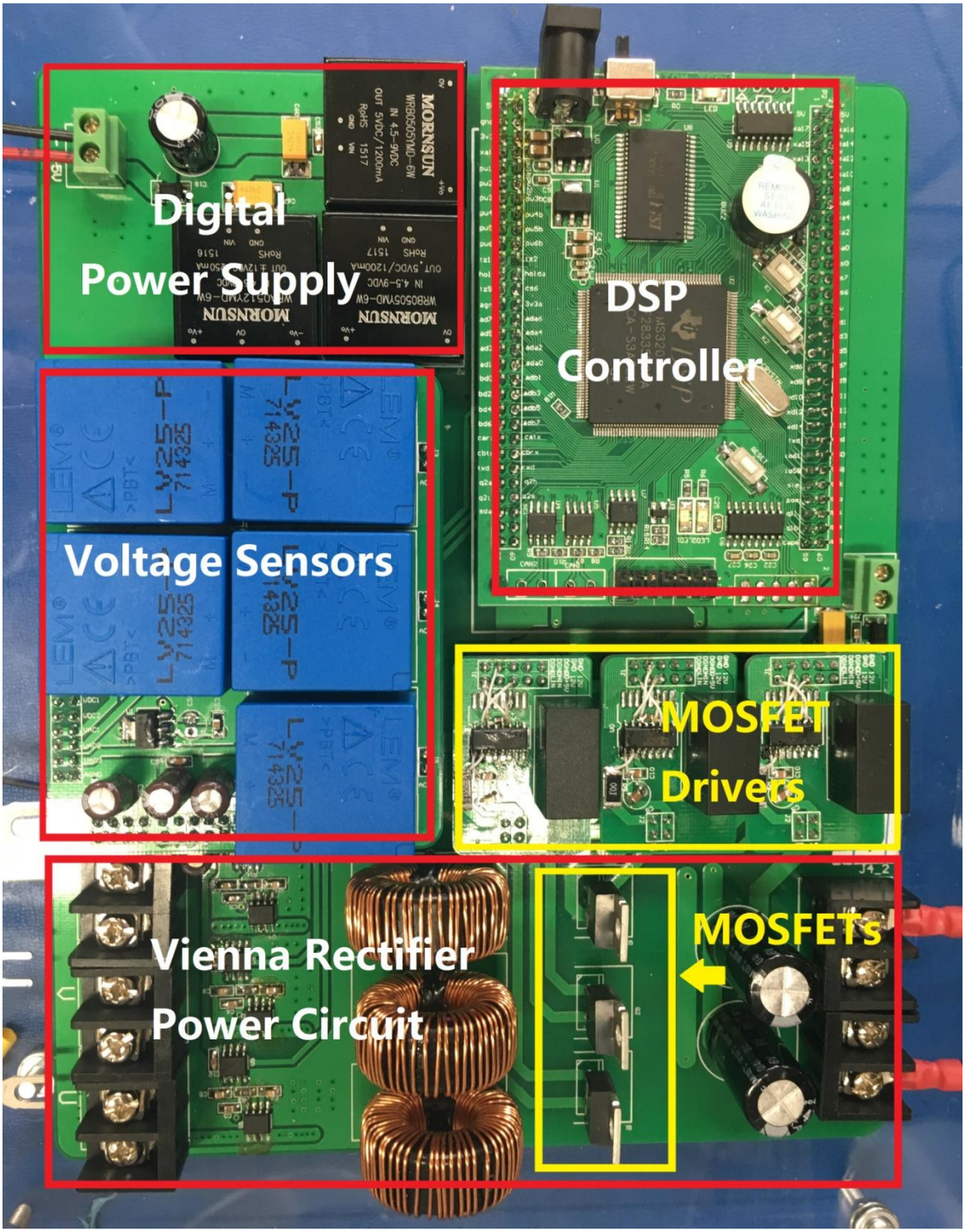


**Fig. 5.9 Photo of the prototype of the Si MOSFET based Vienna rectifier system**

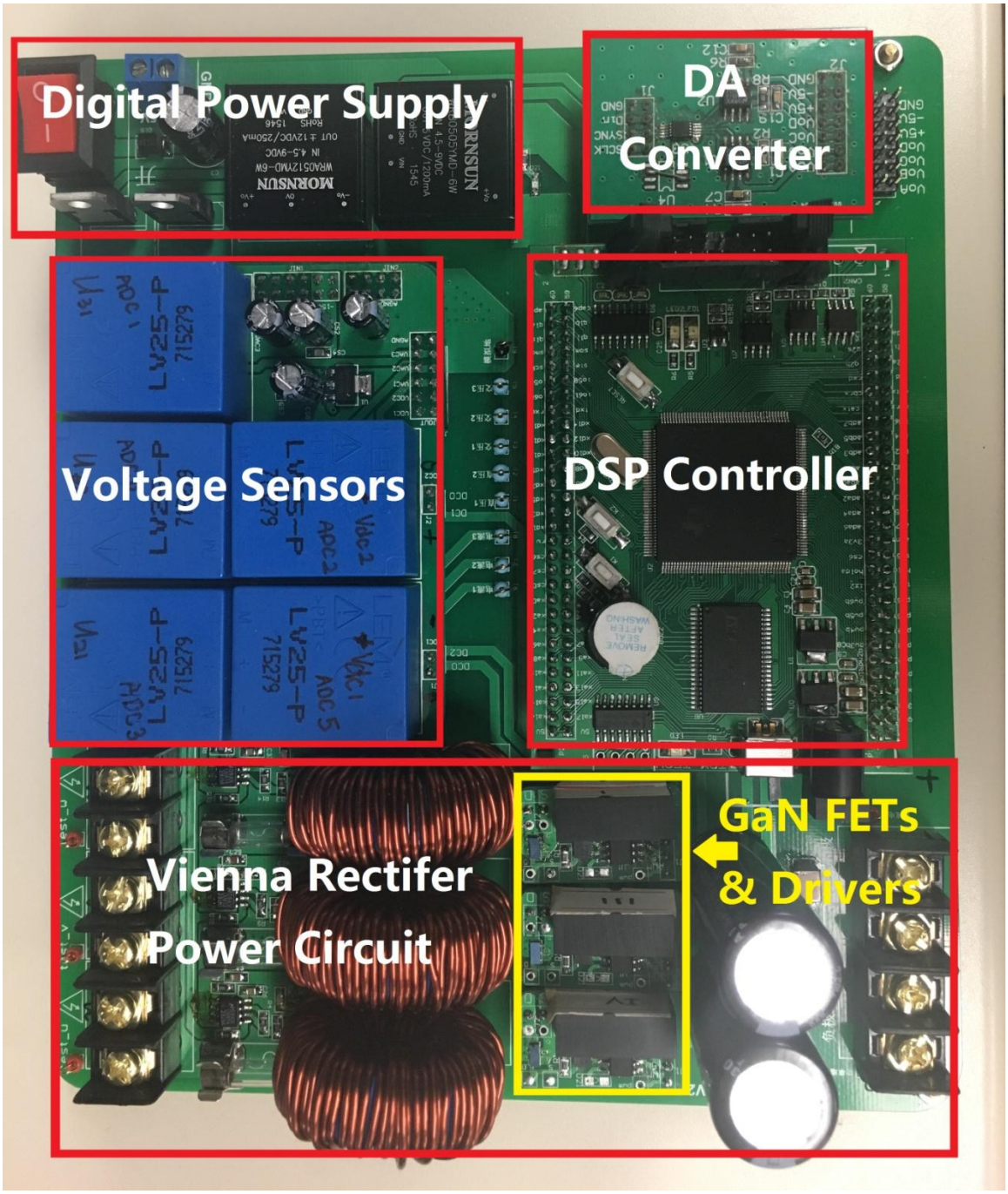


**Fig. 5.10 Photo of the prototype of the GaN FET based Vienna rectifier system**

## 5.2 The Software Design of the Vienna Rectifier

The control system of the prototype of the Vienna rectifier is based on the control circuit, which contains the DSP TMS320F28335 as the key element. The DPS program is written in C language and the compiling and debugging of the program are done in the CCS (Code Composer Studio) environment. The control program of the Vienna rectifier has a main program and an interrupt program. In the main program, the DSP system is initialized. System initializations include parameters initializations and module initializations. For the Vienna rectifier application, GPIO module, ePWM module, ADC module, etc. are utilized and need initializations in the main program. After the initializations of the DSP system, the main program keeps running. The interrupt program runs periodically to implement the control functions of the DSP control system. Signal processing, digit calculation, and pulse generation are carried out in the interrupt program. The flow chart of the thought of the software design in the form of the DSP control program is shown in Fig. 5.11. These functions are written and achieved in the interrupt program of the DSP. Therefore, desired control of the Vienna rectifier system can be carried out.

In general, the control method shown in Fig. 5.11 correlates with the control strategy of the Vienna rectifier introduced in chapter 3 well. They have the same structure, which confirms the correctness of the DSP controller. In the following, detailed descriptions of each function given in Fig. 5.11 will be indicated in sequence.

Since the inputs of the DSP control circuit are eight analog signals generated by the sensing circuit and representing sampled AC voltages, AC currents and DC voltages, the first thing the DSP controller needs to do is to transfer the analog signals into digital signals. This analog-to-digital transformation is carried out by the Analog Digital Converter (ADC) module in the DSP. Calibration process is essential to transfer each analog signal to a corresponding digital signal. The relation between the analog signal

and the corresponding digital signal is linear mapping. In conclusion, the "A/D Calibration" function transfers eight analog signals carrying sample information into eight digital signals without losing any information.

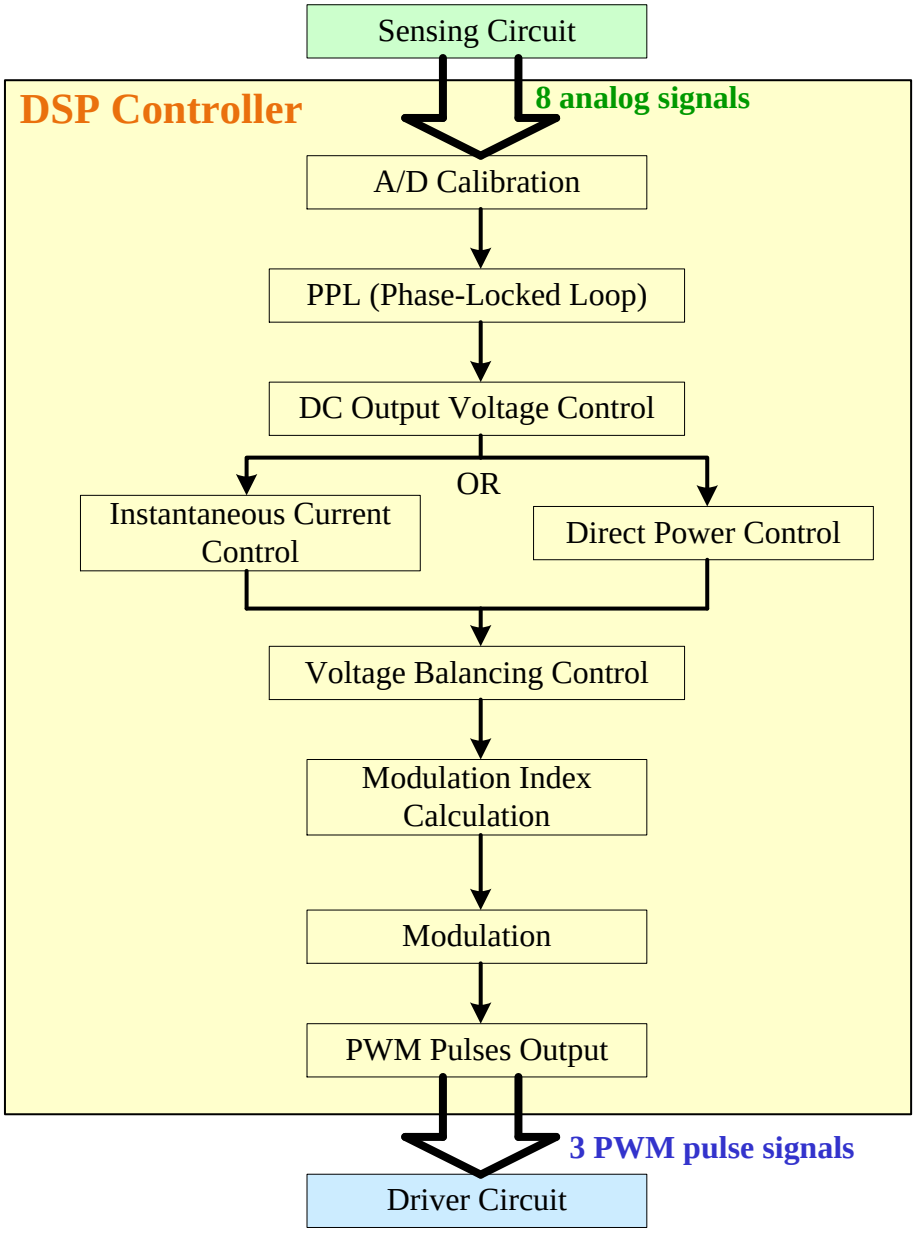


**Fig. 5.11 DSP Control Program Flow Chart**

Based on the digital signals provided by the "A/D Calibration", "Phase-Locked Loop" (PLL) can acquired the actual phase and frequency of the AC voltages. The phase and frequency information will be used in the "Instantaneous Current Control" function.

As it is named, "DC Output Voltage Control" function plays the role of the DC output voltage controller introduced in section 3.4. Given the DC output voltage command, corresponding AC current command (the reference current magnitude) is calculated in this function.

Either the instantaneous current control (ICC) or the direct power control (DPC) can be used as the inner control loop in the whole control system. For the ICC, a modulation index command is generated by comparing the sampled current with the current reference and process the difference. For the DPC, the active power command is calculated based on the current reference and the reactive power command is set to zero. Based on feedback control on the active power and the reactive power, a modulation index command can be calculated to make the active power and reactive power to follow their commands.

The "Voltage Balancing Control" deals with the unbalance voltages on the DC capacitors by generating a compensating component in the form of the modulation index. Since the modulation index influences the conducting duty cycle of the switch in each phase, a change in the modulation index causes changes in charging/discharging time on the DC capacitors and leads to balanced voltages.

By adding the modulation index components generated by the ICC/DPC control function and the voltage balancing control function, the final modulation index commands can be calculated.

The modulation function generates proper PWM pulse signals based on corresponding modulation index commands. And the PWM pulse output function exports the PWM pulses as the output of the DSP control circuit.

# 5.3 Experiment Results of the Vienna Rectifier

Experiments are carried out on both prototypes of the GaN FET based and Si MOSFET based Vienna rectifier systems. And for each system, the instantaneous current control strategy (ICC) and the direct power control strategy (DPC) are both applied as well. As a result, four types of experiments are conducted based on the classification of switching device type as well as control strategy. The experimental results of these four conditions are shown as follows.

## 5.3.1 Si MOSFET Based Vienna Rectifier Prototype with ICC control

Fig. 5.12 shows the experiment results of the Si MOSFET based Vienna rectifier prototype with ICC control operating in steady state under rated conditions ( $f_s$=100 kHz). Four waveforms in the figure are respectively the DC output voltage $U_{DC}$, the line-to-line rectifier input voltage $u_{rab}$, the phase voltage of phase $a$ $u_a$, and the phase current of phase $a$ $i_a$. All experiment results will be given in the same form in this work.

The experiment results shown in Fig. 5.12 are in good correlation with the simulation results shown in Fig. 4.10. The DC output voltage is nicely regulated at the command value (50V) and the AC mains current (phase *a*) has nearly sinusoidal shape and is in phase with AC mains voltage in the same phase. FFT analysis of the AC mains current is done and the results is shown in Fig. 5.13. The THD is 8.29% in this case.

The theoretical analysis results, the simulation results and the experiment results match each other very well. Therefore, the Vienna rectifier system employing Si MOSFET is successfully designed and instantaneous current control strategy is functional in the Vienna rectifier system.

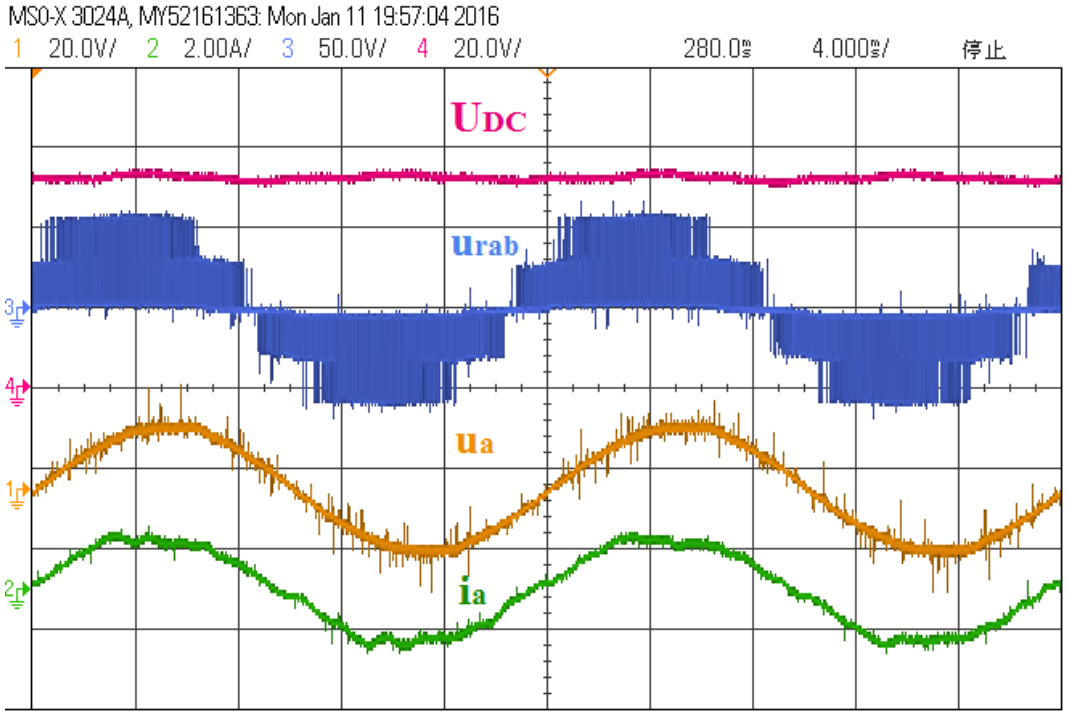


**Fig. 5.12 Experiment results of the Si MOSFET based Vienna rectifier system with ICC control**

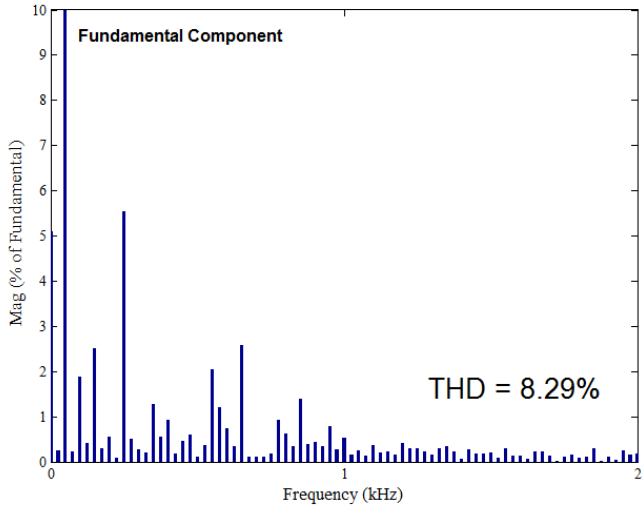


**Fig. 5.13 FFT analysis on AC mains current in the Si MOSFET based Vienna rectifier system with ICC control**

### 5.3.2 Si MOSFET Based Vienna Rectifier Prototype with DPC control

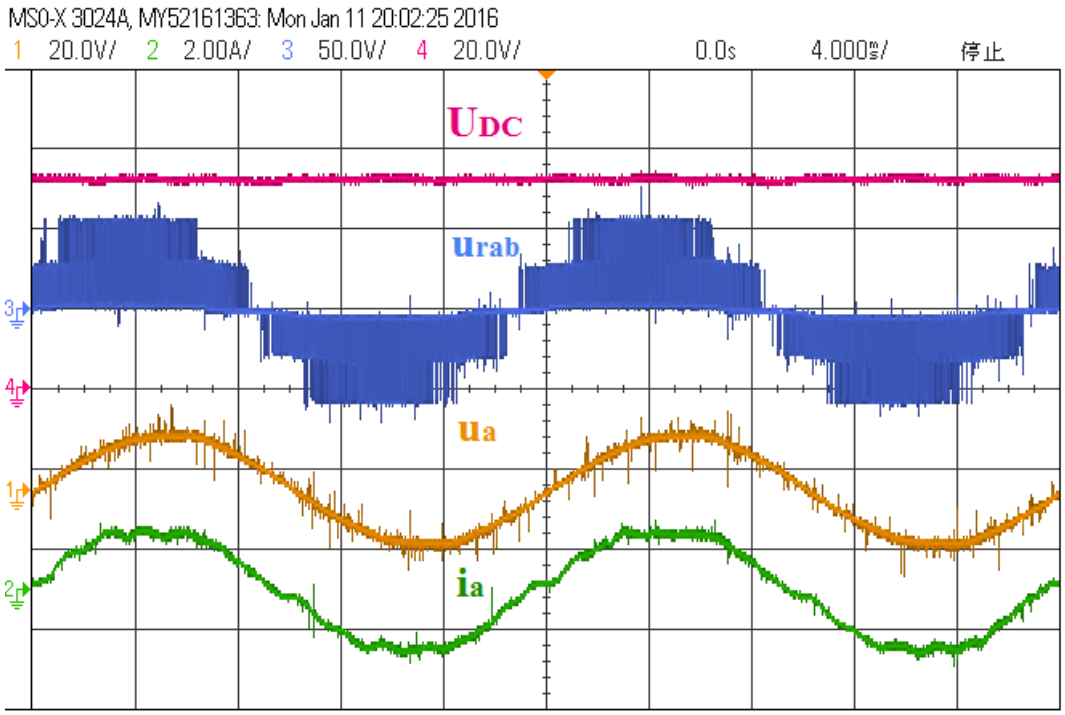


**Fig. 5.14 Experiment results of the Si MOSFET based Vienna rectifier system with DPC control**

Fig. 5.14 shows the experiment results of the Si MOSFET based Vienna rectifier prototype with DPC control operating in steady state under rated conditions ( $f_s$=100 kHz). The experiment results shown in Fig. 5.14 correlates well with the simulation results shown in Fig. 4.14. The DC output voltage is nicely regulated at the command value (50V) and the AC mains current (phase *a*) has nearly sinusoidal shape and is in phase with AC mains voltage in the same phase. FFT analysis of the AC mains current is done and the results is shown in Fig. 5.15. The THD is 7.76% in this case, which is slightly smaller than the THD for the same prototype but using ICC control instead. The

THD comparison proves that better THD is one of the advantages of the DPC over the ICC. The direct power control strategy performs well in the Vienna rectifier system.

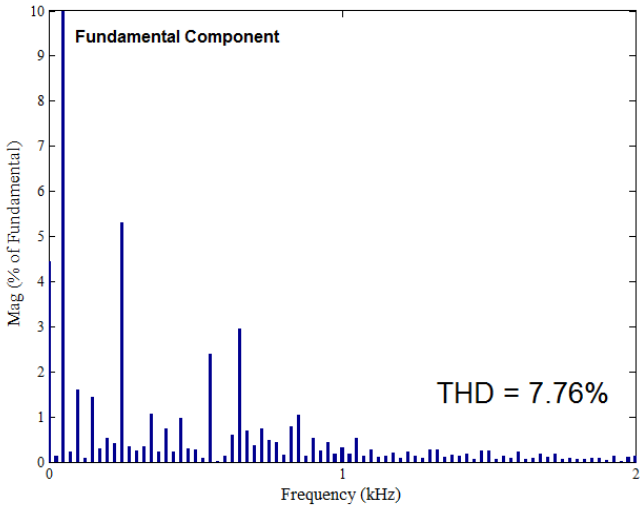


**Fig. 5.15 FFT analysis on AC mains current in the Si MOSFET based Vienna rectifier system with DPC control**

### 5.3.3 GaN FET Based Vienna Rectifier Prototype with ICC Control

Fig. 5.16 shows the experiment results of the GaN FET based Vienna rectifier prototype with ICC control operating in steady state under conditions with $f_s$=50 kHz. The original designed switching frequency for the GaN FET based Vienna rectifier system is 100 kHz, however, due to limited time and technical difficulty on the GaN FET drivers, the switching frequency of the system is only pushed to 50 kHz. In near future, obstacles will be overcome and the switching frequency will be pushed to 100 kHz soon.

The experiment results shown in Fig. 5.16 correlates are in great consistency with the simulation results shown in Fig. 4.10. The DC output voltage is nicely regulated at the command value (50V) and the AC mains current (phase *a*) has nearly sinusoidal shape and is in phase with AC mains voltage in the same phase. FFT analysis of the AC mains

current is done and the results is shown in Fig. 5.17. The THD is 11.31% in this case. The THD value is relatively high compared with that of the Si MOSFET based system. Possible reasons may include the difference in system switching frequency and the immaturity of the newly designed GaN FET drivers. Besides, controller parameters, like PI gains can be further optimized to improve the performance of the system.

In general, the theoretical analysis results, the simulation results and the experiment results match each other very well. Therefore, the Vienna rectifier system employing GaN FET is successfully designed and implemented. This is the first research that successfully applies the GaN devices in a Vienna rectifier system. It proves that GaN power devices have the ability and potential to be applied in rectifying systems and related applications.

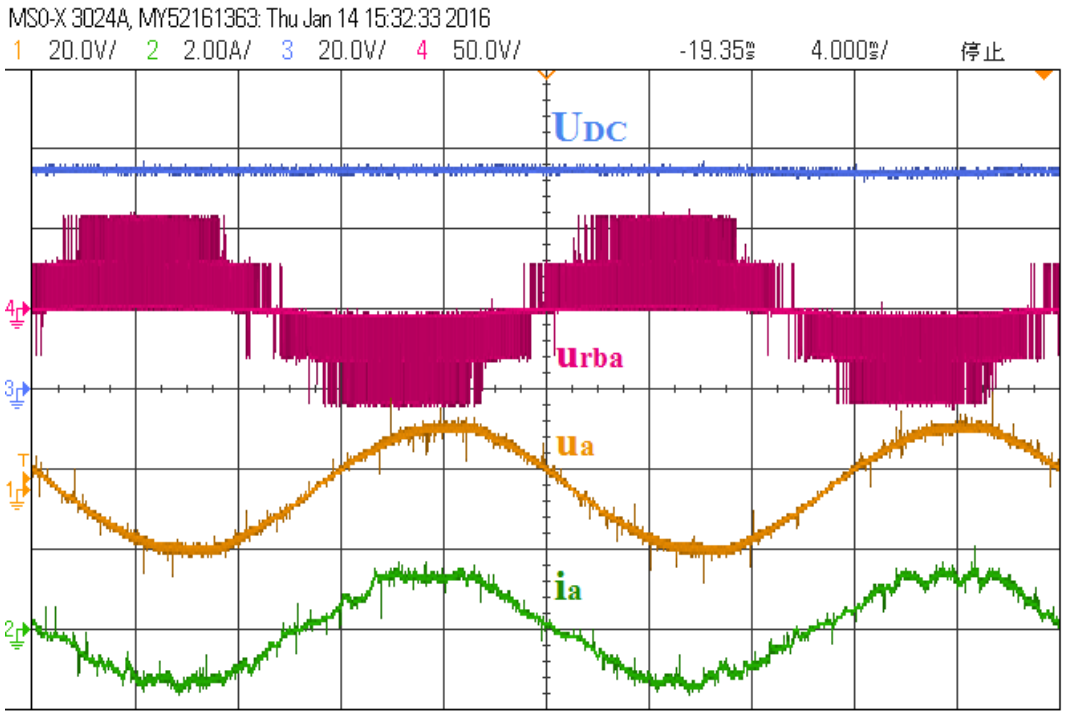


**Fig. 5.16 Experiment results of the GaN FET based Vienna rectifier system with ICC control**

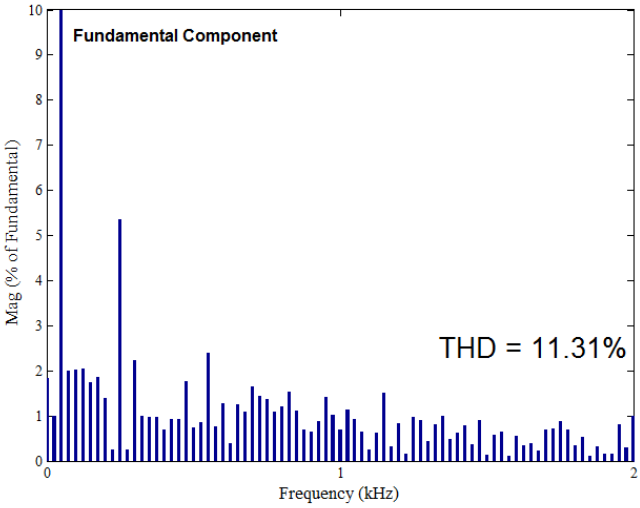


**Fig. 5.17 FFT analysis on AC mains current in the GaN FET based Vienna rectifier system with ICC control**

### 5.3.4 GaN FET Based Vienna Rectifier Prototype with DPC Control

The experiment results of the GaN FET based Vienna rectifier prototype with DPC control operating in steady state under conditions with $f_s$=50 kHz is shown in Fig. 5.18.

The experiment results match the simulation results shown in Fig. 4.14. The DC output voltage is nicely regulated at the command value (50V) and the AC mains current (phase a) has nearly sinusoidal shape and is in phase with AC mains voltage in the same phase. FFT analysis of the AC mains current is done and the results is shown in Fig. 5.19. The THD is 14.8% in this case. Due to limited time, the DPC control in the GaN FET based Vienna rectifier prototype is not fully developed and optimized. But the experiment results still reveal that the DPC control achieves fundamental control functions in the Vienna rectifier and has promising future.

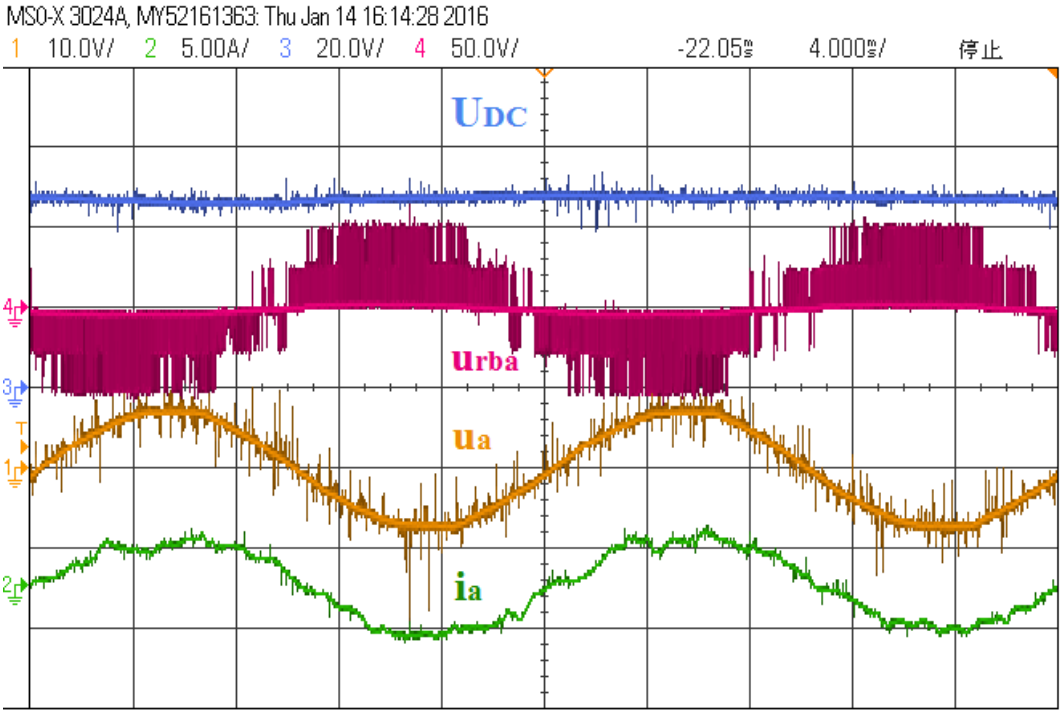


**Fig. 5.18 Experiment results of the GaN FET based Vienna rectifier system with DPC control**

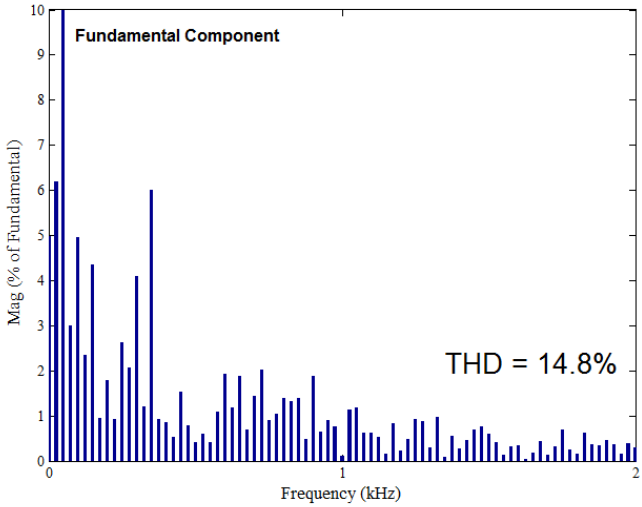


**Fig. 5.19 FFT analysis on AC mains current in the GaN FET based Vienna rectifier system with DPC control**

### 5.3.5 Summary of Experimental Results

To summarize, the experiment results is consistent to the theoretical analysis results and simulation results, which confirms that the design and implementation of the Vienna rectifier system based on both the Si MOSFET and GaN FET are successful. Desired performance of the Vienna rectifier, such as regulated DC output voltage, high quality AC current with sinusoidal shape, and high power factor, can be achieved in both prototypes with either the ICC control or the DPC control.

## 5.4 Comparison between the GaN FET Based and Si MOSFET Based Vienna Rectifiers

Comparison between the GaN FET based and Si MOSFET based Vienna rectifier system can be conducted based on corresponding prototypes and experiment results.

### 5.4.1 Comparison on Power Densities and Sizes of the GaN FET and Si MOSFET Devices and Drivers

By comparing Fig. 5.9 and Fig. 5.10, it can be noticed that the GaN FET based Vienna rectifier system has smaller size compared with the Si MOSFET based Vienna rectifier system, specially the size of the power electronics devices and their drivers. Since the GaN FET devices have small size and good thermal conductivity, the GaN FET gate driver PCB boards takes small space. In the GaN FET based system, the volume of one GaN FET and its driver is $2.83\ \text{cm} \times 1.64\ \text{cm} \times 1.40\ \text{cm} = 6.5\ \text{cm}^3$. In the Si MOSFET based system, the volume of one MOSFET with heat sink is $1.55\ \text{cm} \times 1.16\ \text{cm} \times 2.31\ \text{cm} = 4.15\text{cm}^3$, and the volume of its driver is $3.86\ \text{cm} \times 2.57\ \text{cm} \times$

$1.40\ \text{cm} = 13.89\text{cm}^3$. The total volume for one MOSFET section with heat sink and driver is $18.04\text{cm}^3$. The volume of the Si MOSFET switch and driver is nearly three times the volume of the GaN FET switch and driver. As a result, at an identical operating point, where the GaN FET and MOSFET devices deal with the same power, the power density of the GaN FET switch and driver would be three times of the power density of the MOSFET switch and driver. In conclusion, GaN FET devices are suitable for high power density applications.

### 5.4.2 Comparison on Power Losses on the GaN FET and Si MOSFET Devices

Based on the GaN FET and Si MOSFET parameters given in 5.1, the theoretical power losses on the GaN FET and Si MOSFET devices can be compared.

It can be seen clearly that the on-resistance of GaN FET is nearly nine times smaller than the on-resistance of Si FET, which means the conduction loss of the GaN device should be nine times smaller than that of the Si device.

Compared with the Si device, the GaN device has better parameters in total gate charge, input capacitance, output capacitance and reverse transfer capacitance. Therefore, the switching loss of the GaN device is much smaller than that of the Si device as well.

Better performance in high switching frequency operation applications can be expected with the GaN device, since it has low conduction loss and switching loss.

### 5.4.3 Comparison on Current Qualities of the GaN FET and Si MOSFET Based Vienna Rectifier Systems

The quality of AC mains currents in the GaN FET based and Si MOSFET based prototypes can be compared with experiment results shown in Fig. 5.12, Fig. 5.14, Fig. 5.16, and Fig. 5.18 and corresponding FFT analysis results.

In general, the current quality in the Si MOSFET based prototype is slightly better than the current quality in the GaN FET. However, many possible reasons cause this result. Firstly, the GaN FET driver is newly designed and immature, which leads to limitation on switching frequency of the system. The switching frequency of the GaN FET prototype experiment is half of the switching frequency of the Si MOSFET prototype experiment. Considering the fact that the higher the switching frequency the better the current quality, it is positive for GaN FET prototype to have improved current quality when the switching frequency can be pushed to the same level as the Si MOSFET prototype. Furthermore, the gains of controllers and other controlling related parameters can be optimized in the GaN FET prototype, which also makes contributions to improving the current quality. In a word, the current quality of the GaN FET prototype is similar to that of the Si MOSFET in unfavorable conditions and the GaN FET based Vienna rectifier system has promising future potentials in achieving high current quality performance.

# *Chapter 6*

# *Conclusions, Contributions and Future Work*

This thesis presents a Vienna rectifier system utilizing the GaN FET power devices. Several advantages of applying the GaN FET power devices in the Vienna rectifier system are verified. Besides, direct power control (DPC) strategy is used to control the Vienna rectifier system and it has outstanding control performance. Theoretical analysis and simulation are carried out. Two prototypes of the Vienna rectifier are built with GaN FET devices and Si MOSFET devices on a similar scale for practical comparison. In this chapter, conclusions and contributions of this thesis are summarized. Recommended future works are proposed.

## 6.1 Conclusions

- **The Vienna rectifier topology has advantages of low input current harmonics, low blocking voltage stress on the power semiconductor devices, high power density, high efficiency, and high reliability.**

The Vienna rectifier is a three-phase three-level three-switch PWM rectifier with controlled output voltage, regulated input current and unidirectional power flow. It is a boost system with boost inductor current in continuous conduction mode. The input current has low harmonics and high quality and the power factor of the mains is very high. The voltage stress on the switching devices is low and the switching losses are low as well. The Vienna rectifier outstands in the respect of high power density, high efficiency, high reliability, low complexity and low realization effort.

- **The GaN FET devices has advantages of low ON-resistance, fast switching speed, nice thermal conductivity, small size and high reliability.**

Wide bandgap semiconductor material such as gallium nitride (GaN) has many advantages including wide band gap, high electron saturation velocity, high critical

breakdown electric field, high thermal conductivity, etc. These material features guarantee better characteristics of the GaN power devices, such as low ON-resistance, fast switching speed, nice thermal conductivity, small size and high reliability. Thus GaN power devices are suitable for high frequency, high power density, and high temperature applications.

- **The Vienna rectifier system has better performance with high switching frequency, which matches the application potential of the GaN FET.**

The simulation results of the Vienna rectifier system reveal that when the switching frequency is higher, the Vienna rectifier performance is better. To be more specific, the input current quality and waveform is improved with increased switching frequency. Moreover, with high switching frequency, the value and size of the inductor can be reduced, hence the volume of the system can be minimized and the power density of the system is increased.

Since the GaN FET has significant advantages in high frequency applications, it should be employed in the high frequency Vienna rectifier systems to achieve its full potential and maximize the excellence of the Vienna rectifier.

- **The GaN FET based Vienna rectifier have higher power density compared with the Si MOSFET based Vienna rectifier.**

Comparing the two prototypes of the Vienna rectifier with GaN FET and Si MOSFET devices, it can be seen that the GaN FET device and driver module has much smaller volume compared with the Si MOSFET device and driver module. Considering that two prototypes are working under similar power level, the power density of the GaN FET and driver module is higher than that of the Si MOSFET and driver module. On the system level, the volume of the GaN FET based Vienna rectifier is smaller than the Si MOSFET based Vienna rectifier, so that the power density is higher in the GaN FET based system.

- **The GaN FET based Vienna rectifier has lower power losses on the switches and higher efficiency comparing with the Si MOSFET based Vienna rectifier.**

Comparing the device characteristics related to conduction loss and switching loss of the GaN FET device and Si MOSFET device, it can be concluded that under the same operation condition, the power losses on the GaN FET device is smaller than that on the Si MOSFET device. Therefore, the efficiency of the GaN FET based Vienna rectifier is high.

- **Direct power control (DPC) has better controlling performance in both steady state operation and transient state operation in the Vienna rectifier.**

Simulation results show that the direct power control (DPC) strategy generates well regulated output voltage and better input current waveform in the steady state, and it also has better dynamic response in the transient state. As a result, DPC is a good control candidate for the Vienna rectifier system.

## 6.2 Contributions

- **This is the first research that utilizes GaN FET device in the Vienna rectifier applications and studies the advantages.**

Promising potentials for applying the GaN power devices in the rectifier and converter applications are verified through this research. GaN power devices are proved to have advantages in high power density, high frequency, high temperature applications.

- **Direct power control (DPC) strategy is used to control the Vienna rectifier and it has outstanding controlling performance.**

Direct power control (DPC) strategy effectively controls the Vienna rectifier. In the steady state operation, DPC improves the input current waveform. In the transient state operation, DPC shows fast dynamic response. As a result, DPC is a good control strategy for the Vienna rectifier.

## 6.3 Future Work

- **Optimization of the GaN FET based Vienna rectifier system.**

As mentioned in chapter 5, due to time limitations and immaturity of the GaN FET driver design, the performance of the GaN FET based Vienna rectifier prototype has not been optimized. This optimization may include redesign of the GaN FET driver, selecting new controller parameters (gains), etc. After the optimization, the GaN FET based Vienna rectifier should be able to operate at 100 kHz or even higher switching frequency well. And great performance should be expected as well. Based on the optimization, more experiments and analysis can be done on the GaN FET and Si MOSFET based prototypes, such as measurement of power losses on the switches and so on.

- **Improving control strategy for the Vienna rectifier system.**

In this work, the instantaneous current control and direct power control are used to control the Vienna rectifier system. Both of these control strategies achieve functionality, while direct power control wins over the instantaneous current control in both the steady state operation and the transient state operation. As a result, there is large space to improve the control strategy for the Vienna rectifier system and direct power control can be a good candidate for further study.

- **Exploring more development and applications of GaN power devices in high frequency and high power density power electronics fields.**

Great advantages and promising potentials of the GaN power devices in high frequency and high power density applications can be seen from this research. More efforts are needed to explore the enormous benefits of the GaN power devices and possible applications.

# *Appendix*

It is left blank.

# *Bibliography*


[1] "IEEE Recommended Practices and Requirements for Harmonics Control in Electric Power Systems", IEEE Std. 519, 1992.

[2] R. Ridley, “Three-phase power factor correction circuits—part 1,” in Proc. HFPC’94, 1994, pp. 278–321.

[3] B. Singh, K. A.K. Al. Haddad, and A. Chandra, “A review of active filters for power quality improvement,” IEEE Trans. Ind. Electron., vol. 46, pp. 960–971, Oct. 1999.

[4] G. Seguier, Power Electronic Converters AC/DC Conversion. New York: McGraw-Hill, 1986.

[5] P. Enjeti and I. Pitel, “Design of three-phase rectifier systems with clean power characteristics,” presented at the IEEE PESC’99 (Tutorial), Charleston, SC, June 27 July 1, 1999.

[6] H. Mao, F. C. Y. Lee, and D. Boroyevich, “Review of high-performance three-phase power-factor correction circuits,” IEEE Trans. Ind. Electron., vol. 44, pp. 437–446, Aug. 1997.

[7] J.W. Kolar and H. Ertl, “Status of the techniques of three-phase rectifier systems with low effects on the mains,” in Proc. IEEE INTELEC’99, 1999, Paper 14-1.

[8] B. Singh, B. N. Singh, A. Chandra, K. Al-Haddad, A. Pandey and D. P. Kothari, "A review of three-phase improved power quality AC-DC converters," in *IEEE Transactions on Industrial Electronics*, vol. 51, no. 3, pp. 641-660, June 2004.

[9] J. Kolar, M. Hartmann, and T. Friedli, “Three-Phase PFC and AC-AC Converter Systems,” in Tutorial, IEEE Applied Power Electron. Conf. and Exp. (APEC ’11), 2011.

[10] P. Pejovic, “Three-Phase High Power Factor Rectifier Based on the Third Harmonic Current Injection with Passive Resistance Emulation,” in Proc. of the 31st Ann. IEEE Power Electron. Spec. Conf. (PESC ’00), vol. 3, 2000, pp. 1342–1347.

[11] H. Ertl and J. W. Kolar, “A constant output current three-phase diode bridge rectifier employing a novel electronic smoothing inductor,” IEEE Trans. Ind. Electron., vol. 52, no. 2, pp. 454–461, Apr. 2005.

[12] K. Mino, M. L. Heldwein, and J. W. Kolar, “Ultra compact three-phase rectifier with electronic smoothing inductor,” in Proc. 20th IEEE Appl. Power Electron. Conf. Expo., Mar. 6–8, 2005, vol. 1, pp. 522–528.

[13] N. Mohan, “A Novel Approach to Minimize Line-Current Harmonics in Interfacing Power Electronics Equipment with 3-Phase Utility Systems,” IEEE Trans. Power Del., vol. 8, no. 3, pp. 1395–1401, 1993.

[14] R. Naik, M. Rastogi, and N. Mohan, “Third-Harmonic Modulated Power Electronics Interface with Three-Phase Utility to Provide a Regulated DC Output and to Minimize Line-Current

Harmonics," IEEE Trans. Ind. Appl., vol. 31, no. 3, pp. 598–602, 1995.

[15] H. Yoo and S.-K. Sul, "A Novel Approach to Reduce Line Harmonic Current for a Three-Phase Diode Rectifier-Fed Electrolytic Capacitor-Less Inverter," in Proc. of the 24th Ann. IEEE Appl. Power Electron. Conf. and Exp. (APEC '09), 2009, pp. 1897– 1903.

[16] ——, "A new Circuit Design and Control to Reduce Input Harmonic Current for a Three-Phase AC Machine Drive System Having a Very Small DC-Link Capacitor," in Proc.of the 25th Ann. IEEE Appl. Power Electron. Conf. and Exp. (APEC '10), 2010, pp. 611–618.

[17] R. Greul, S. D. Round, and J. W. Kolar, "Analysis and Control of a Three-Phase, Unity Power Factor Y-Rectifier," IEEE Trans. Power Electron., vol. 22, no. 5, pp. 1900–1911, 2007.

[18] J. Biela, U. Drofenik, F. Krenn, J. Miniboeck, and J. W. Kolar, "Three-Phase Y-Rectifier Cyclic 2 Out of 3 DC Output Voltage Balancing Control Method," IEEE Trans. Power Electron., vol. 24, no. 1, pp. 34–44, 2009.

[19] R. Greul, S. D. Round, and J. W. Kolar, "The Delta-Rectifier: Analysis, Control and Operation," IEEE Trans. Power Electron., vol. 21, no. 6, pp. 1637–1648, 2006.

[20] T. Nussbaumer, M. Baumann, and J. W. Kolar, "Comprehensive Design of a Three-Phase Three-Switch Buck-Type PWM Rectifier," IEEE Trans. Power Electron., vol. 22, no. 2, pp. 551–562, 2007.

[21] D. Bortis, S. Waffler, J. Biela, and J. W. Kolar, "25-kW Three-Phase Unity Power Factor Buck–Boost Rectifier with Wide Input and Output Range for Pulse Load Applications," IEEE Trans. Plasma Sci., vol. 36, no. 5, pp. 2747–2752, 2008.

[22] A. R. Prasad, P. D. Ziogas, and S. Manias, "An Active Power Factor Correction Technique for Three-Phase Diode Rectifiers," IEEE Trans. Power Electron., vol. 6, no. 1, pp. 83–92, 1991.

[23] J. W. Kolar, H. Ertl, and F. C. Zach, "A Comprehensive Design Approach for a Three-Phase High-Frequency Single-Switch Discontinuous-Mode Boost Power Factor Corrector Based on Analytically Derived Normalized Converter Component Ratings," IEEE Trans. Ind. Appl., vol. 31, no. 3, pp. 569–582, 1995.

[24] J. W. Kolar and F. C. Zach, "A Novel Three-Phase Utility Interface Minimizing Line Current Harmonics of High-Power Telecommunications Rectifier Modules," in Proc.of the Int. Telecom. Energy Conf. (INTELEC '94), 1994, pp. 367–374.

[25] ——, "A Novel Three-Phase Utility Interface Minimizing Line Current Harmonics of High-Power Telecommunications Rectifier Modules," IEEE Trans. Ind. Electron., vol. 44, no. 4, pp. 456–467, 1997.

[26] Y. Zhao, Y. Li, and T. A. Lipo, "Force Commutated Three Level Boost Type Rectifier," IEEE Trans. Ind. Appl., vol. 31, no. 1, pp. 155–161, 1995.

[27] M. L. Heldwein, S. A. Mussa, and I. Barbi, "Three-Phase Multilevel PWM Rectifiers Based on

Conventional Bidirectional Converters," IEEE Trans. Power Electron., vol. 25, no. 3, pp. 545–549, 2010.

[28] G. Gong, M. L. Heldwein, U. Drofenik, J. Miniboeck, K. Mino, and J. W. Kolar, "Comparative Evaluation of Three-Phase High-Power-Factor AC-DC Converter Concepts for Application in Future More Electric Aircraft," IEEE Trans. Ind. Electron., vol. 52, no. 3, pp. 727–737, 2005.

[29] L. Hoffmann, C. Gautier, S. Lefebvre and F. Costa, "Optimization of the driver of GaN power transistors through measurement of their thermal behavior," IEEE Trans. Power Electron., vol. 29, no. 5, pp. 2359-2366, Aug. 2013.

[30] A. Yoshikawa, H. Matsunami, and Y. Nanishi, in Wide Bandgap Semiconductors, Springer. pp.2, 2007.

[31] Microsemi PPG, "Gallium Nitride (GaN) versus Silicon Carbide (SiC) In The High Frequency (RF) and Power Switching Applications,", digikey.

[32] R. muller and T. Kamins, in Device electronics for integrated circuits, 3th ed., Johan Wiley & Sons, eq. 1.1.12, pp.15, 1986.

[33] C. Raynaud, D. Tournier, H. Morel and D. Planson, "Comparison of high voltage and high temperature performances of wide bandgap semiconductors for vertical power devices," Diamond and Related Materials, vol. 19, no. 1, pp. 1-6, Jan. 2010.

[34] P. Neudeck, R. S. Okojie and L. Chen, "High-temperature electronics-a role for wide bandgap semiconductors?," in Proc. IEEE90, 2002, no. 6, pp.1065-1076.

[35] T. Funaki, J. Balda, J. Junghans, A. Kashyap, H. Mantooth, F. Barlow, T. Kimoto and T. Hikihara, "Power conversion with SiC devices at extremely high ambient temperatures," IEEE Trans. Power Electron., vol. 22, no. 4, pp. 1321-1329, Jul. 2007.

[36] M. Khan, G. Simin, S. Pytel, A. Monti, E. Santi and J. Hudgins, "New developments in gallium nitride and the impact on power electronics," in Power Electron. Specialists Conf. (PESC), 2005, pp. 15-26.

[37] "GaNpowIR-An Introduction", International Rectifier, Feb. 2010.

[38] J. Casady, and R. Johnson, "Status of silicon carbide (SiC) as a wide-bandgap semiconductor for high-temperature applications: A review," Solid-State Electron., vol. 39, no. 10, pp. 1409-1422, Oct. 1996.

[39] A. Witek, Diamond and Related Materials 7, pp. 962–964, 1998.

[40] C. Mion, "Investigation of the thermal properties of gallium nitride using the three omega technique," Ph.D. dissertation, EE, NCSU, Raleigh, NC, 2006.

[41] H. Shibata, Y. Waseda, H. Ohta, K. Kiyomi, K. Shimoyama, K. Fujito, H. Nagaoka, Y. Kagamitani, R. Simura and T. Fukuda, "High thermal conductivity of gallium nitride (GaN) crystals grown by HVPE process," Materials Trans., vol. 48, no. 10, pp. 2782-2786, Sept. 2007.

[42] N. Kaminski, Nando, “State of the art and the future of wide band-gap devices,” in Power Electron. Appl. (EPE), 2009, pp. 1-9.

[43] S. Davis, “Schottky diodes: the old ones are good, the new ones are better,” Power Electronics Technology, Mar. 2011.

[44] A. Lidow, “Is it the end of the road for silicon in power conversion?,” in Integrated Power Electron. Systems (CIPS), 2010, pp. 1-8.

[45] “GaNpowIR-An Introduction”, International Rectifier, Feb. 2010.

[46] N. Ikeda, S. Kaya, J. Li, Y. Sato, S. Kato and S. Yoshida, “High power AlGaN/GaN HFET with a high breakdown voltage of over 1.8 kV on 4 inch Si substrates and the suppression of current collapse,” in IEEE Power Semiconductor Devices and IC's (ISPSD), 2008, pp. 287-290.

[47] Y. Niiyama, T. Shinagawa, S. Ootomo, H. Kambayashi, T. Nomura and S. Kato, “High-power operation of normally-off GaN MOSFETs,” Furukawa Rev., vol. 36, pp. 1-5, 2009.

[48] M. Rodriguez, Y. Zhang, and D. Maksimovic, “High-frequency PWM buck converters using GaN-on-SiC HEMTs,” IEEE Trans. Power Electron., vol. 29, no. 5, pp. 2462-2473, Aug. 2013.

[49] L. Su, F. Lee and J. Huang, “Enhancement-Mode GaN-Based High-Electron Mobility Transistors on the Si Substrate With a P-Type GaN Cap Layer,” IEEE Trans. Electron Devices, vol. 61, no. 2, pp. 460-465, Jan. 2014.

[50] Michael. Briere, “The status of GaN power device development at International Rectifier,” APEC Exhibitor Presentation, Mar. 2013.

[51] http://news.panasonic.com/global/press/data/2015/09/en150930-5/en150930-5.html

[52] J. W. Kolar and F. C. Zach, "A novel three-phase utility interface minimizing line current harmonics of high-power telecommunications recti- fier modules," in IEEE Trans. Ind. Electron., vol. 44, no. 4, pp. 456–466, Aug. 1997.

[53] H. Chen and D. C. Aliprantis, “Analysis of squirrel-cage induction generator with VIENNA rectifier for wind energy conversion system,” IEEE Trans. Energy Convers., vol. 26, no. 3, pp. 967–975, Sep. 2011.

[54] C. Qiao and K. M. Smedley, “Three-phase unity-power-factor starconnected switch (VIENNA) rectifier with unified constant-frequency integration control,” IEEE Trans. Power Electron., vol. 18, no. 4, pp. 952–957, Jul. 2003.

[55] A. Lidow, J. Strydom, R. Strittmatter, C. Zhou, "GaN: A Reliable Future in Power Conversion: Dramatic performance improvements at a lower cost," IEEE Power Electronics Magazine., vol. 2, no. 1, pp. 20-26, Mar. 2015.

[56] A. Lidow, J. Strydom, M. de Rooij, and Y. Ma, "GaN transistorsfor efficient power conversion," Power Conversion Publications, 2012

[57] J. Wang, Y. Li, Y. Han "Integrated Modular Motor Drive Design With GaN Power FETs" IEEE

Trans.Industry Applications, vol. 51, no. 4, pp. 3198 - 3207, 2015

[58] R. Burgos, R. Lai, Y. Pei, et al, "Space Vector Modulator for Vienna-Type Rectifiers Based on the Equivalence Between Two- and Three-Level Converters: A Carrier-Based Implementation", IEEE Trans. Power Electronics, vol. 23, no. 4, pp. 1888-1898, 2008

[59] U. Drofenik and J. W. Kolar, "Comparison of Not Synchronized Sawtooth Carrier and Synchronized Triangular Carrier Phase Current Control for the VIENNA Rectifier I," in Proc. of the IEEE Int. Symp. on Industrial Electronics (ISIE '99), vol. 1, 1999, pp. 13–19.

[60] H. Kanaan, K. Al-Haddad, and F. Fnaiech, "Modelling and Control of Three-Phase/Switch/Level Fixed-Frequency PWM Rectifier: State-Space Averaged Model," IEE Proceedings -Electric Power Applications, vol. 152, no. 3, pp. 551–557, 2005.

[61] J. Kolar, F. Zach, "A Novel Three-Phase Utility Interface Minimizing Line Current Harmonics of High-Power Telecommunications Rectifier Modules," IEEE Trans. Ind. Electron., vol. 44, no. 4, pp. 456–467, 1997.

[62] J. Kolar, U. Drofenik, and F. Zach, "Space Vector Based Analysis of the Variation and Control of the Neutral Point Potential of Hysteresis Current Controlled Three-Phase/Switch/Level PWM Rectifier Systems," in Proc. of the Internat. Conf. on Power Electron. and Drive Systems, vol. 1, 1995, pp. 22–33.

[63] U. Drofenik, "Optimierung und Experimentelle Analyse des Stationären Betriebsverhaltens eines VIENNA Rectifier I," Ph.D. dissertation, Vienna University of Technology, 2003.

[64] H. Akagi, Y. Kanazawa, A. Nabae, "Instantaneous reactive power compensators comprising switching devices without energy storage components," IEEE Trans. on Industry Applications, 1984, 20(3): 625-630.

[65] T. Noguchi, H. Tomiki, S. Kondo, "Direct power control of PWM converter without power-source voltage sensor," IEEE Trans. on Industry Applications, 1998, 34(3): 473-479.